Order Number 9224016

The nature of illite/smectite clays and smectite illitization in Paleozoic K-bentonites

Cetin, Kenan, Ph.D.

University of Cincinnati, 1992

U·M·I
300 N. Zeeb Rd.
Ann Arbor, MI 48106

THE NATURE OF ILLITE/SMECTITE CLAYS AND SMECTITE ILLITIZATION IN PALEOZOIC K-BENTONITES

A dissertation submitted to the

Division of Graduate Studies and Research
of the University of Cincinnati

in partial fulfillment of the
requirements for the degree of

DOCTOR OF PHILOSOPHY

in the Department of Geology
of the College of Arts and Sciences

1992

by

Kenan Cetin

M.S., Middle East Technical University, Turkey, 1987

B.S., Middle East Technical University, Turkey, 1984

Committee Chair: Warren D. Huff

UNIVERSITY OF CINCINNATI

March 6 19 92

I hereby recommend that the thesis prepared under my supervision by Kenan Cetin

entitled The Nature of Illite/Smectite Clays and Smectite Illitization in Paleozoic K-Bentonites.

be accepted as fulfilling this part of the requirements for the degree of Doctor of Philosophy

Approved by:

ABSTRACT

Alkylammonium ion exchange, x-ray powder diffraction (XRD), x-ray fluorescence spectroscopy (XRF), and high resolution transmission electron microscopy (HRTEM) have been used to study the chemistry and the physical properties of illite/smectite (I/S) clays. The samples represent Paleozoic K-bentonites and include the full range of I/S compositions commonly found in nature. The data have been used to evaluate current models of I/S interstratification and the mechanism of formation of illite during bentonite diagenesis.

XRD results show a progressive sequence of illite polytypes from 1Md to 1M to 2M1 with increasing illite proportion and degree of ordering in the I/S. Chemical analyses of the <0.2 μm size fraction indicate that the increases in the amount of tetrahedral Al^{+3} for Si^{+4} substitution and the amount of fixed-K are the principal factors controlling the increases in the proportion of illite and the degree of ordering in I/S. Extrapolation of the chemical data suggests a montmorillonitic and a phengitic end-member compositions, respectively, for smectite and illite. Both chemical and XRD data are consistent with a layer-by-layer transformation mechanism of smectite to illite in which randomly distributed high-,

intermediate-, and low-charge interlayers of a precursor smectite preferentially incorporate K^+ ions in response to an increasingly negative tetrahedral charge.

The magnitude and distribution of layer charges determined by alkylammonium ion exchange are characteristic of smectite in I/S with 15-100% expandabilities, confirming the two-component nature of I/S in this range. This result also provides strong support for the layer-by-layer transformation mechanism in which the expandable layers in I/S retain their smectitic charge. The neoformation mechanism proposed for the formation of illite in bentonites (**Nadeau et al., 1985; Nadeau and Bain, 1986**) appears to be unlikely because such a mechanism requires precipitation of illite particles with surface charges significantly higher than that of a smectite.

Both the XRD and HRTEM data for alkylammonium exchanged I/S with <15% expandabilities suggest the presence of expandable, vermiculite-like charged domains. Alkylammonium ion-expanded interlayer thicknesses measured on HRTEM images further suggest a vermiculitic rather than smectitic charge distribution between illite packets. Thus, samples with very high illite/smectite ratios can be better described as illite/vermiculite in view of the layer charge density of the expandable component. The HRTEM data also

demonstrate that the fundamental particles postulated by Nadeau and coworkers are secondary, not primary, crystallites produced by disintegration of interstratified crystallites along the expandable interlayers during sample preparation.

ACKNOWLEDGEMENTS

First and foremost, I wish to express my sincerest gratitude to Dr. Warren D. Huff, my advisor, who not only introduced me to the clay mineral research but also was a source of insightful advice, guidance and inspiration, virtually on a daily basis. Without his initiating the project as well as reading several drafts of the manuscript, I could not have completed the research. His words of wisdom and support on a personal level greatly helped me in resolving my personal difficulties and enriched my perspective for science in particular, and life at large.

I am grateful to Dr. Craig Dietsch and Dr. J. Barry Maynard, minor advisors, for many fruitful discussions, continuous support, encouragement, and valuable improvements to an early version of the manuscript. I want to thank Dr. Maynard also for his help in every step of the XRF analyses.

My special thanks go to Dr. Attila Kilinc for always being there as a solid support and also for initiating my coming to Cincinnati.

I am thankful to Mark Phillips, our x-ray diffraction specialist, for putting up with my "get me out of trouble" blues.

Many thanks go to Earny Clark of U.C. Materials Science Department for training me on the Philips CM20 TEM.

I would like to take this opportunity to thank my fellow graduate friends, Carlos Abreau, Mark Barnhill, Bruce Brasswell, Zeki Camur, Tammie Gerke, Scott Ritger, and many others who made my stay at Cincinnati a pleasurable one.

Last but not least, I want to express my deepest gratitude and passion to Michelle, my companion, for her patient, continuous, and sincere support the last two years in my battles with graduate life.

This research was facilitated by a research grant from the Clay Minerals Society, and partial financial support by the Department of Geology, University of Cincinnati, and the University of Cincinnati Research Council.

TABLE OF CONTENTS

LIST OF TABLES

General Introduction

Chapter 1

Chapter 2

Appendix A

LIST OF FIGURES

General Introduction

Chapter 1

Appendix A

GENERAL INTRODUCTION

Statement of the Problem

Illite/smectite (I/S) is an interstratified clay mineral that exhibits properties of both illite and smectite. Many workers have observed that smectite-rich I/S minerals change with time to illite through a progressive increase in the proportion of illite layers upon burial and heating. Termed smectite illitization, this reaction (also frequently termed transition or conversion) has been identified in sedimentary diagenetic environments (**Burst, 1969; Dunoyer de Segonzac, 1970; Perry and Hover, 1970; Weaver and Beck, 1971; Hower et al., 1976; Boles and Franks, 1979; Srodon, 1984a**), hydrothermal environments (**Eslinger and Savin, 1973; Inoue et al., 1978; McDowell and Elders, 1980; Inoue and Utada, 1983; Horton, 1985**),contact metamorphic environments (**Nadeau and Reynolds, 1981**) as well as in bentonites (**Huff and Türkmenoglu, 1981; Velde and Brusewitz, 1982; Brusewitz, 1986, 1988**).

Powder X-ray diffraction (XRD) has been the essential tool used to reveal smectite illitization which is recognized to involve the following mineral sequence:

Smectite → Random I/S → Ordered I/S → Illite.

Over the course of the transition, an XRD peak appears at low values of 2θ and migrates to higher angles. The peak

shift indicates development of short-, intermediate-, and finally long-range ordering of illite and smectite layers **(Hoffman and Hower, 1979; Bethke et al., 1986)**. The type of interlayer order in I/S can be used as a measure of the thermal histories of the associated sediments and rocks **(Hoffman and Hower, 1979; Horton, 1985; Burtner and Warner, 1986)**. Although the smectite-to-illite transition is widely accepted to take place within the general framework of evolution described above, there is considerable uncertainty about: 1) the physical and chemical nature of crystallites that make up the I/S minerals, and 2) the mechanism(s) of conversion during illitization. At present, there are two, apparently incompatible I/S models: 1) the Markov (MacEwan crystallite) model, and 2) the fundamental particle model (Fig.1).

The Markovian model of I/S, first introduced by **Hendrics and Teller (1942)** and **MacEwan (1956, 1958)**, and applied by **Reynolds and Hower (1970)** to calculate XRD patterns of I/S, considers that I/S is composed of silicate layers 10Å thick that are separated by K-filled illite and hydrous smectite interlayers **(Reynolds, 1980)**. The interlayers are stacked along the crystallographic c-axis to form coherent crystallites, usually referred to as MacEwan crystallites, of various ordering types. Ordering types are identified by their Reihweite or R value

(**Jagodzinski, 1949**), ranging from 0 to 3, where the integer indicates the number of unlike nearest neighbors in the stacking sequence. Thus, R0 indicates randomly interstratified I/S and R3 indicates long-range ordered I/S. One-dimensional XRD coherent domain thickness considerations indicate that crystallites are predominantly 5 to 15 silicate layers thick (50 to 150Å). Based on this model, **Hower et al. (1976)**, and **Hoffman and Hower (1979)** suggested a transformation mechanism in which smectite interlayers, in response to an increase in net negative layer charge caused by tetrahedral Al^{+3} for Si^{+4} substitution, collapse about interlayer K^{+} ions to form illite layers. In this model, the transition is made without disrupting the stack of layers. Using computer methods, **Bethke and Altaner (1986)** showed that the Markovian model for smectite illitization can explain: 1) the occurrence of randomly interstratified I/S, 2) the transition to ordered interstratifications, and 3) the development of long-range ordering.

The fundamental particle model **(Nadeau et al., 1984; 1985)**, based heavily on transmission electron microscope (TEM) observations of dispersed I/S, proposes that I/S is composed of fundamental smectite and illite particles (Fig. 1). In this model, a fundamental smectite particle is defined as a single, 10Å thick silicate layer. Illite

particles are at least 20Å thick and are composed of two smectite particles held together by interlayer K^+. If a sample consisted of all 20Å illite particles, it would be equivalent to a perfectly ordered 50/50 R1 illite/smectite in the Markovian model, and it would contain no smectite particles. An I/S, which in the sense of Markovian model has less than 50% smectite, has illite particles that have grown to 30, 40, 50Å or more in the fundamental particle model. The fundamental particle model further proposes that the illite particles are capable of absorbing water or organic molecules and that interparticle diffraction between particles, stacked on an X-ray slide, gives the appearance of smectite interlayers in regularly ordered I/S minerals. In effect, the fundamental particle model implies that the materials yielding the XRD patterns of I/S do not necessarily contain chemically distinct illite and smectite layers. **Nadeau et al. (1984, 1985)**, in contrast to the more classical model of transformation of precursor smectite to illite, suggested a neoformation model whereby smectite is converted to illite by dissolution of smectite particles and reprecipitation of 20Å thick fundamental illite particles from solution. In this model, illite particles of greater thickness either precipitate or grow from thinner particles as diagenesis proceeds, a process called Ostwald ripening **(Eberl and Srodon, 1988)**.

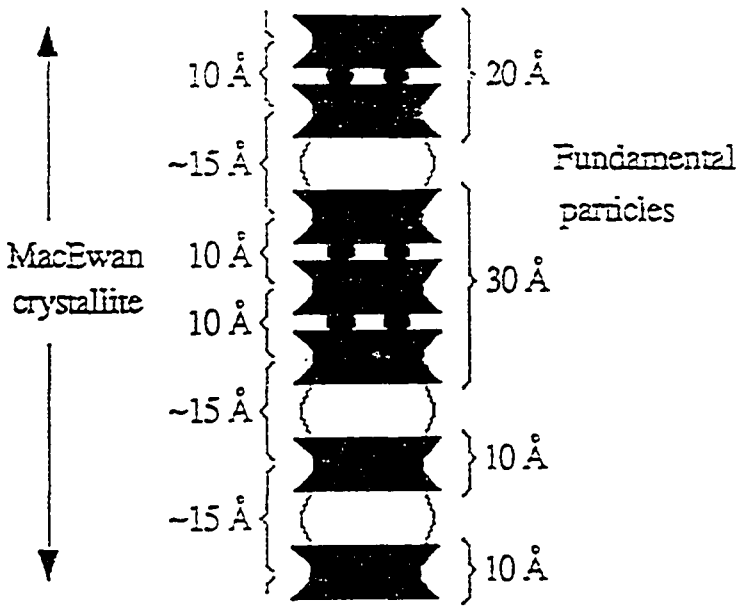

Fig. 1: Interstratified illite/smectite according to the MacEwan crystallite (left) and the fundamental particle model (right). (modified from **Altaner and Bethke, 1988**).

Several studies with different approaches have been undertaken to resolve the forementioned problems concerning the nature of I/S and the smectite-to-illite conversion mechanism. **Inoue et al. (1987)**, using TEM to study the morphology of I/S minerals in a hydrothermal system, identified three mineral phases, each with a distinctive shape. The first has a flaky morphology whenrandom I/S is dominant between 100% and 50% expandability (= percent smectite). The second has a lath morphology and occurs between about 50% to as little as 5% expandability. The third phase is in the form of hexagonal plates and has almost no expandability. On the basis of these observations, they proposed that both transformation and neoformation took place in these clays - transformation of smectite to illite by K-fixation in the flakes, and neoformation as the flakes dissolve and reprecipitate in the form of laths and hexagonal plates that subsequently grow by the Ostwald ripening process. **Inoue et al.(1988)** provides further support for evolution of illite by neoformation controlled by the Ostwald ripening process in I/S with less than 50% expandabilities. **Eberl and Srodon (1988)** deduced a similar process for the growth of illite using XRD diagrams and the Warren-Averbach technique **(Warren and Averbach, 1950).**

Studies by high resolution electron microscopy

(HRTEM) of dispersed I/S minerals **(Bell, 1986; Klimentidis and Mackinnon, 1986; and Vali and Köster, 1986)** appear to support the Markovian model because they show ordered sample domains that are closer in thickness to MacEwan crystallites than to fundamental particles. These studies, however, are not fully conclusive because the sample preparation techniques used did not allow these workers to obtain a representative data set of basal spacings from dispersed particles. **Ahn and Peacor (1986)**, after studying ion-thinned samples of shales, stated that what really existed in rocks were segregated megacrystals of smectite and illite tens of layers thick. They interpreted interstratification as an artifact due to disintegration of megacrystals in the course of X-ray sample preparation. Recently, these authors reinterpreted their observation **(Ahn and Peacor, 1989)** on the basis of computer simulations of **Guthrie and Veblen (1989a)**, and they now recognize megacrystals as ordered I/S crystals. **Ahn and Buseck (1990)**, using ultra high resolution TEM imagery of ion-thinned chips of shale and bentonite samples, stated that coherently diffracting sample domains they observed are thicker than the fundamental particles. They suggested that the smectite interlayers in I/S, being loosely bonded, are more easily cleaved than illite interlayers, and that thin flakes similar in thickness to fundamental particles can be

derived during sample preparation from larger primary crystallites having two types of interlayers. **Veblen et al. (1990)** and **Srodon et al. (1990)** reported that illite-to-smectite ratios in undisturbed I/S as determined from HRTEM images are consistent with those from XRD. These workers deduced, as did **Ahn and Buseck (1990)**, that fundamental particles only a few silicate layers thick are secondary crystallites that are separated along smectite interlayers of larger crystals.

In summary, most of the recent HRTEM data accumulated appear to provide support for the existence of MacEwan crystallites in I/S. However, none of these studies provide a clear understanding whether or not the crystal edges (or interfaces between fundamental particles) in ordered I/S are smectitic. This is central to the controversy between the fundamental particle and the MacEwan crystallite models because ordered I/S is considered to be a single phase (i.e. illite) in the fundamental particle model. In most of the recent HRTEM studies of I/S, the original textures of the samples are preserved. Such samples, because of their intact nature, may naturally have areas of lattice fringes that are thicker than fundamental particles simply because they may consist of aggregates of fundamental particles having a high degree of face-to-face orientation **(Nadeau, 1985)**. The difficulty of interpretation of HRTEM images,

largely owing to focusing problems **(Guthrie and Veblen, 1989)**, further makes the reliability of expandability measurements on undisturbed samples uncertain.

Purpose:

In this study, a series of I/S clays from K-bentonites ranging from random to long-range ordered and having 70% to <5% expandability has been examined. The purpose of the study is three-fold:

1) to characterize the layer charge properties of the expandable component in these I/S clays, using the alkylammonium exchange method. **Nadeau et al. (1985)** pointed out that their investigations did not take into consideration either the surface charge or any charge distribution across the silicate layers, and indicated the need for information on layer charge in I/S minerals. The alkylammonium exchange method **(Lagaly and Weiss, 1969; Lagaly, 1981)** has been extensively used to characterize smectites and vermiculites, and has the potential of revealing whether or not the expandable component, particularly in short- and long-range ordered I/S, has a smectitic charge;

2) to study by HRTEM the texture, structure, and size of particles in both untreated and alkylammonium ion exchanged, well-dispersed I/S samples with special emphasis on the ordered, more illitic end of the I/S series. HRTEM

of well-dispersed I/S permanently expanded by alkylammonium ions at its interlayers may show whether or not extremely small particles have expanding interlayers within them; and

3) to characterize smectite illitization in bentonites on the basis of XRD, chemical analysis, HRTEM, and alkylammonium ion exchange data.

The primary focus of the review in the remainder of this section is to give further details on the concepts that are frequently encountered in the literature dealing with smectite illitization, interstratification and interlayer order in I/S, and layer charge of smectite and illite.

Interstratification and Interlayer Stacking Order

The terms interstratification, interlayering, and mixed-layering describe phyllosilicate structures in which two or more kinds of layers occur in a vertical stacking sequence along the crystallographic c-axis. Such mixing is possible because the a-b geometry of most silicates is fundamentally the same, varying only in site occupancies and interatomic dimensions. The existence of interstratified clay minerals has been known for many years and their widespread occurrence was documented by the comprehensive work of **Weaver (1956)**.

Interstratification can be random, for which no discernible pattern exists in the sequence of component

layers; ordered, according to various periodic stacking schemes; or partially ordered, an intermediate case between two extremes. Ordering types are commonly described using a terminology based on the term Reichweite, first defined by **Jagodzinski (1949)**, and usually denoted by R (**Kakinoki and Komura, 1965; Sakharov and Drits, 1973**). R describes the number of neighbor-to-neighbor interactions between layer types. Random interstratifications have a Reichweite of 0 (R0) and show no interactions among neighbors. Reichweite 1 (R1) minerals have ordering of nearest neighbors. In minerals with Reichweite 2 and 3 order (R2 and R3), ordering is dependent on the next-nearest and thrice-removed neighbors. R1 and R2 are usually referred to as short- and intermediate-range ordering, respectively while R3 and R>3 are considered as long-range ordering (**Altaner and Bethke, 1988**).

Randomly interstratified minerals are recognized in XRD patterns by the presence of aperiodic 001 reflections at angles that cannot be predicted by the Bragg law for a single phase. Reflections occur between the nominal positions of 001 peaks of both end-member components in the mixture, and the positions of these reflections are fixed by the proportions of the end-members in the interstratification (**Mering, 1949**) and the nature of ordering (**Reynolds, 1980**). The observed reflections are

thus composites of the two end-member reflections. For R1 ordered minerals containing two end-members in equal proportions, reflections, called superstructure or superlattice reflections, occur and correspond to the sum of the thicknesses of the individual layer types. Superlattice reflections follow the Bragg law.

The minerals that are usually involved in interstratification include chlorite, vermiculite, smectite, illite, glauconite, biotite, serpentine, kaolinite, and talc. Of these, interstratified I/S are the most common in nature, and the most widely studied (**Moore and Reynolds, 1989**).

In interstratified I/S minerals, identification of the type of ordering and estimation of proportions of illite and smectite are based on XRD patterns of ethylene glycol (EG)-solvated samples because these patterns tend to maximize the differences between the expanding and non-expanding constituents. Figure 2 shows a calculated XRD pattern of a randomly interstratified (R0) illite/EG-smectite containing 50% illite, and demonstrates that 001 reflections of the mixture occur between the nominal positions of illite and smectite. The solid vertical lines mark the positions of the smectite 001 reflections, and the dashed lines designate the same for illite. Composite peaks whose positions depend on the proportions of illite and

smectite occur near 10° 2θ for the illite 001 and EG-smectite 002 reflections, 16° for the illite 002 and EG-smectite 003 reflections, 20° for the illite 002 and smectite 004 reflections, and 26.6° 2θ for the illite 003 and smectite 005 reflections. It should be noted that a strong but broad reflection occurs at 5.2° 2θ at the smectite 001 position. The smectite 001 is not displaced because no illite peak is nearby. Instead, it becomes progressively broader and weaker as the proportion of illite increases.

A perfectly R1 ordered I/S of the same composition (50/50 illite and smectite) is distinguished from the randomly interstratified sample in Figure 2 by the presence of a periodic sequence of superstructure reflections called 001*, 002*, 003*, etc., (Fig. 3a). An increase in the proportion of illite to more than 50% causes some degree of randomness, and leads to weakening and disappearance of the 001* superstructure reflection. Thus, in interstratified I/S samples containing more than 50% illite, R1 ordering is diagnosed by a weak 001* superstructure near 3° 2θ and a dominating component of the second-order superstructure reflection 002* in the 6-7° 2θ region (Fig. 3b).

A peak between 7° and 9° 2θ in addition to a peak around 9-10°θ suggests long-range ordering (R≥3). Figure 3c shows a calculated pattern for 90% illite with R3 ordering.

The broad shoulder at about 8° 2θ, or d=11.1Å contains components of the illite 001 reflection and the fourth order of a 47Å superstructure whose unit cell consists of three 10Å illite layers and one 17Å EG-smectite layer. This peak denotes the presence, in the interstratified crystallites, of the repeating unit-cell pattern IIIS (where I and S represent illite and smectite, respectively) randomly mixed with additional illite layers.

The proportion of illite is estimated by comparing the position of the composite 002/003 reflection near 17° 2θ with the position of the same peak in computer simulated XRD models after a general peak-to-peak match of the patterns is established. In the absence of a computer program to generate models, however, estimates can be made using a differential quantity (**Moore and Reynolds, 1989**), δ2θ, the difference between the positions of composite 001/002 and 002/003 reflections in degrees 2θ (Table 1).

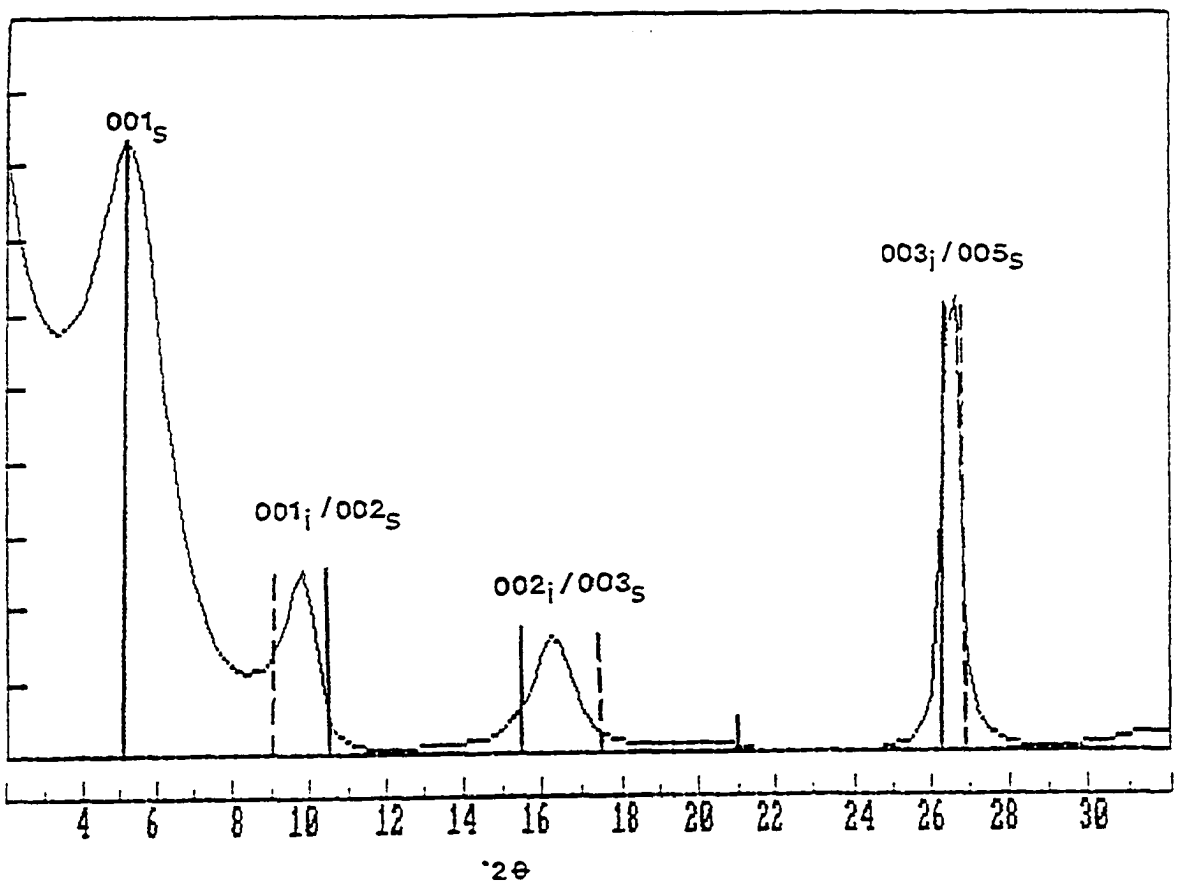

Fig. 2: Interstratified illite/EG-smectite, 50% illite, RO, and the locations of the 001 reflections for the pure phases. Dashed line represents pure illite and solid lines represent smectite.

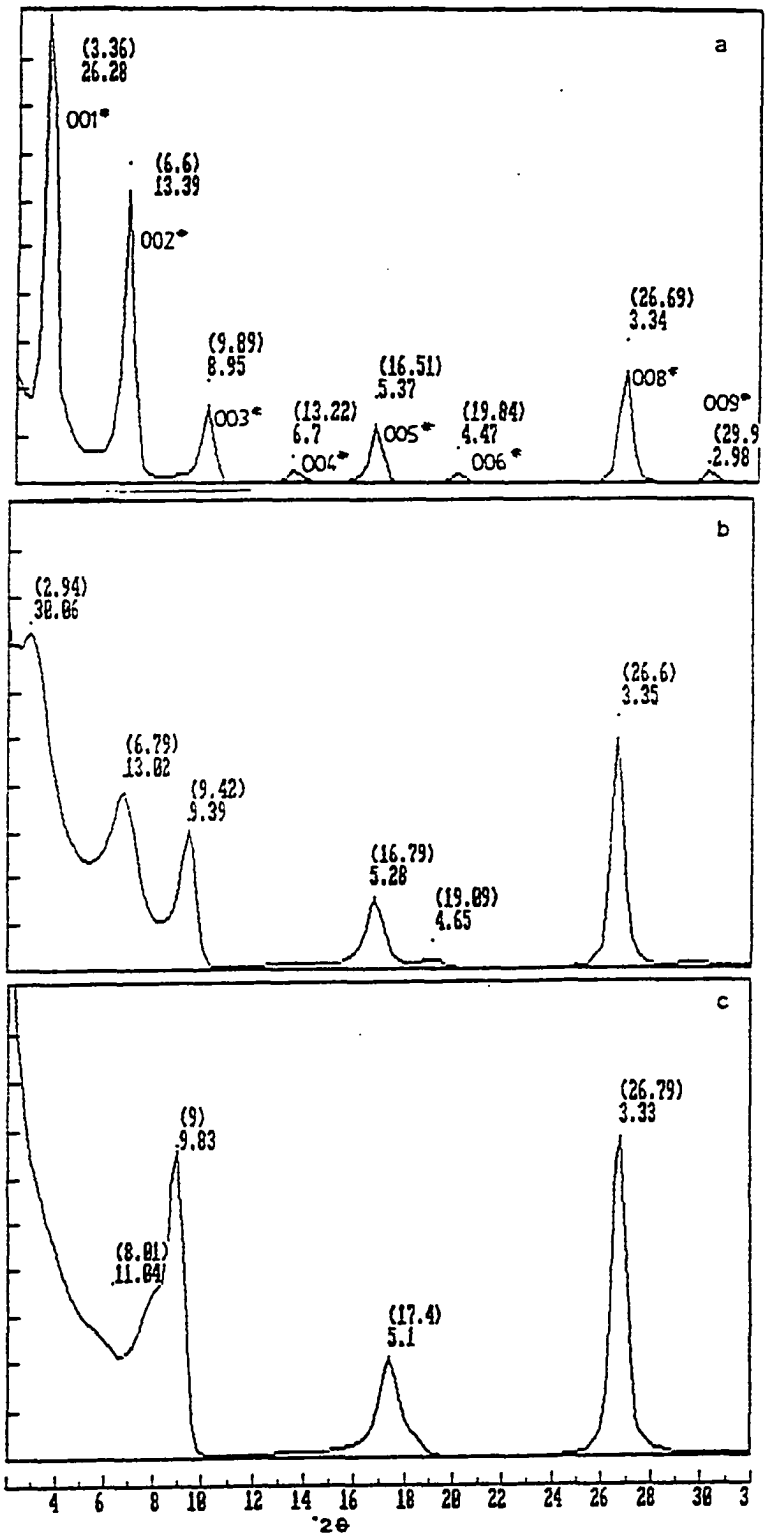

Fig. 3: Ethylene glycol-solvated illite/smectite: (a) 50% illite, R1, (b) 70% illite, R1, and (c) 90% illite, R3.

Table 1: The positions (CuKα) of useful reflections for estimating percent illite in illite/EG-smectite (from **Moore and Reynolds, 1989**).

		001/002		002/003		
% illite	Reichweite(R)	d(Å)	°2θ	d(Å)	°2θ	°δ2θ
10	0	8.58	10.31	5.61	15.80	5.49
20	0	8.67	10.20	5.58	15.88	5.68
30	0	8.77	10.09	5.53	16.03	5.94
40	0	8.89	9.95	5.50	16.11	6.16
50	0	9.05	9.77	5.44	16.29	6.52
60	1	9.22	9.59	5.34	16.60	7.01
70	1	9.40	9.41	5.28	16.79	7.38
80	1	9.64	9.17	5.20	17.05	7.88
90	3	9.82	9.01	5.10	17.39	8.38

Determination of layer charge density

Ionic substitutions in tetrahedral or octahedral sheets of layer silicates frequently result in a residual, usually negative, charge imbalance. Termed layer charge or layer charge density, this charge imbalance is a particularly important property of 2:1 clay minerals because it determines the cation-retention capacity of clays, influences the selectivity of clays for various cations during ion-exchange reactions, and affects the ability of clays to adsorb water or various polar organic molecules. Furthermore, the magnitude of the layer charge serves as a criterion for the classification of 2:1 clay minerals (**Bailey, 1980**). Various methods have been described for determining layer charge (**Keller, 1945, 1955; Lagaly and Weiss, 1969; Mortland, 1970**) but they often give different results, depending on the nature of the mineral, experimental conditions, and the assumptions upon which the methods are based. Cation exchange capacity (CEC) is probably the most commonly used measure of a interlayer charge. CEC is expressed as moles of exchangeable cations per unit mass of clay, and therefore CEC is not a direct measure of layer charge density. Measured CECs may vary with both experimental conditions and clay properties; notably pH, exchanging cations, the clay's exposed surface area, and chemical composition.

CEC and total surface area (SA) measurements may be combined to estimate the layer charge density (LCD=CEC/SA). The total surface area of expanding 2:1 phyllosilicates is measured by adsorption of water **(Newman, 1983)**, or polar organics, such as ethylene glycol **(Dyal and Hendrics, 1950)** or ethylene glycol monoethyl ether **(Carter et al.,1965)**. **Jonas and Roberson (1966)**, for example, used the extent of interlayer hydration as a measure of layer charge. Unfortunately, the extent of interlayer swelling and hence the amount of solvent adsorbed is partially dependent on the layer charge density **(Harward et al., 1969)**. Thus, the combination of CEC and surface area determinations is a relatively inaccurate method of measuring layer charge density.

Philen et al. (1971) characterized layer charge by the competitive adsorption of two divalent organic cations, diquat and paraquat. The separation of charges in these ions is about 3.5Å for diquat and 7.0Å for paraquat. This difference apparently accounts for the observed relationship between the layer charge density and the relative preference a clay exhibits for diquat versus paraquat in exchange relations. A shorter charge separation allows diquat to more closely satisfy the closely spaced charge sites on vermiculite. A greater contribution of van der Waals forces in addition to the electrostatic

attraction causes smectites to prefer paraquat.

Layer charge density can also be estimated by calculating structural formulas. A total elemental analysis is required for these calculations, and then cations are assigned to structural positions based on the assumption of a -22 framework anionic charge per formula unit. The resulting layer charge is expressed as a charge per formula unit, which converts to charge per unit area upon division by the surface area per unit cell.

There are two major problems with calculated structural formulas. First, the specimens must be mono-minerallic. Very few smectites or even vermiculites are truly monominerallic since most contan traces of mica, kaolinite, quartz, carbonates or metal hydrous-oxides. Structural formulas and the estimated layer charge densities will reflect these contaminants. The second problem results from the assumption of a -22 anionic charge per formula unit. It is nearly impossible to accurately determine the anionic charge of a clay, and even a slight deviation from -22 will have a major impact on estimated layer charge.

The characterization of smectite and vermiculite interlayer charge densities has been greatly advanced by the development of the alkylammonium ion exchange method. Since the early work of **Jordan (1949a, 1949b)**, considerable

attention has been given to the adsorption of alkylammonium cations by 2:1 phyllosilicates **(Weiss and Kantner, 1960; Sutherland and MacEwan, 1961; Brindley and Hoffman, 1962; Walker, 1967; Theng et al., 1967; Macintosh et al., 1971)**. Much of the early work has been summarized by **Weiss (1963)**. Sample preparation, alkyl carbon chain length, and the nature of the clay were all found to influence interlayer alkylammonium conformation and the observed basal spacings. However, with consistent sample preparation, **Weiss (1963)** observed a linear relationship between layer charge density and the extent of basal expansion. He proposed the use of dodecylammonium and octadecylammonium clay derivatives for the determination of layer charge density among vermiculites and high-charge smectites. **Lagaly and Weiss (1969), Stull and Mortier (1974), Lagaly et al. (1976), Rüehlicke and Köhler (1981), Hausler and Stanjec (1988)** and **Ghabru et al. (1989)** further refined the use of alkylammonium ions in determining layer charge density.

Alkylammonium-clay derivatives are prepared by the following stoichiometric exchange of the interlayer cations with various straight chain alkylammonium cations:

$$R\text{-}NH_4^+ + \text{Na-Clay} = Na^+ + R\text{-}NH_4\text{-Clay}.$$

Twelve or thirteen alkylammonium derivatives are prepared using alkylammonium chloride cations that have from six

(hexylammonium) to eighteen (octadecylammonium) carbons in their alkyl chains. The derivatives are washed free of excess organic cations, dried, and analyzed by X-ray diffraction to observe the basal spacing imposed by the exchange on each derivative. The packing density and various interlayer alkylammonium configurations depend primarily on the layer charge density. Thus the layer charge density can be estimated by following the change in basal spacing as a function of the size of the alkylammonium cations (Appendix A). The method estimates the interlayer charge density which for smectite represents approximately 80% of the total charge.

The alkylammonium ion exchange method has the advantage over other methods of estimating interlayer charge because it provides not only an estimate of mean interlayer charge of an expanding clay but also the extent of heterogeneity of the interlayer charge across the silicate layers. Furthermore, the presence of non-expanding minerals or other contaminants has little effect on the basal spacing and does not preclude the estimation of interlayer charge (Lagaly and Weiss, 1969; Lagaly, 1981). The results are influenced by incomplete exchange of interlayer cations with alkylammonium cations and incomplete drying of the prepared samples (Lagaly et al., 1976). However, because these problems can be avoided with

proper and consistent sample preparation (**Lagaly et al., 1976; Stull and Mortier, 1974**), and because the method does not require chemical analyses, it is increasingly being used to determine the interlayer charge of expanding 2:1 layer silicates.

Layer Charge Characteristics of Smectite and Illite

A fundamental property of mica-type layer silicates is layer charge. A first comprehensive study of smectites based on the Hoffmann-Endell-Wilm structure were published by **Ross and Hendrics (1945)**. Impressed by the extensive data in this paper, a charge density of 0.33 per formula unit for montmorillonites had been generally adopted. In the 1950's, however, evidence began to accumulate that homogeneous smectites actually had heterogeneous charge densities.

Beavers and Larsen (1953) observed that Wyoming Bentonite had several discrete electromagnetic mobilities. **Byrne (1954)** noticed a lack of regular periodicity along the c-axis of montmorillonite treated with dodecylamine and piperidine. He suggested that montmorillonites consist of a mixed-layer sequence, with components differing in chemical composition or in the presence of structural irregularities. **McAtee (1958)** separated natural bentonites

by centrifugation and found two phases; one dominated by sodium and the other by calcium and magnesium. He postulated that the two phases had differences in isomorphous substitution. **Jones and Roberson (1966)** observed that smaller size fractions of Texas bentonite expanded more than larger size fractions. They interpreted this as evidence of a continuous variation in structural charge with particle size. **Goulding and Talibudeen (1980)** employed differential and integral thermodynamic functions in evaluating K-Ca equilibrium exchange isotherms and microcalorimetric measurements. Their analysis separated groups of homoeergitic exchange sites within a given clay specimen. Later, **Talibudeen and Goulding (1983)** found evidence of four main groups of exchange sites in six smectites. The swelling behavior of these clays was influenced by the proportions of different groups of sites that each clay had. **Hsieh et al.(1984)** studied the expansion of eight smectites relative to ethylene glycol vapor pressure. They observed that expansion from 14 Å to 17 Å occurs over a range of pressures, which was interpreted as further evidence of layer charge heterogeneity.

The alkylammonium ion exchange method has contributed significantly to the characterization of layer charge heterogeneity in smectites. Due to heterogeneity,

alkylammonium exchanged smectites exhibit mono-to-bilayer transitions over a range of carbon chain lengths (**Lagaly and Weiss, 1969**). The apparent basal spacing of each transition sample is determined by the relative proportions of monolayers and bilayers. Thus, by observing the changes in basal spacing associated with mono-to-bilayer transition, **Stull and Mortier (1974)** separated the total layer charge of Wyoming bentonite into nine charge-density classes, ranging from 0.36 to 0.22 per formula unit. **Lagaly and Weiss (1976)** examined over 200 layer silicates by alkylammonium ion exchange and observedthat over 90% of the natural smectites have heterogeneous layer charge densities.

Based on the evidence accumulated by numerous researchers using the variety of techniques to determine the layer charge noted above, it is clear that layer charge heterogeneity in most smectites is the rule rather than the exception. The Nomenclature Committee of AIPEA (Association Internationale pour l'Etude des Argiles) currently accepts a charge of 0.2-0.6 per half cell formula unit for smectites (**Bailey, 1980**).

The composition, and thus the layer charge of illite is difficult to determine, because illite samples, including the original Fithian illite described by **Grim et al.(1937)**, usually are physical mixtures of non-expanding

10Å material (i.e. discrete illite) and predominantly illitic, ordered interstratified I/S **(Srodon, 1984b)**. As a result, an indirect method for estimating the composition of end-member illite by extrapolation of data for I/S has been used by several workers.

The first attempt at such an extrapolation was made by **Hower and Mowatt (1966)** who plotted expandability (=percentage of smectite layers) against fixed interlayer cation content to determine the K content of illite. This plot gave a straight line that extrapolated to about 0.75 fixed-K which , with 0.05 exchangeable cations per layer, gave a layer charge of 0.80 for pure illite. **Srodon et al. (1986)** followed this approach, using a broader sample set and a more precise technique for determining expandability. Their results appeared to indicate that end-member illite is actually composed of at least two kinds of illite layers, one with a layer charge of 0.55, and the other with a layer charge of about 1.0, giving rise to an average layer charge of about 0.8 equivalents per formula unit.

The highest reported layer charge for an illite is for an authigenic diagenetic illite from the Rotliegend formation in the southern North Sea basin **(Nadeau and Bain, 1986)**. This illite has a layer charge of 0.87 equivalents per formula unit. **Meunier and Velde (1989)**, in a study to determine solid solution relations between I/S minerals and

illite, proposed that interlayering in I/S minerals does not reach the illite end-member with a charge of 0.87, but instead stops at a bulk composition with a charge of 0.75 because of crystallographic incompatibilities. **Eberl and Srodon(1988)**, using a technique that corrects the expandability measurements for the presence of nonswelling surfaces at the ends of stacks of illite particles, determined that best extrapolated value for the mean layer charge per illite layer is about 0.9 equivalents, a value that they suggest to be independent of illite origin and expandability.

At present, the proposal that illite has a larger layer charge (i.e. 0.9 equivalents) than previously suspected (i.e. 0.75 equivalents) is also supported by an extrapolation of data for Silverton sericites (0.98 equivalents, **Eberl and Srodon, 1988**), by a combination of NMR and XRF data for an I/S sample (0.95 equivalents, **Altaner et al., 1988**), and by chemical analysis of the Kaube sericite, a nonswelling illite (0.87 equivalents, **Srodon and Eberl, 1984**).

Smectite Illitization and Layer Charge

As noted in preceding sections, numerous workers have studied smectite illitization. These studies point to a trend in which the layer charge density increases with increasing diagenetic grade (i.e. **Hower et al., 1976; Srodon et al., 1986; Nadeau et al., 1985**). **Hower et al. (1976)**, for example, explained formation of illite layers as a response to the increase in net negative layer charge due to increasing tetrahedral Al^{+3} for Si^{+4} substitution. More recently, **Eberl et al. (1986)** provided additional experimental evidence that increased net negative layer charge (or increased layer charge deficiency) is necessary for K-fixation and formation of illite layers. They showed that high-charge smectite can produce I/S containing as many as 50% illite layers when subjected to wetting and drying in the presence of K^+ ions whereas low-charge smectite can produce only a few percent illite layers. According to **Srodon et al. (1986)**, based on the chemistry of I/S from three different bentonite sequences, a layer charge threshold of -0.55 equivalents per formula unit is required to dehydrate interlayer K^+ ions and fix it between adjacent 2:1 layers, forming 20Å thick illite units. For the further dehydration and fixation of K^+ ions between adjacent 20Å thick illite units, thereby forming 40Å thick illite units, a charge of -1.0 is required due to

polarization effects (**Sawhney,1967**).

Meuneir and Velde (1989), using bulk chemical composition and percent smectite data for several I/S sequences, concluded that the expandable component of I/S has a maximum charge of 0.66. This conclusion appears to be in agreement with the requirement of at least 0.55 charge deficiency for initial K-fixation and formation of 20Å illite units (**Srodon et al., 1986**). This maximum of 0.66, however, fails to explain continued K-fixation and thickening of illite particles (**Inoue et al., 1988**), a process that necessitates the presence of high-charged (>0.7) expandable interlayers in highly illitic I/S minerals. Indeed, several workers have recently reported the presence of high-charged, vermiculite-like components in highly illitic I/S clays treated with alkylammonium ions (**Vali and Hesse, 1990; Vali et al., 1991**). However, the exact nature of the layer charge including both its magnitude and distribution along and across the silicate layers in highly illitic I/S is not fully documented. Therefore characterization of the layer charge in I/S, including highly illitic I/S, comprises one of the main objectives of this dissertation.

Thermodynamic Status of Interstratified I/S Minerals

One of the most important questions concerning the thermodynamic description of interstratified I/S minerals is whether the smectite and illite components should be regarded as two, independent phases or, as members of a single-phase solid solution. **Garrels (1984)**, using natural aqueous solution compositions in apparent equilibrium with the clay fraction of rocks (using data from **Aagaard and Helgeson, 1983**), constructed stability diagrams for both the two-phase case and one-phase solid solution case. He concluded that the two-phase solubiliy model better explained the data. Inasmuch as the evidence available to Garrels was not definitive, he suggested criteria for distinguishing between these two models and proposed long-term equilibration experiments to resolve the problem. **Garrels's (1984)** results were substantiated by the long-term mineral solubility experiments by **Rosenberg et al. (1985)** and **Sass et al. (1987)** who concluded that randomly interstratified I/S behaves as a two-phase assemblage (see also **Kittrick, 1984**).

Inoue et al. (1987, 1988), on the other hand, identified three morphologically distinct phases in an I/S sequence from a hydrothermally altered system. They consider two of the phases as solid solutions, and the other as a phase with little variation in its chemical

composition. They described the first solid solution as randomly interstratified smectite varying from 100% to about 50% expandable layers, undergoing K-fixation, and the second solid solution, which varies from nearly 50% to as little as 5% expandable layers, as illite maturing by Ostwald ripening. According to this model, the third phase is pure illite with less than 5% expandable layers and a distinct hexagonal particle morphology.

Another solid solution scheme for interstratified I/S has recently been suggested by **Meuneir and Velde (1989)**. According to this scheme, I/S minerals form a partial solid solution series with three components: a high-charge illite (layer charge=0.87) that behaves as a compositional pole, a low-charge montmorillonite (layer charge=0.33), and a high-charge montmorillonite (charge=0.66). They propose that very illitic I/S with a maximum charge of about 0.75 observed in several bentonite sequences represents the final diagenetic bulk composition, and that the solid solution series is incomplete toward the high-charge illite pole. They further propose that high-charge illite in the final bulk composition is not reached during diagenesis because high-charge illite component cannot replace a smectite component in all proportions from 0 to 100% due to crystallographic incompatibilities.

CHAPTER 1: PHYSICAL AND CHEMICAL PROPERTIES OF ILLITE/SMECTITE MINERALS IN SOME PALEOZOIC K-BENTONITES

INTRODUCTION

K-bentonites are altered volcanic ash beds whose clay fractions are generally dominated by interstratified illite/smectite (I/S). They differ from conventional bentonites which are usually smectite-rich. The main process during bentonite diagenesis is smectite illitization, the conversion of smectite-rich clay to illite-rich clay. Currently, both the physical and chemical nature of I/S minerals, and the mechanism of smectite-to-illite conversion are subjects of controversy. Until recently, illite-rich clays in bentonites were accepted as being products of a layer-by-layer transformation process. In this process, illite layers form from smectite layers within a fixed layer sequence in response to an increase in the total layer charge due to increasing tetrahedral Al^{+3} for Si^{+4} substitution, and selective incorporation of K^{+} ions into interlayer spaces (**Hower et al., 1976; Hoffman and Hower, 1979; Eberl and Hower, 1976; Eberl, 1978; Srodon et al., 1986**).

Nadeau et al.(1984, 1985) proposed an alternative model for interstratified I/S minerals which views illitic clays as populations of fundamental smectite and illite particles. In this model, referred to as the fundamental particle model, the layer sequence is not fixed within interstratified crystallites. Furthermore, illitic clays

are viewed as composed of thicker illite particles which, by adsorbing exchangeable cations, water, and/or organic molecules at their interfaces, behave like smectite interlayers.

Using the fundamental particle model, **Nadeau et al. (1984, 1985)** and **Nadeau and Bain (1986)** proposed that a neoformation process, rather than a transformation process, better explains the smectite-to-illite conversion in K-bentonites, as well as in shale/sandstone sequences. In this neoformation process, smectite particles dissolve, and thin, fundamental illite particles crystallize and grow both in number and thickness as diagenesisproceeds. Such a neoformation process is supported by an earlier study **(Boles and Franks, 1979)** which suggested that dissolution of smectite in Gulf Coast shales does occur, but it is not supported by data from other studies of K-bentonites **(Altaner et al., 1984; Srodon et al., 1986)**.

The main purpose of this study is to characterize the physical and chemical nature of I/S minerals from K-bentonites, and to evaluate the models of smectite illitization in K-bentonites. For this purpose, a suite of fourteen samples of Paleozoic K-bentonites - which effectively encompasses the range of I/S compositions and ordering types common in nature - have been selected. This section documents the detailed XRD characteristics and

chemical composition of I/S minerals in these selected samples.

EXPERIMENTAL PROCEDURE

Samples

All but one sample used in this study are from K-bentonite beds that occur in Llandovery, Wenlock, and Ludlow (Silurian) strata of southern England, Wales, Scotland, and Northern Ireland (Fig. 1). These K-bentonite beds are preserved both in shallow-water carbonate sequences and slope/submarine fan deposits. Individual beds range from 2 cm to 1 m in thickness (Appendix C), and consist of white to yellowish and greenish gray plastic clay with minor amounts of non-clay minerals such as zircon, apatite, quartz, and biotite. A detailed account of the stratigraphy, mineralogy, and tectonic setting of these beds are given by **Huff and Morgan (1990)**. One sample is from the Rocklandian (middle Ordovician) Millbrig K-bentonite in central Kentucky (**Scharpf, 1990**). It is composed mainly of a clay fraction of interstratified I/S, and a non-clay fraction chiefly of biotite, with minor alkali feldspars, zircon, apatite, and Fe-Ti oxides (**Günal, 1979**).

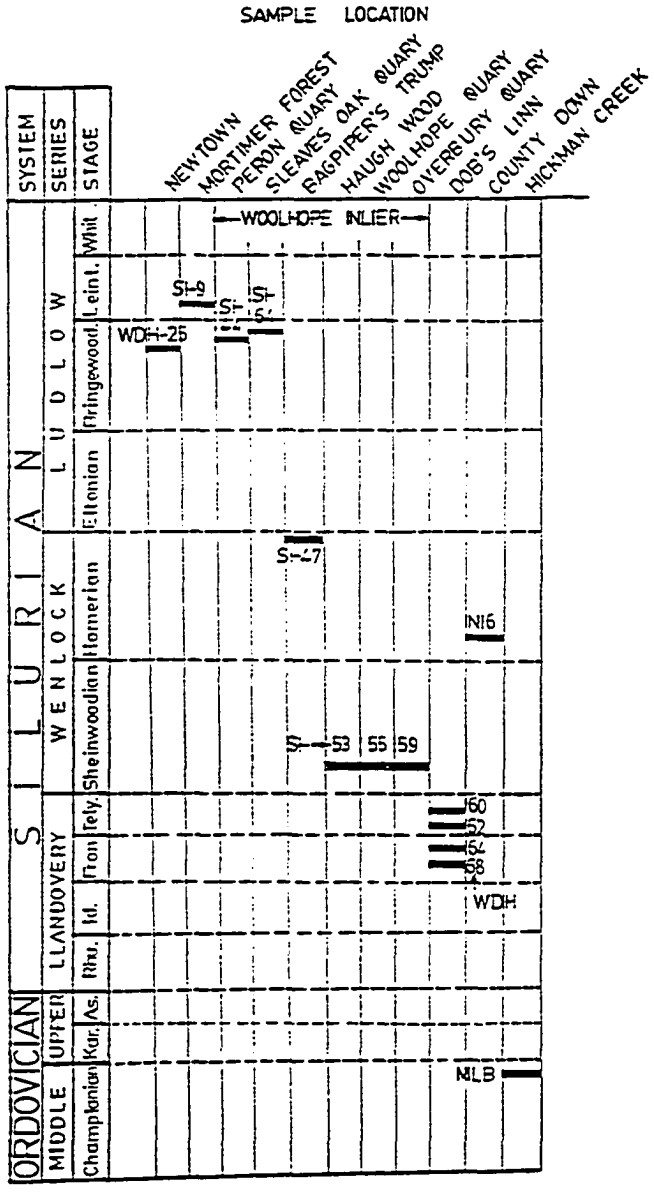

Figure 1: Schematic columnar section showing sample age and locations. Sample thickness and detailed location data are given in Appendix C.

Sample Preparation

Between ten and fifteen grams of each sample was dispersed in distilled water by gentle crushing, agitation in a blender, and ultrasonic vibration. The clay suspensions were then centrifuged using a Sharples super-centrifuge, to obtain the <0.2μm fraction. No chemicals were used for sample treatments, except two samples (WDH-68 and NI-6) to which small amounts of 0.01 N sodium pyrophosphate were added for a complete dispersion. Supercentrifuge overflow suspensions were concentrated by repeated settling and decantation, and were stored in capped beakers for subsequent analyses.

X-ray Powder Diffraction

Oriented mounts of the <0.2μm fraction were prepared on petrographic glass slides by the smear method of **Gibbs (1968)**. The mounts were x-rayed air-dried as well as after ethylene glycol solvation for at least 24 hours by the vapor method. XRD was also conducted on randomly oriented powder mounts, prepared by a sideward-packing technique **(Austin et al. 1989)** for the determination of illite polytypes. The reflections that are used in the determination of the polytypes are presented in Table 1. All XRD analyses were performed on a Siemens D-500 3kW automated powder x-ray diffractometer using Cu-Kα

radiation. The relative proportions of illite and smectite and the type of interlayer order in I/S were determined by comparison of XRD patterns of the ethylene glycol-solvated samples with computer simulated XRD patterns generated by the NEWMOD program for two-component layering (**Reynolds, 1985**).

Table 1: Diagnostic reflections used in the determination of two common polytypes of illite in I/S samples (modified from **Bailey, 1980**).

	1M				$2M_1$		
	d	I	hkl		d	I	hkl
*	3.66	50	112		3.88	30	113
*	3.07	50	112		3.72	30	023
	2.93	10	113	*	3.49	30	114
	2.69	20	023	*	3.20	30	114
					2.98	35	025
					2.86	30	115

d: spacing.

I: relative intensity (on a scale of 100).

hkl: lattice indices.

* : Most diagnostic reflections.

Chemical Analysis

Major elements were determined on pressed powder pellets of the <0.5μm fraction of the samples. Analyses were performed using a Rigaku 3070 x-ray spectrometer to measure Kα elemental intensities. Pellets were prepared using a Spex 3624B x-press, and finely ground, air-dried powders of the samples. The Kα intensities from the samples (averages of two analyses per sample), were converted to weight % using multiple regression equations obtained on a set of standard samples. Loss on ignition (LOI) for the samples were determined after ignition at 900°C for about 40 minutes. The precision of the reported values has been estimated to be ±2 relative percent.

Structural formulas were calculated by normalizing the cation analyses to a theoretical structure containing 11 oxygens (-22 anionic charge per one-half formula unit). All K was assumed to be fixed and non-exchangeable. Na and Ca were assumed to be exchangeable interlayer cations. All Fe was treated as Fe_2O_3. The chemical analysis (weight %) and structural formulas (half formula unit) are presented in Table 2. Note that structural formulas for some samples are corrected for minor kaolinite and quartz. Exclusion of Ti, Mn, P, and S, all not considered to be structurally held, accounts for totals less than 100%. Note also that TOTAL values in Table 2 are calculated on a hydrous basis.

Table 2: **Chemical analyses (wt.%) and structural formulas (half cell) for I/S clays.**

	Samples						
	SI-59	SI-64	SI-55	SI-44	SI-53	SI-9	MLH
SiO2	64.29	65.35	61.73	60.56	58.20	59.64	57.80
Al2O3	22.23	18.30	23.25	23.70	28.09	24.68	26.51
Fe2O3	2.19	2.17	2.09	1.74	1.41	1.46	1.59
MgO	4.22	3.76	3.94	4.42	3.50	4.48	3.76
K2O	2.82	5.13	4.53	5.49	6.07	6.33	7.60
CaO	2.10	2.90	2.02	1.71	0.86	1.68	1.22
Na2O	0.19	0.92	0.27	0.36	0.30	0.19	0.12
TOTAL	98.04	98.52	97.83	97.99	98.44	98.46	98.60
LOI	12.23	9.51	13.99	13.73	12.07	11.40	10.70
Si	3.91	3.87	3.81	3.76	3.56	3.70	3.72
Al	0.09	0.13	0.19	0.24	0.44	0.30	0.28
Tetrahedral charge	−0.09	−0.13	−0.19	−0.24	−0.44	−0.30	−0.28
Al	1.50	1.17	1.50	1.49	1.59	1.51	1.47
Fe+3(Total)	0.10	0.10	0.10	0.08	0.07	0.07	0.06
Mg	0.38	0.35	0.36	0.41	0.32	0.41	0.46
Sum	1.98	1.62	1.96	1.98	1.98	1.99	1.99
Octahedral charge	−0.44	−1.49	−0.48	−0.47	−0.38	−0.44	−0.49
Net layer charge	−0.53	−1.62	−0.67	−0.71	−0.82	−0.74	−0.77
K	0.22	0.40	0.36	0.43	0.48	0.50	0.60
Na	0.02	0.10	0.03	0.04	0.04	0.02	0.03
Ca	0.14	0.19	0.13	0.11	0.06	0.11	0.07
Interlayer charge	0.52	0.88	0.65	0.69	0.64	0.74	0.77
% Illite (XRD)	30	45	52	55	57	60	70
% Illite from Kfix/Kfix/max	29	53	47	57	63	66	79
Corrected for Kaolinite (%)		2			1		
Quartz (%)		2					

(continued next page)

Table 2 (continued from previous page)

	SI-47	WDH-62	WDH-64	WDH-60	WDH-68	WDH-25	NI-6
SiO2	59.77	55.07	53.30	54.52	58.49	56.26	59.14
Al2O3	23.85	29.78	33.16	30.70	26.47	29.43	23.55
Fe2O3	1.23	1.63	1.17	1.48	2.06	1.85	2.06
MgO	4.97	2.83	2.18	2.79	2.08	2.79	4.21
K2O	7.60	8.63	8.70	8.84	8.75	8.07	7.51
CaO	1.11	0.58	0.20	0.40	0.11	0.21	2.32
Na2O	0.28	0.29	0.12	0.20	0.93	0.22	0.14
TOTAL	98.83	98.82	98.83	98.94	98.89	98.84	98.93
LOI	10.00	9.49	9.02	8.95	9.49	9.03	7.11
Si	3.61	3.46	3.34	3.42	3.66	3.51	3.63
Al	0.39	0.54	0.66	0.58	0.34	0.49	0.37
Tetrahedral charge	-0.39	-0.54	-0.66	-0.58	-0.34	-0.49	-0.37
Al	1.56	1.66	1.79	1.69	1.61	1.67	1.37
Fe+3(Total)	0.07	0.08	0.06	0.07	0.10	0.09	0.10
Mg	0.35	0.27	0.20	0.26	0.19	0.32	0.39
Sum	1.98	2.01	2.05	2.02	1.90	2.08	1.86
Octahedral charge	-0.41	-0.24	-0.05	-0.20	-0.49	-0.08	-0.81
Net layer charge	-0.80	-0.78	-0.71	-0.78	-0.83	-0.57	-1.81
K	0.61	0.69	0.69	0.71	0.70	0.64	0.60
Na	0.01	0.04	0.02	0.02	0.11	0.03	0.02
Ca	0.08	0.04	0.01	0.03	0.01	0.01	0.16
Interlayer charge	0.78	0.81	0.73	0.79	0.83	0.69	0.94
% Illite (XRD)	83	89	89	90	90	95	97
% Illite from Kfix/Kfix/max	80	91	91	93	92	84	79
Corrected for Kaolinite (%)							
Quartz (%)							2

RESULTS

X-ray diffraction

XRD results show that the clay mineral composition of the <0.2μm fraction of the samples is dominated by interstratified I/S. Minor amounts of discrete illite, kaolinite, quartz, and chlorite occur in several samples. Samples show both random (R0) and ordered interstratification of various types ranging from R0 to R3 and various mixtures of these, and generally exhibit higher illite content at higher degrees of ordering.

Modeling: Samples SI-59 (Fig. 2) and SI-64 (Fig. 3) show random interstratification, and are best modeled by assuming a diffracting crystallite domain thickness (N) between 3 and 7 silicate layers, and compositions of 30% and 45% illite for each, respectively. Comparison of experimental XRD patterns for these samples (Fig. 2a and Fig. 3a) with computer models (Fig. 2b, c and Fig. 3b, c) shows that models with a thin diffracting crystallite domain range (i.e. N=3-7) simulate both the peak positions and intensities in the experimental patterns better than those using crystallite domains of a broader thickness range (N=3-14). Note that best fit models for these samples (Fig. 2b and Fig. 3b) also have peaks for discrete illite

and kaolinite which were added to their respective I/S models.

The XRD pattern for SI-55 (Fig. 4a) is also typical of random interstratification as it displays a strong reflection near 17Å. However, the presence of a superstructure (superlattice) reflection near 30Å (Fig. 4a) indicates ordered domains in the sample. Note that the superstructure reflection is not readily apparent in the coarser clay fraction of the sample (Fig. 4b). Indeed, the best fit computer model for this sample is obtained when an R0 I/S (N=3-5) containing 50% illite is mixed with an R1 ordered I/S (N=3-14) containing 60% illite in the proportion 90% and 10% respectively (Fig. 4c). The illite content for sample SI-55 calculated from this mixture by simple proportioning is 52%. The simulated pattern in Figure 4c also has 7% discrete illite and 7% kaolinite added by the mixing function, and clearly shows that the broad shoulder at 8-10° 2θ in the finer clay fraction of the sample (Fig. 4a) is caused by discrete illite.

Samples SI-44, SI-53, and SI-9, like SI-55, are best modeled by mixing random (R0) I/S with R0.5 and R1 ordered I/S in various proportions. A mixture of an R0 I/S (N=3-5) containing 50% illite and an R1 ordered I/S (N=3-14) containing 65% illite produces the best fit model for SI-44 (Fig. 5) when mixed in the proportion 72% and 28%,

respectively. An R0.5 I/S (N=3-14) with 55% illite and R0 ordered I/S (N=3-7) with 60% illite produce the best model for sample SI-53 when mixed in the proportion 65% and 35%, respectively (Fig. 6). In order to obtain the best fit for SI-9 (Fig. 7), an R1 ordered I/S (N=3-14) with 60% illite layers is added to a mixture of R0.5 ordered I/S (N=3-14) with 60% illite and R0 I/S (N=3-7) with 60% illite, using the respective proportions of 10%, 48%, and 42%. Illite content of these mixtures is calculated as 55%, 57%, and 60% for SI-44, SI-53, and SI-9, respectively.

Samples MLH and SI-47 are representatives of I/S with short-range and intermediate-range order. The XRD pattern for MLH (Fig. 8) is best modeled assuming a composition of 70% illite and complete R1 order. Sample SI-47 (Fig. 9) is, in terms of its peak positions - particularly 002/003 I/S peak near 17° 2θ - best modeled assuming a composition of 83% illite, R=1.5 order, and a crystallite domain thickness N=5-9 (Fig. 9b). On the other hand, two mixtures also produce reasonably good models for this sample: (1) an R1 ordered I/S (N=3-14) containing 75% illite and an R2 ordered I/S (N=3-14) containing 85% illite mixed in the proportion 75% and 25% respectively (Fig. 9c); and (2) an R1 ordered I/S (N=3-14) containing 75% illite and an R3 ordered I/S (N=3-14) containing 90% illite mixed in the proportion 90% and 10%, respectively (Fig. 9d).

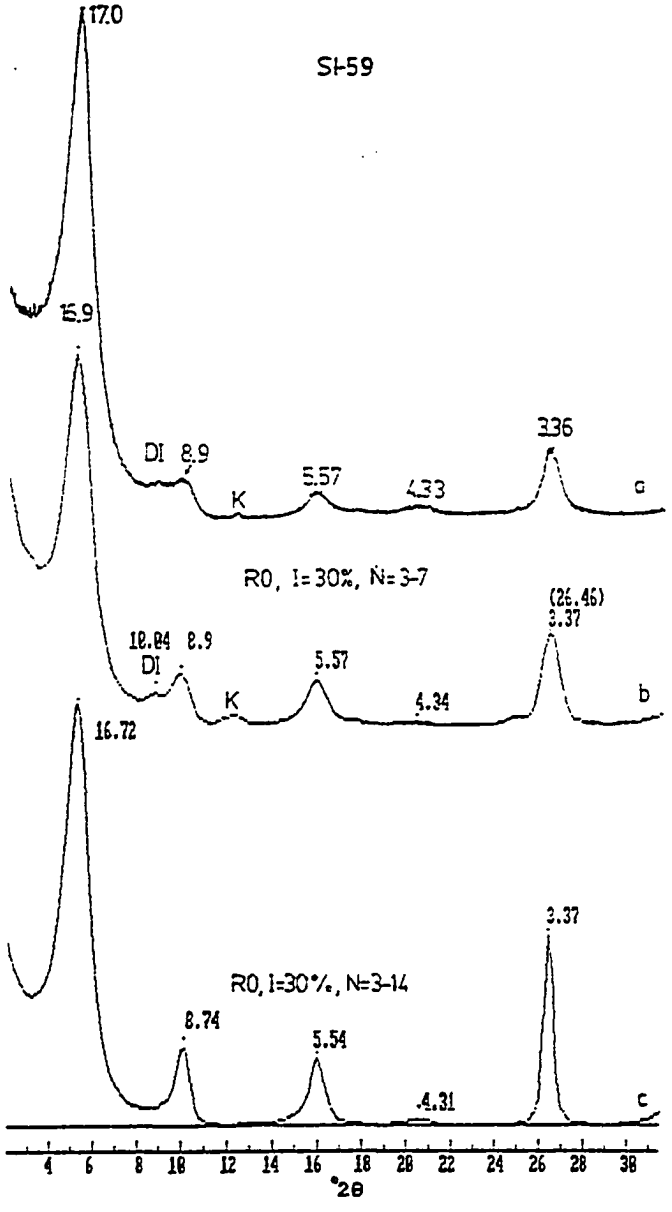

Figure 2: Observed XRD pattern for ethylene glycol-solvated sample SI-59 (a), and calculated XRD patterns for random (R0) I/S with 30% illite (b and c). Values of N represent thickness of diffracting domains. Values by the peaks represent basal spacings in Angstrom. Here and in subsequent figures: DI=discrete illite, K=kaolinite.

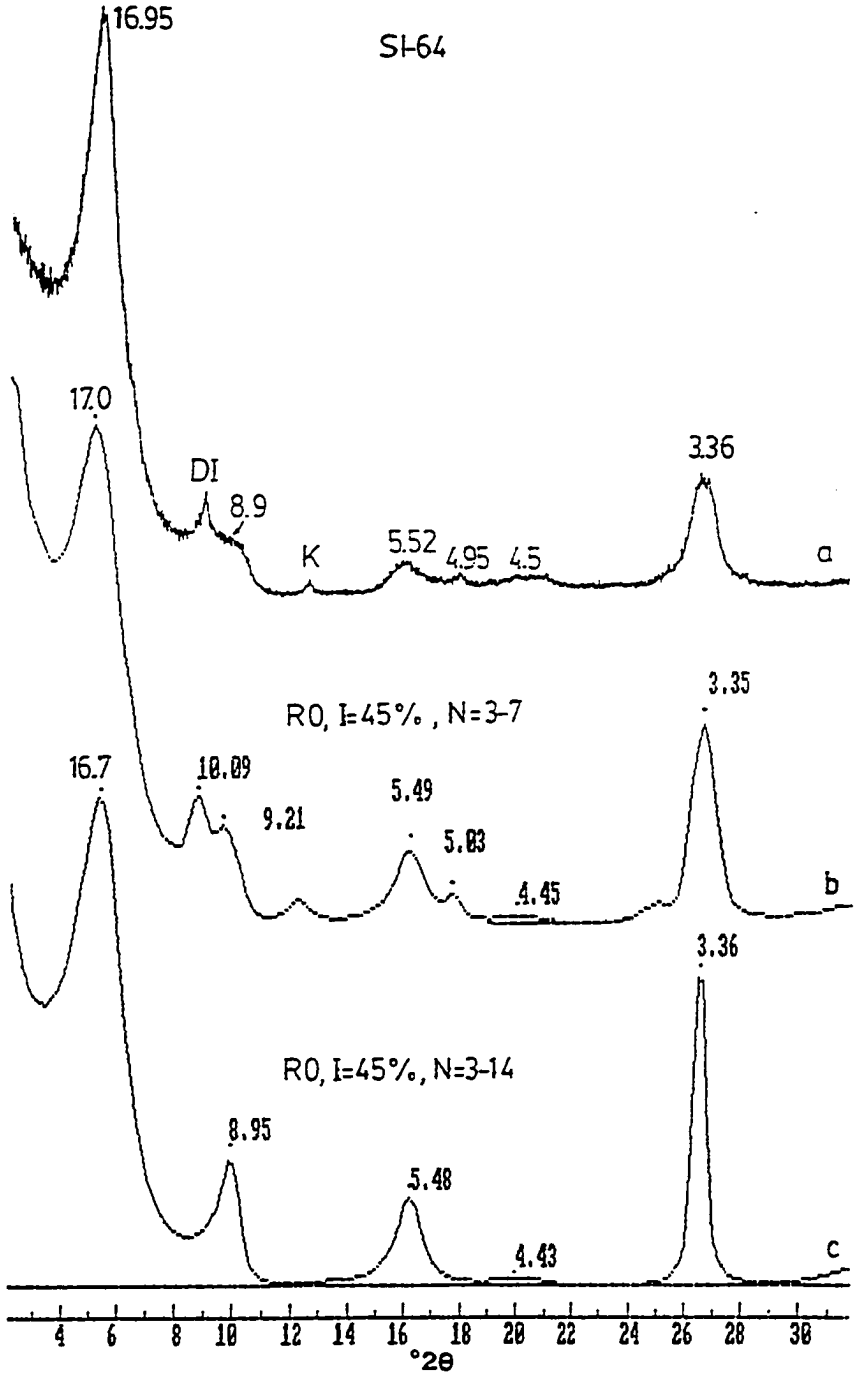

Figure 3: Observed XRD pattern for ethylene glycol-solvated sample SI-64 (a) and calculated XRD patterns for random (RO) I/S with 45% illite (b and c).

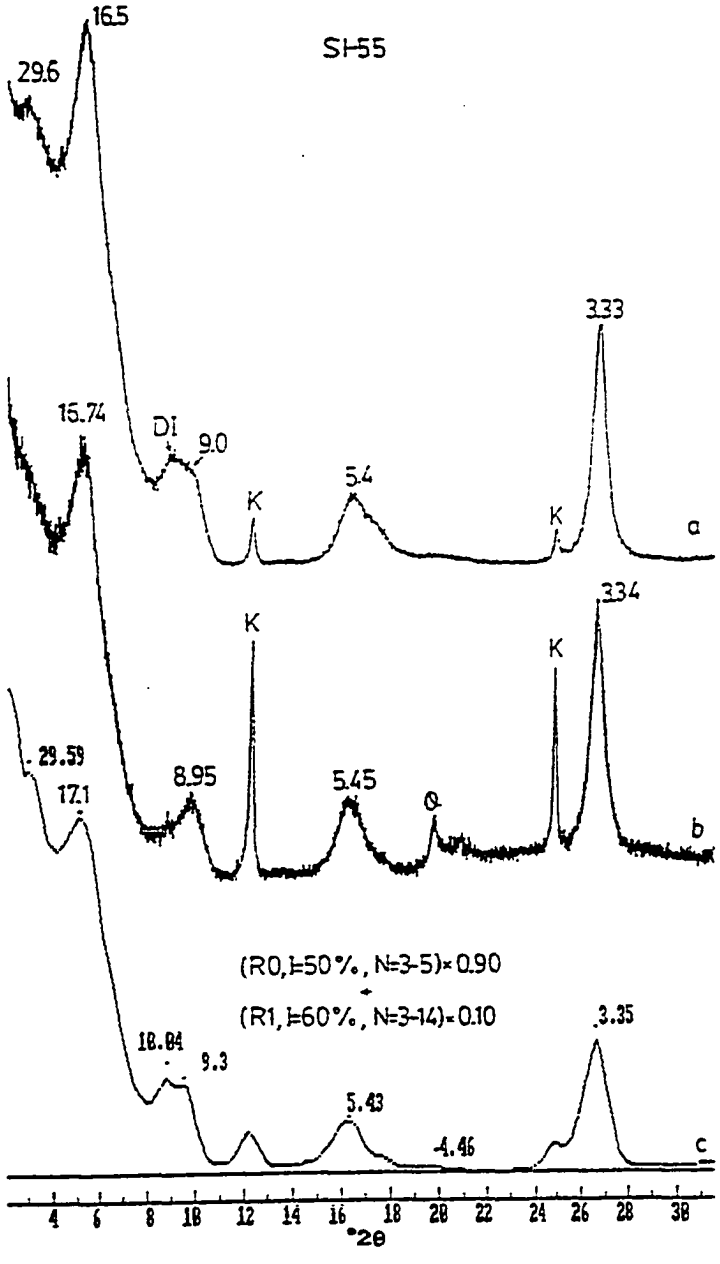

Figure 4: XRD patterns for ethylene glycol-solvated sample SI-55: (a) <0.2 μm fraction, (b) coarse clay fraction, and (c) calculated pattern for an I/S mixture with 52% illite (see text). Q=quartz.

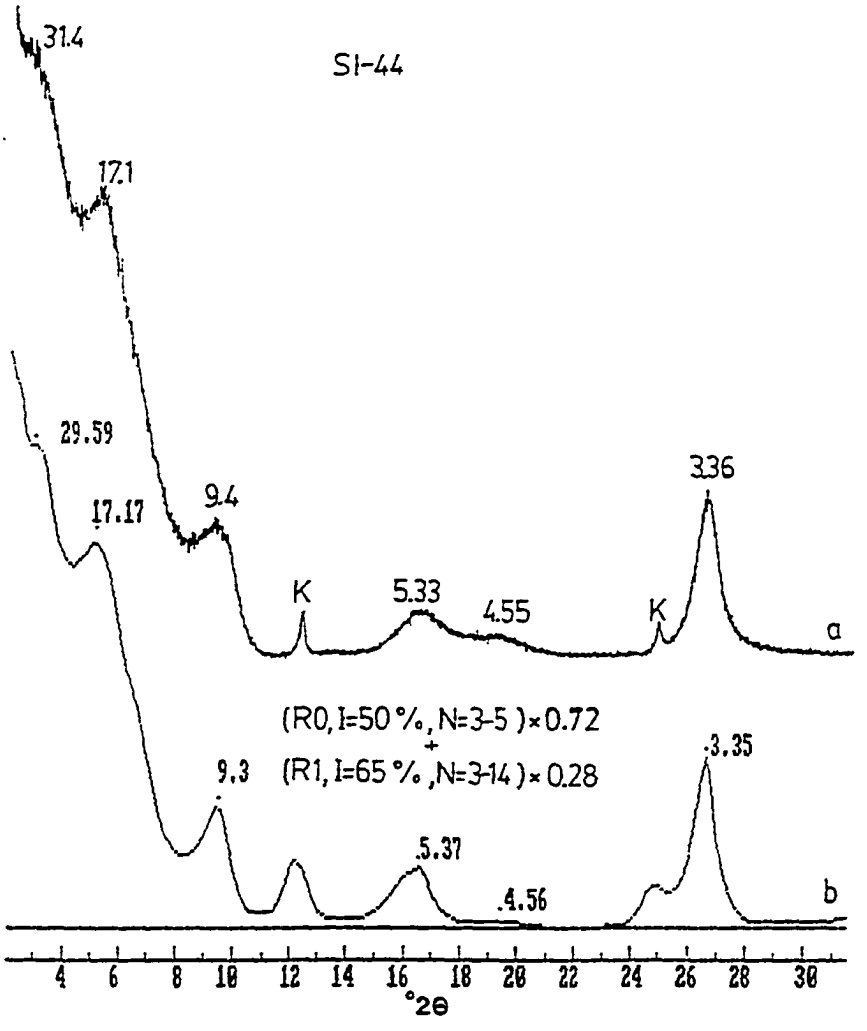

Figure 5: Observed XRD pattern for ethylene glycol-solvated sample SI-44 (a) and calculated pattern for an I/S mixture with 55% illite (b).

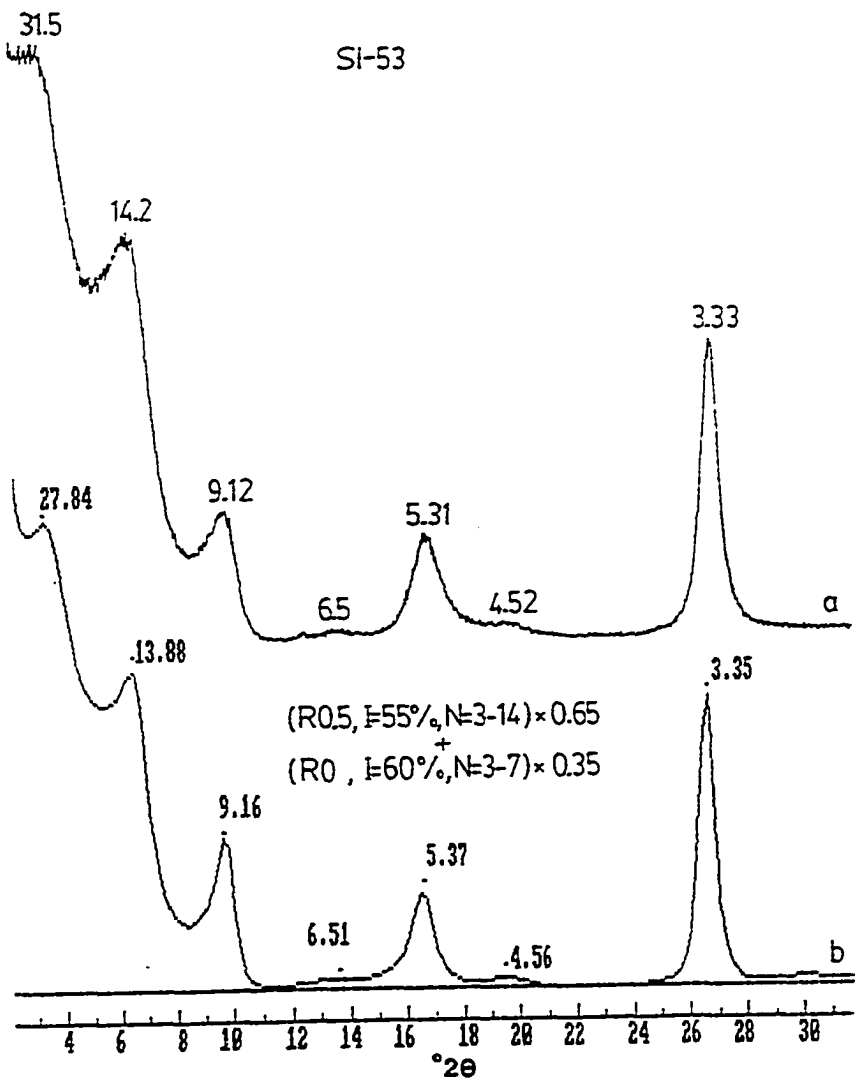

Figure 6: Observed XRD pattern for ethylene glycol-solvated sample SI-53 (a), and calculated XRD pattern for n I/S mixture with 57% illite (b).

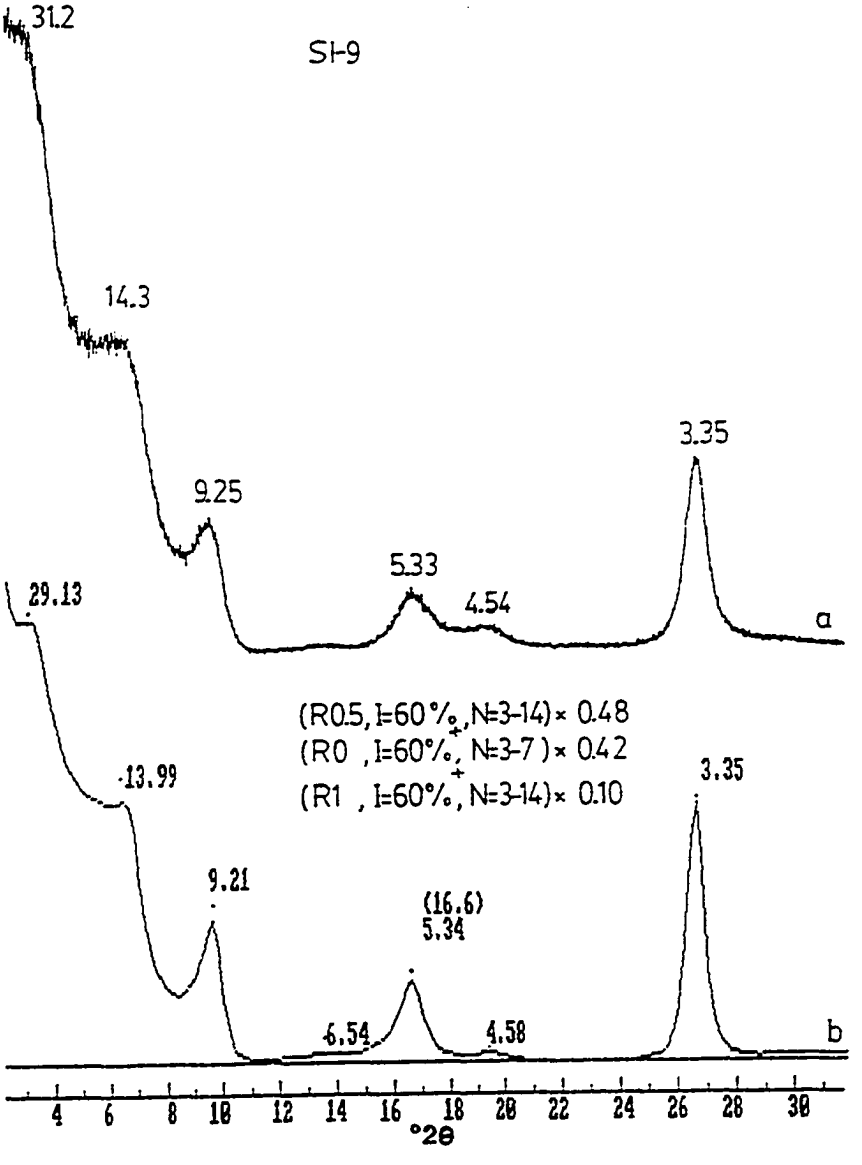

Figure 7: Observed XRD pattern for ethylene glycol-solvated sample SI-9 (a) and calculated XRD pattern for an I/S mixture with 60% illite (b).

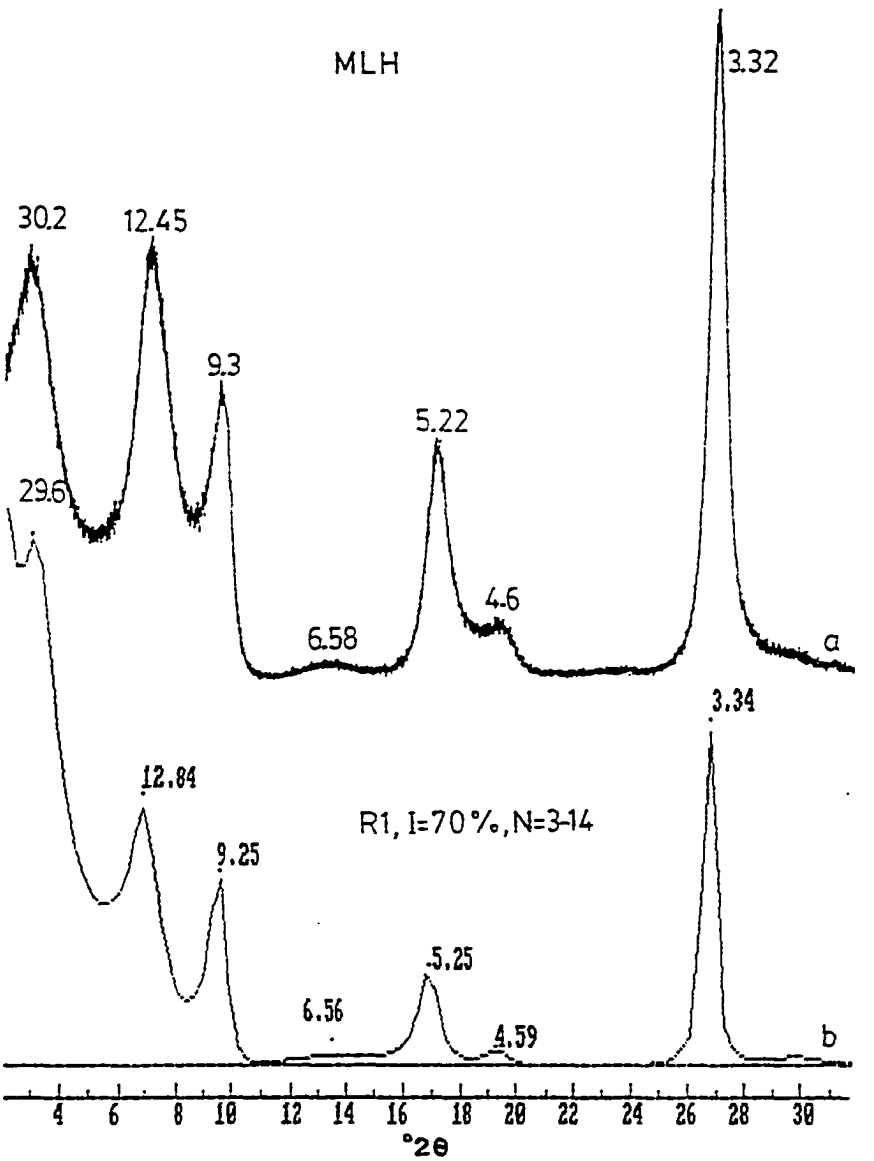

Figure 8: Observed XRD pattern for ethylene glycol-solvated sample MLH (a) and calculated XRD pattern for an R1 ordered I/S with 70% illite.

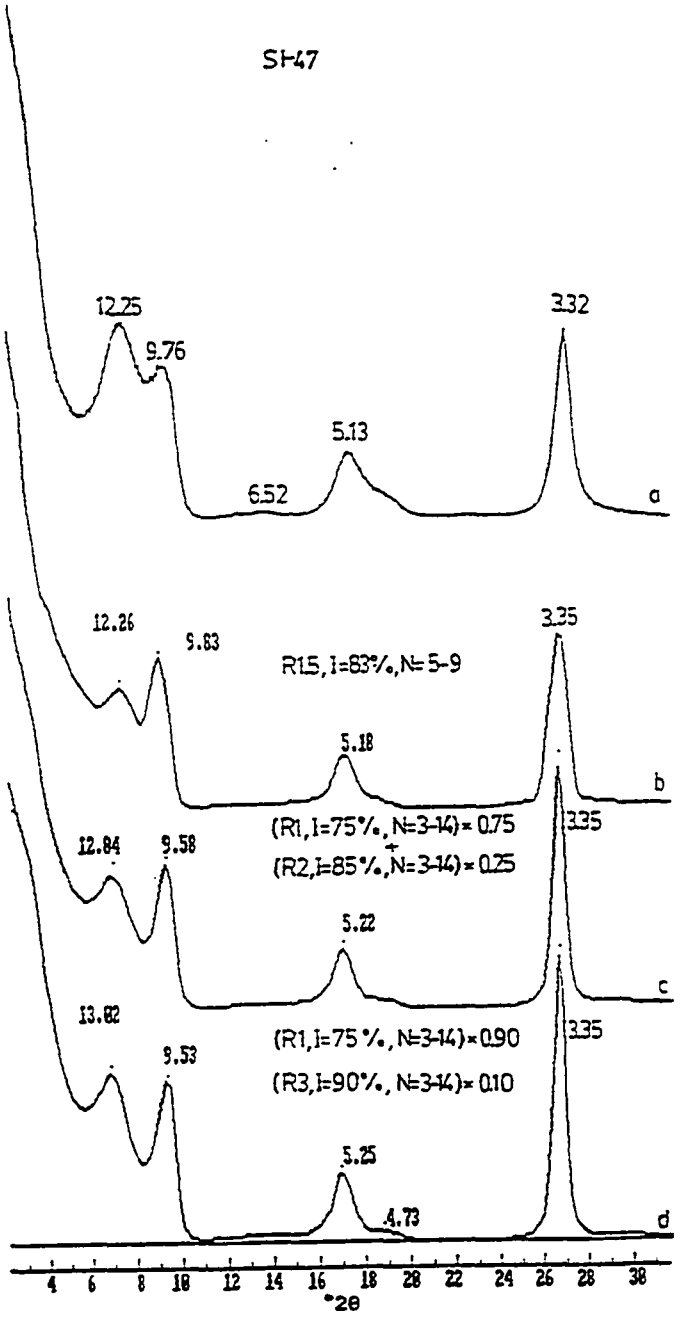

Figure 9: Observed XRD pattern for ethylene glycol-solvated sample SI-47 (a), and best-fit calculated pattern (b). Also shown are two I/S mixtures (c), and (d) with 78% and 77% illite, respectively, that also model the observed pattern reasonably well.

Samples WDH-25, WDH-60, WDH-62, WDH-64, and NI6 are all representatives of long-range order. WDH-62 (Fig. 10a) is best modeled assuming a composition of 89% illite and R=2.5 or incomplete R3 order (Fig. 10b). WDH-64 (Fig. 10c) has the same composition and slightly better ordering than WDH-62 (Fig. 10d). Samples WDH-60 and WDH-68 (Fig. 11a and 11b) are both best modeled as R3 ordered I/S containing 90% illite (Fig. 11c). Samples WDH-25 and NI6 (Fig. 12a and 12c) are the most illitic clays studied and they are best modeled assuming illite compositions of 95% and 97%, respectively, and R3 order for both (Fig. 12b and 12d). A diffracting crystallite domain thickness of N=3-14 is assumed in the modeling of these six samples. The <0.2μm clay fraction of these highly illitic samples have only I/S except for NI6, which has a minor amount of chlorite (Fig. 12c).

Illite Polytypes: Stacking of the 2:1 layers parallel to the crystallographic c-axis results in the growth of mica crystals. Theoretically, there are six simple ways, with periodicities between one and six, in which 2:1 layers may be stacked, giving rise to the 1M, $2M_1$, $2M_2$, 3T, and 6H polytypes (**Yoder and Eugster, 1955**). In nature, however, only the 1M, $2M_1$, and 3T as well as a disordered 1Md variety of 1M, are commonly identified among dioctahedral micas such as muscovite (**Bailey, 1980**). The $2M_2$ polytype is

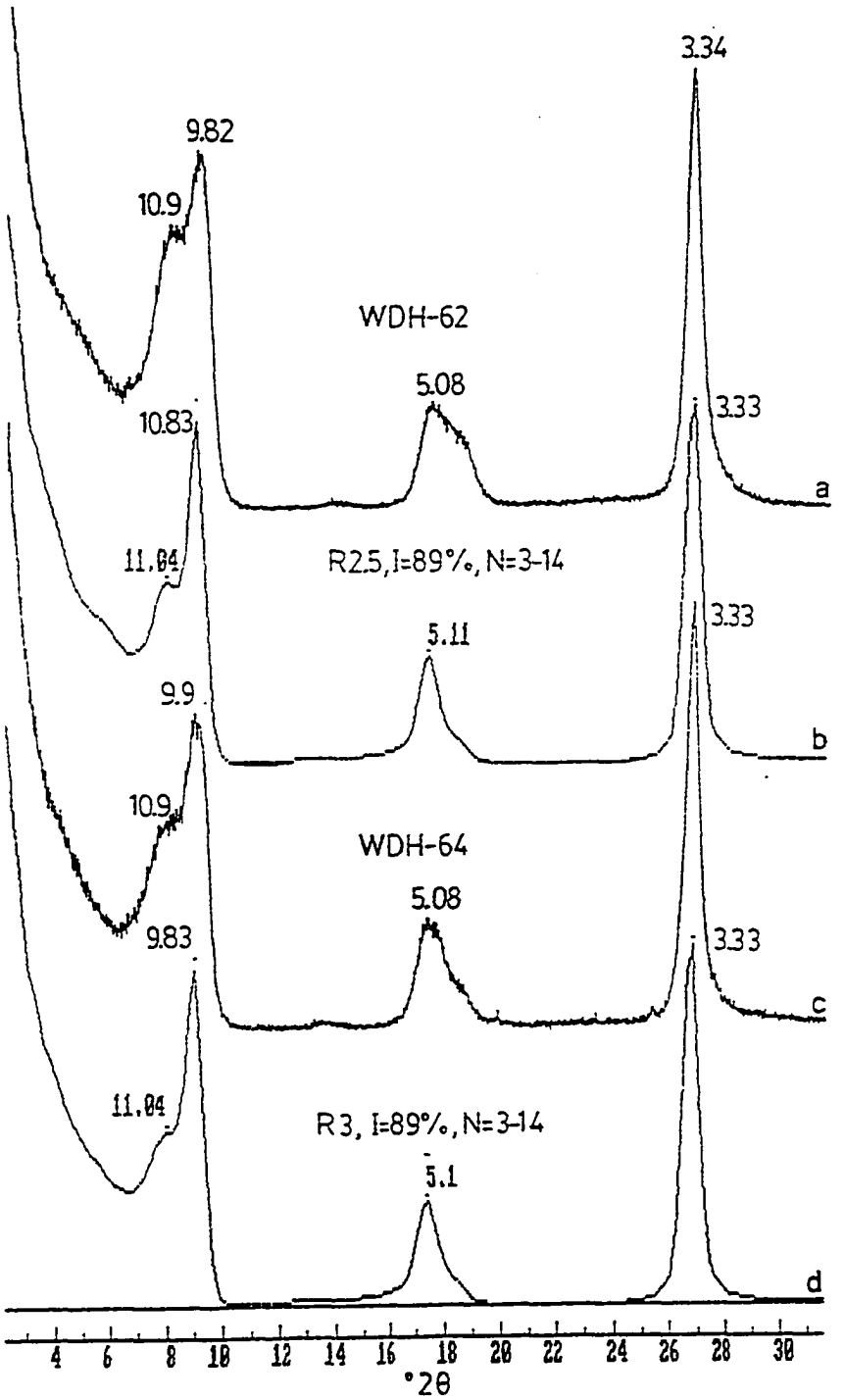

Figure 10: Observed XRD patterns for ethylene glycol-solvated samples WDH-62 (a) and WDH-64 (c), and their respective calculated models (b and d).

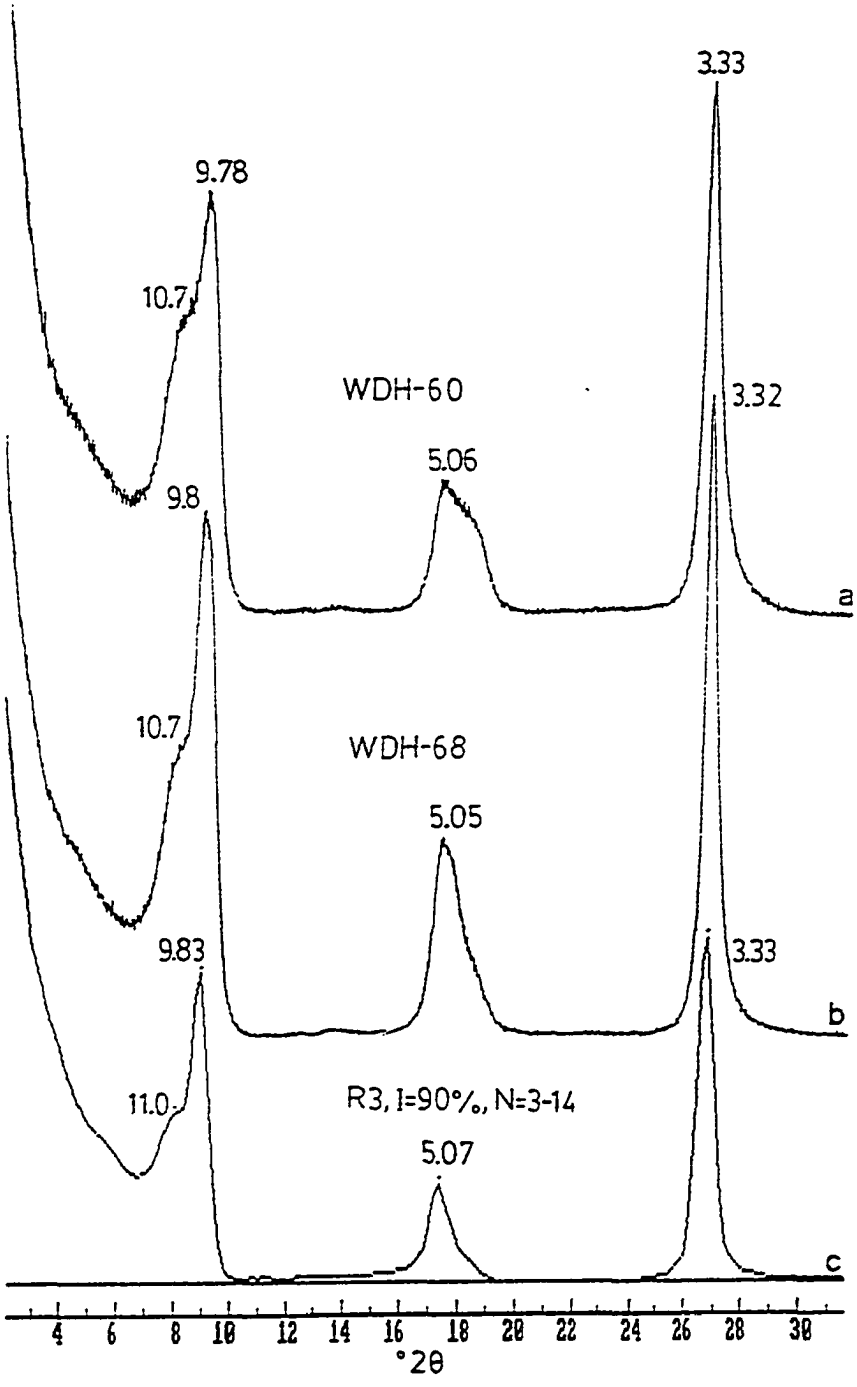

Figure 11: Observed XRD patterns for ethylene glycol-solvated samples WDH-60 (a) and WDH-68 (b), and calculated XRD pattern for an R3 ordered I/S with 90% illite (c).

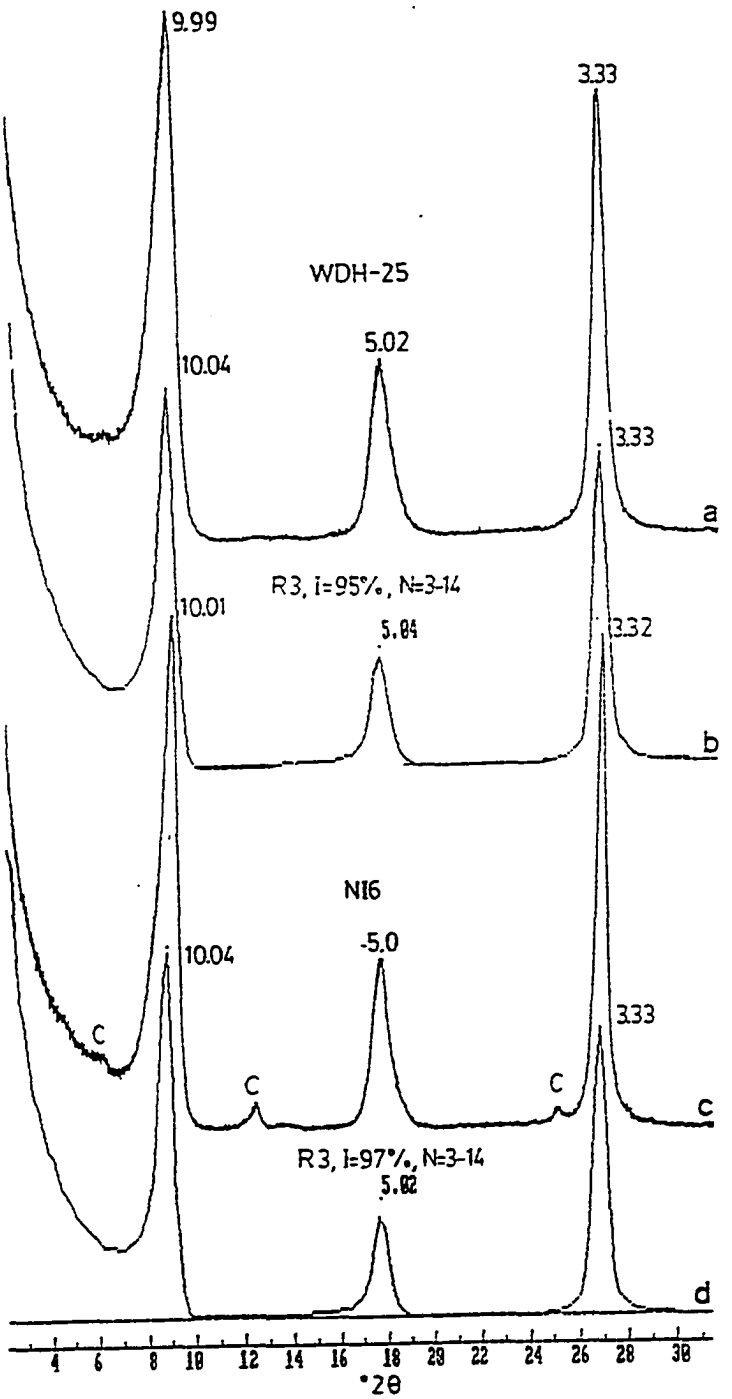

Figure 12: Observed XRD patterns for ethylene glycol-solvated samples WDH-25 (a) and NI6 (c), and their respective calculated patterns (b and d).

very rarely reported (i.e. **Shimoda, 1970**). All of the polytypes known from muscovites also exist in illitic materials (**Levinson, 1955; Yoder and Eugster, 1955 Srodon and Eberl, 1984**). The 1M, $2M_1$, $2M_2$, and 3T polytypes are identified by their diagnostic reflections on XRD patterns of randomly-oriented sample powders. There exists, however, some confusion concerning the definition and identification of 1Md illite polytype (**Austin et al., 1989**). On XRD patterns, the 1Md polytype is usually recognized on the basis of the lack of diagnostic 1M polytype reflections and the presence of an elevated background between 20° and 34° 2θ. Identifying 1Md in this way is now suggested to be appropriate provided that 1M is the only ordered polytype in an I/S mixture (**Austin et al., 1989**). This suggestion is adopted in the present study.

The XRD patterns of the randomly oriented powder mounts of the samples reveal a systematic change in polytype with the increase in the illite content (Fig. 13). Samples SI-59, SI-64, SI-55, SI-44, and SI-53, all of which have <60% illite, show none of the diagnostic reflections for 1M or $2M_1$ polytypes (Table 1). Furthermore, they all show an elevated background between 20° and 34° 2θ indicating disorder (**Austin et al., 1989**). Therefore, the dominant type of mica polytype in these samples is considered to be 1Md.

XRD patterns for samples SI-9 and MLH, which have 60% and 70% illite, respectively, show one of the diagnostic 1M reflections at 3.66Å whereas the pattern for SI-47 shows both diagnostic 1M reflections, namely $11\bar{2}$ at 3.66Å and 112 at 3.07Å. Inasmuch as their reflections are poorly defined, and weak in intensity, these samples are mixtures of 1Md and 1M polytypes.

Six samples with about 90% or more illite, WDH-62, WDH-64, WDH-60, WDH-68, WDH-25, and NI6 (Fig. 13), show most of the diagnostic reflections for both 1M and 2M1 polytypes (Table 1). Some reflections become more intense as illite content in the samples increases, though most remain as broad bands. These samples with broad reflections at or close to the positions of the diagnostic 1M and $2M_1$ polytype reflections are considered to be mixtures of these two polytypes with some disorder. Sample NI6, however, is clearly a mixture of 1M and $2M_1$ polytypes as its XRD pattern shows each diagnostic 1M and $2M_1$ reflections as sharp and distinct peaks.

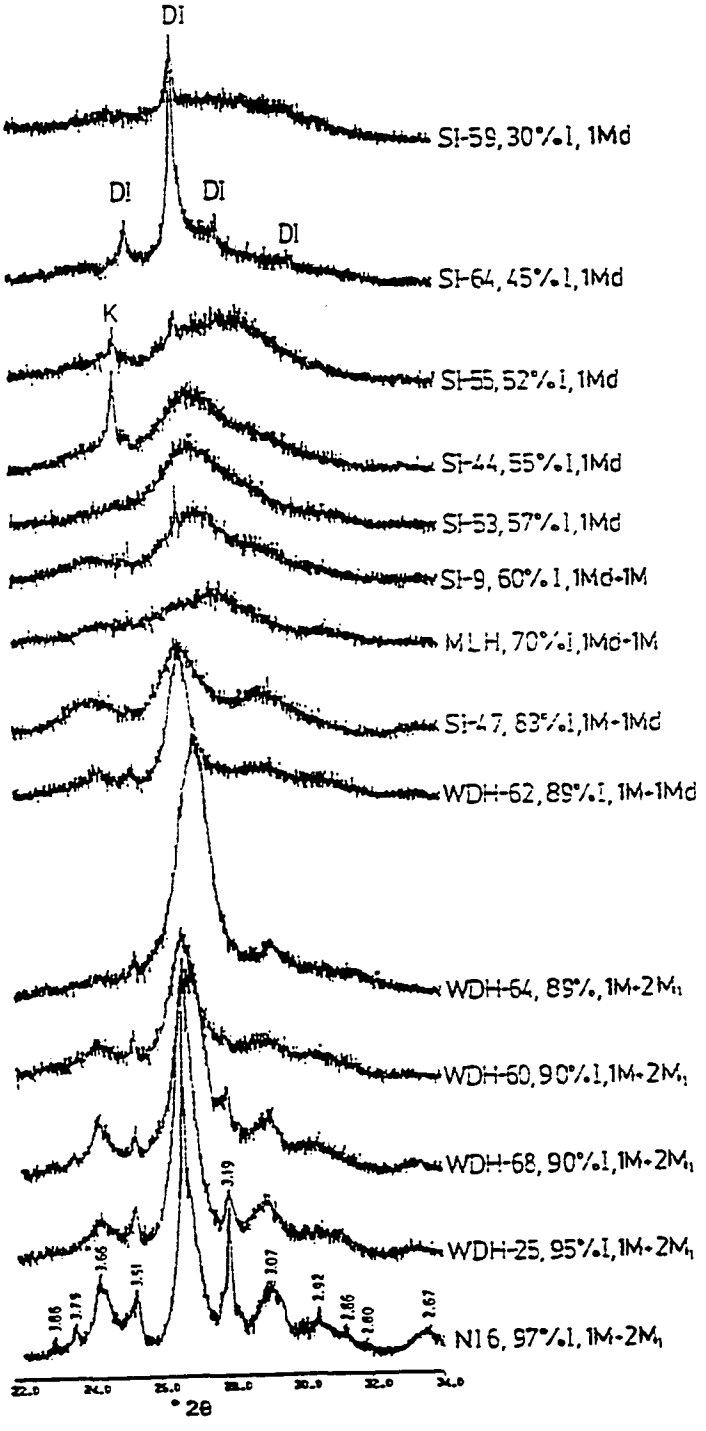

Figure 13: XRD patterns of random powder mounts of I/S, showing evolution of 1M and $2M_1$ illite polytypes with increasing proportion of illite. Positions of the diagnostic reflections are labeled on the bottom pattern. K= kaolinite.

Chemical Analysis

The chemical analyses of I/S cast into structural formulas (Table 2) provide an important tool for evaluating the smectite-to-illite transition during bentonite diagenesis in that they can be used to infer the amount and type of ionic substitutions, and associated layer charge modifications and interlayer exchange reactions. The chemical data are commonly represented on X-Y plots using the proportion of illite from XRD data as independent variable (X). These, in turn, can be used to infer the causes for observed physical changes and the processes involved in the transition.

Most samples yield balanced structural formula, indicating the validity of procedures used in the course of chemical analysis. Three samples (SI-64, WDH-25, and NI6), however, give greatly unbalanced structural formula and values for octahedral occupancy that are significantly different from the ideal value of 2.00 (Table 2). This is attributed to the very high amounts of S and P measured by XRF in these samples, P being due to contamination from the dispersion agent. High values of P and S result in poor estimation of elemental proportions because of the interdependency of elemental intensities in the multiple regression program used. Therefore, these three samples are excluded from the plots presented here. However, the

chemical trends described below would still be applicable even if they had not been excluded.

Ionic substitutions: The tetrahedral and octahedral ionic substitutions over the course of the smectite-to-ilite transition can be evaluated from the plots of total Si, and octahedral Al, Mg, and Fe vs. illite percent (from XRD), which are presented in Figures 14 and 15.

Si has an inverse linear relationship with illite percent in the samples with a correlation coefficient of r^2= 0.77 (Fig. 14a). A very similar trend is observed when Si is plotted versus fixed-K with a correlation coefficient of r^2= 0.79 (Fig. 14b). Fixed-K is determined by XRF and thus is independent of the XRD-derived illite percent in the samples. Therefore, the linear relationship between fixed-K and Si provides an independent test that the linear decrease in Si is real. For 0% illite, the regression lines in Figure 14a and 14b extrapolate to 4.14 and 4.16 Si cations per half formula unit, respectively, which is very close to the ideal value of 4.00.

The variation in the quantity of octahedral Al vs. illite percent is better approximated by a model with two regression lines, rather that one, intersecting at about 70% illite layers (Fig. 15a). From Figure 15a the following features are observed:

1) octahedral Al has a value of about 1.5 cations per

formula unit, and does not vary significantly in the 30-70% illite range.

2) ordered I/S samples, particularly those with about 90% or more illite layers, have higher octahedral Al, averaging about 1.65 cations per half formula unit. The amounts of Mg and Fe are slightly lower with highly illitic samples although their variations with illite percent are statistically not significant as indicated by the correlation coefficients of r^2= 0.35 and r^2= 0.22, respectively (Fig. 15b and 15c).

Layer charge: Progressively lower amounts of Si in the samples reflect greater extent of Al^{+3} for Si^{+4} substitution and a corresponding increase in the negative tetrahedral charge with increasing illite percent. The octahedral charge of the samples are uniformly negative and varies between 0.38 and 0.49 (average for 7 samples is 0.45) in the <80% illite range. In the highly illitic samples, because of increased Al, despite slightly less Mg and Fe, the octahedral charge decreases to less than 0.25 (Table 2). Octahedral charge for these samples remains less than 0.32 and averages 0.22 even if recalculated assuming that all Fe is reduced. Total layer charge density increases with percentage of illite layers (Fig. 16a) showing some scatter of data points along a straight

regression line (r^2= 0.48). For 0% illite, this line extrapolates to 0.53, and for 100% illite to 0.83.

An evaluation of the nature of the charge or the source of the charge throughout the range of illite percent in the samples is possible from Figure 16b, where percentage of tetrahedral charge in total charge (Tetrahedral/Net Charge X 100, or Tc%, in Fig. 16b) is plotted versus proportion of illite. One clear feature observed in Figure 16b is that octahedrally charged silicate layers in these samples become increasingly tetrahedrally charged as the proportion of illite layers increases. Although several data points do not closely fit the straight regression line, the correlation coefficient of r^2= 0.78 indicates an approximate linear relationship. Additional support for this trend is provided by a very similar trend observed when percentage of tetrahedral charge in total charge is plotted versus fixed-K (Fig. 16c). Furthermore, the data are in good agreement with published analyses of I/S (Fig. 16d) from Silurian K-bentonites from Sweden (**Brusewitz, 1986**), Carboniferous K-bentonites from Poland (**Srodon et al., 1986**), and Cretaceous bentonites from Montana (**Nadeau and Bain, 1986**).

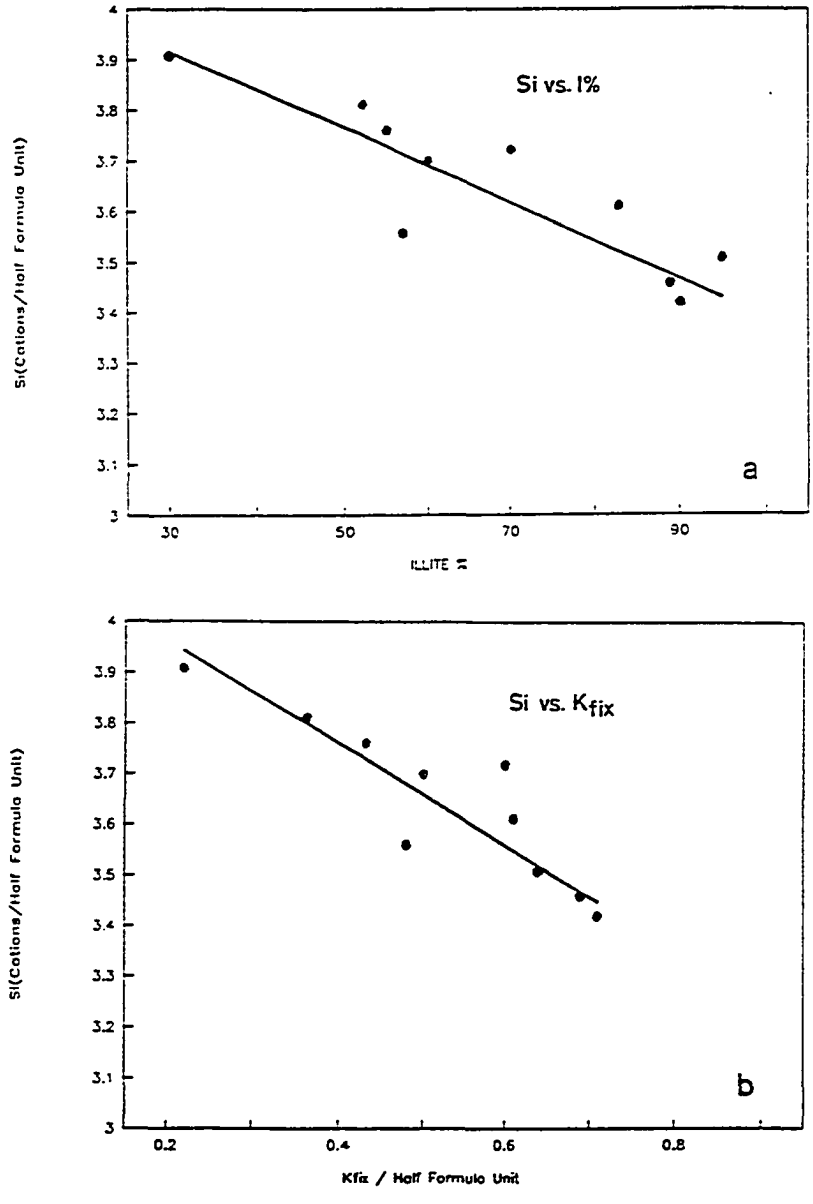

Figure 14: Variation of amount of Si with illite % (a) and fixed-K (b) in I/S samples.

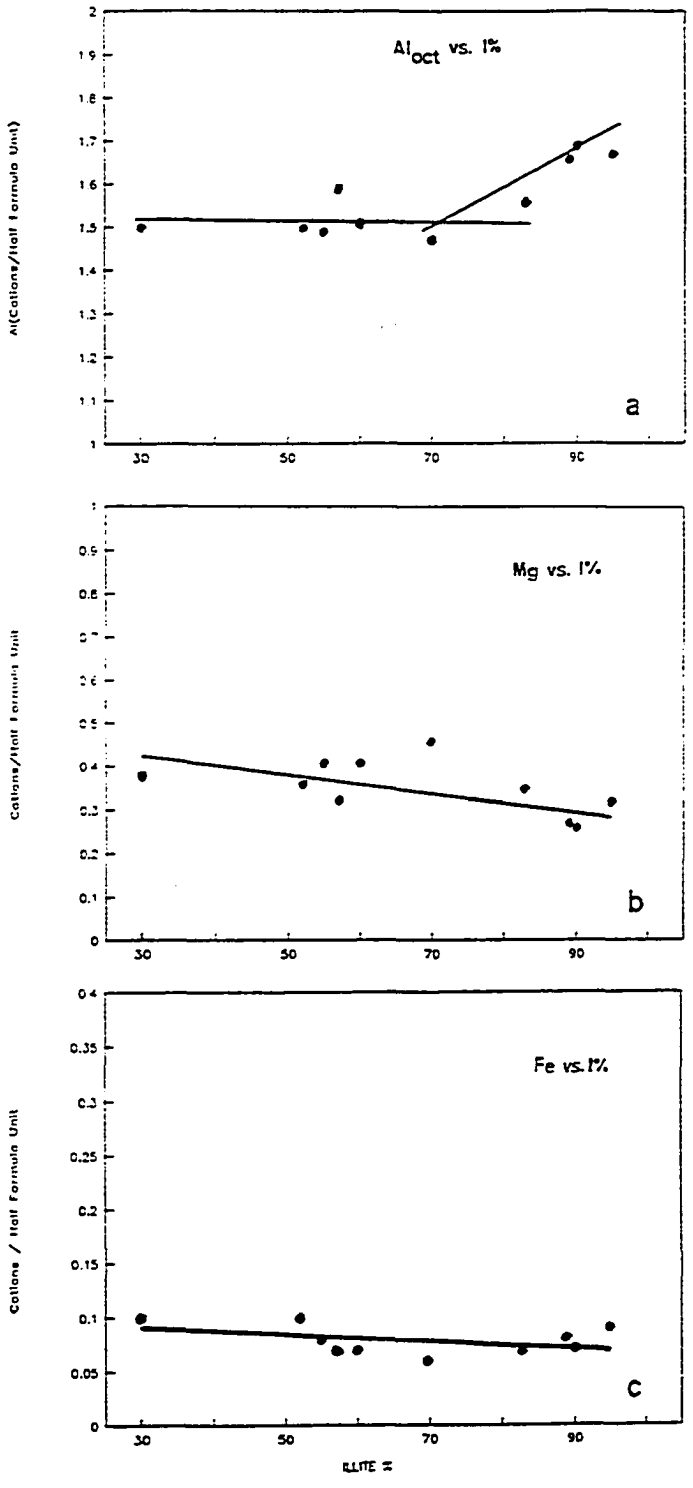

Figure 15: Variations of octahedral Al (a), Mg (b), and Fe (c) with illite %.

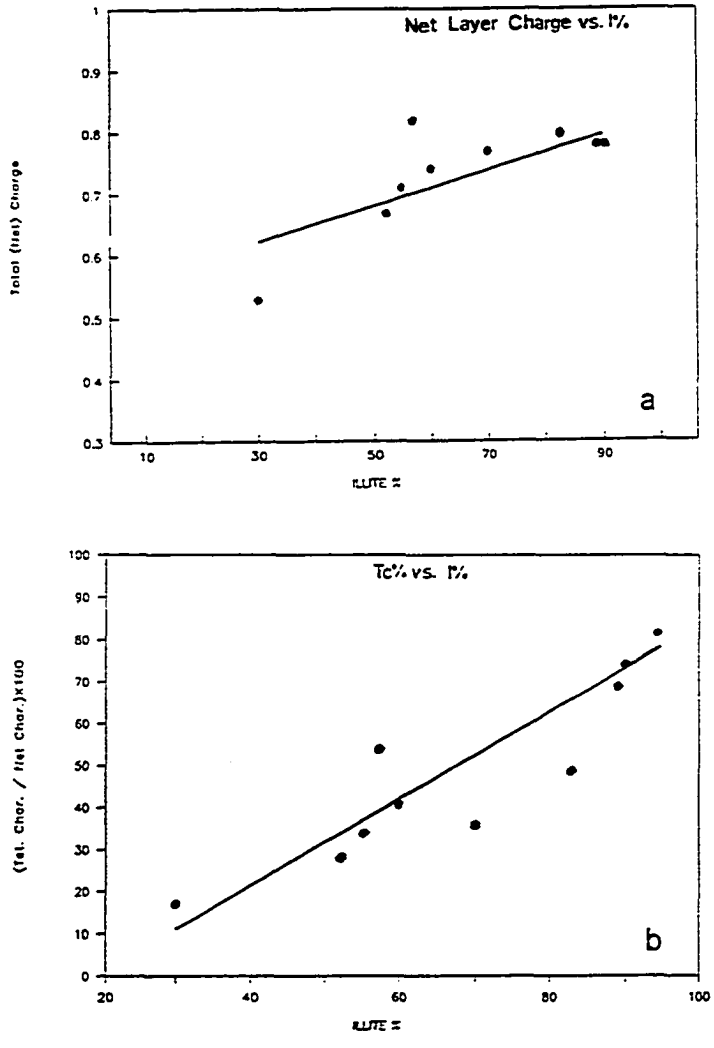

Figure 16: Variation of net layer charge with illite % (a) and variations of Tc% (percentage of tetrahedral charge in net charge) with illite % (b) and with fixed-K (c). Variation of Tc% in other Paleozoic K-bentonites calculated from published data (**Brusewitz, 1986; Nadeau and Bain; Srodon et al., 1986** + this study) is also shown (d).

(Figure 16 continued next page)

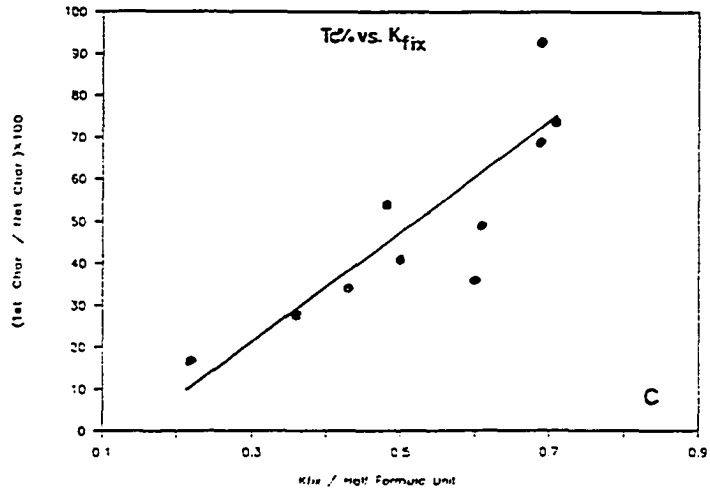

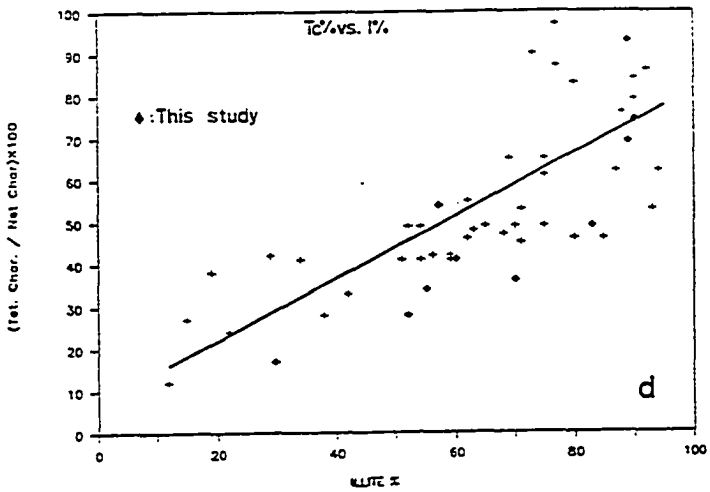

Non-exchangeable and exchangeable cation content: An understanding of the smectite-to-illite diagenetic transition requires an evaluation of the interlayer content of both components in intermediate I/S minerals. Because, by definition, illite interlayers are non-expanding and are associated with non-exchangeable cations, such an evaluation becomes possible by studying plots of the variation of fixed-K (K_{fix}), the sum of exchangeable cations($E^+ = Na^+ + Ca^{++}$), and the interlayer charge ($=K_{fix} + Na^+ + Ca^{++}$) with respect to illite percent. Such plots are presented in Figure 17. From these plots the following features are observed:

1) Data points in K_{fix} vs. illite percent plot (Fig. 17a) can be fitted by a single regression line having a correlation coefficient of $r^2 = 0.93$. This line extrapolates to about 0.03 fixed-K for 0% illite and to about 0.76 fixed-K for 100% illite.

2) Data points for the sum of exchangeable cations vs. illite percent can also be fitted by a regression line with a correlation coefficient of $r^2 = 0.82$ (Fig. 17b). This line extrapolates to 0.45 for 0% illite and to 0.05 sum of exchangeable cations per half formula unit. The regression line in a plot of the sum of exchangeable cations vs. fixed-K (Fig. 17c) extrapolates to 0.46 equivalents of exchangeable cations for $K_{fix}=0.00$, and to about 0.86

fixed-K per half formula unit for E^{+}= 0.00.

3) Interlayer charge increases as illite percent increases, and shows a trend that can be fitted by a regression line having a relatively poor correlation coefficient of r^2= 0.62 (Fig. 17c). However, because total (net) charge and interlayer charge closely balance for most samples (Table 2; also compare Fig. 16a and 17c) both trends are believed to be real. For 0% illite, the regression line in Fig. 17c extrapolates to 0.49, and for pure illite to 0.81 equivalents per half formula unit.

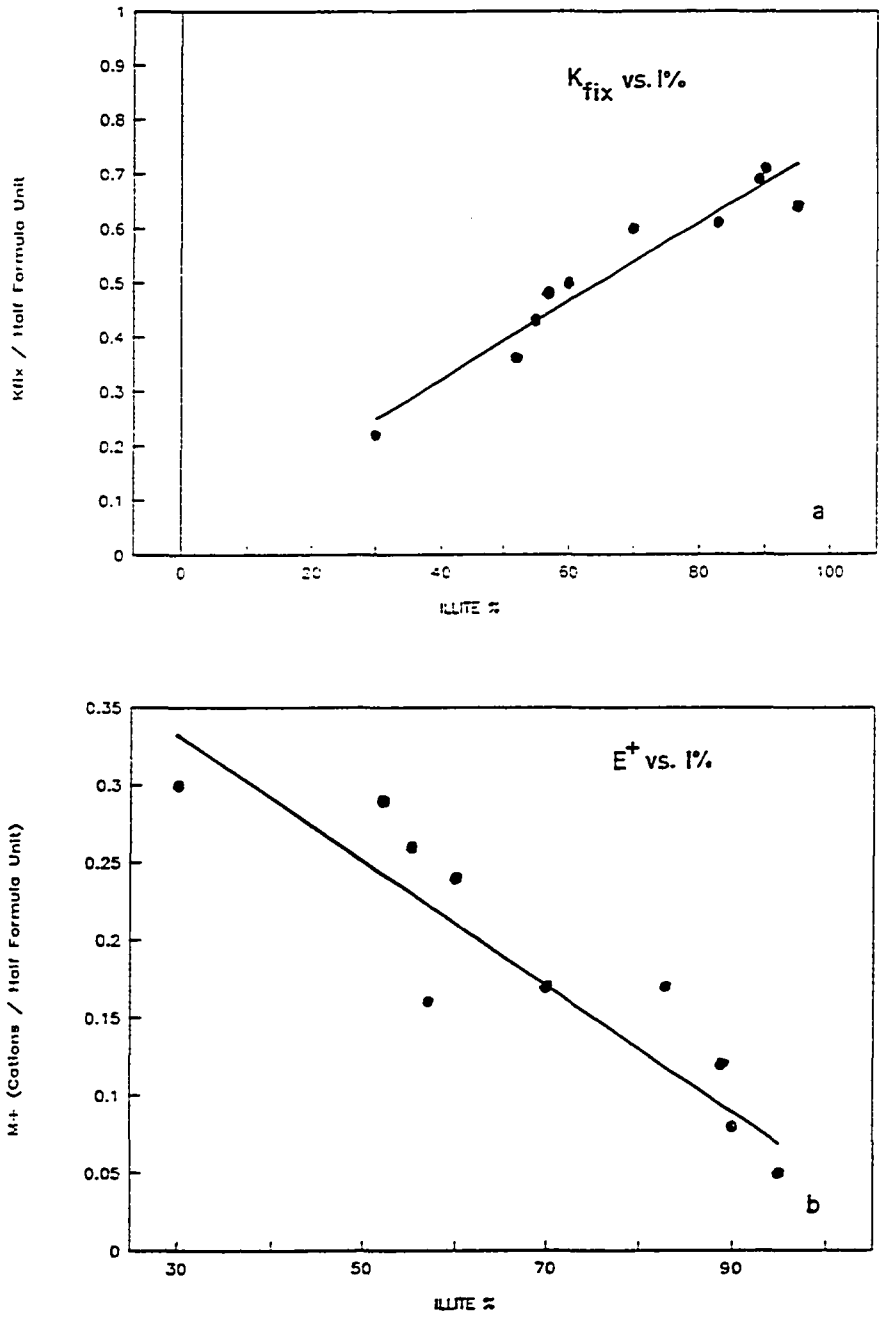

Figure&d@ 17: Variations of the K content with illite % (a), and sum of exchangeable cations with illite % (b) and fixed-K (c). Variation of interlayer charge is also shown (d).

(Figure 17 continued next page)

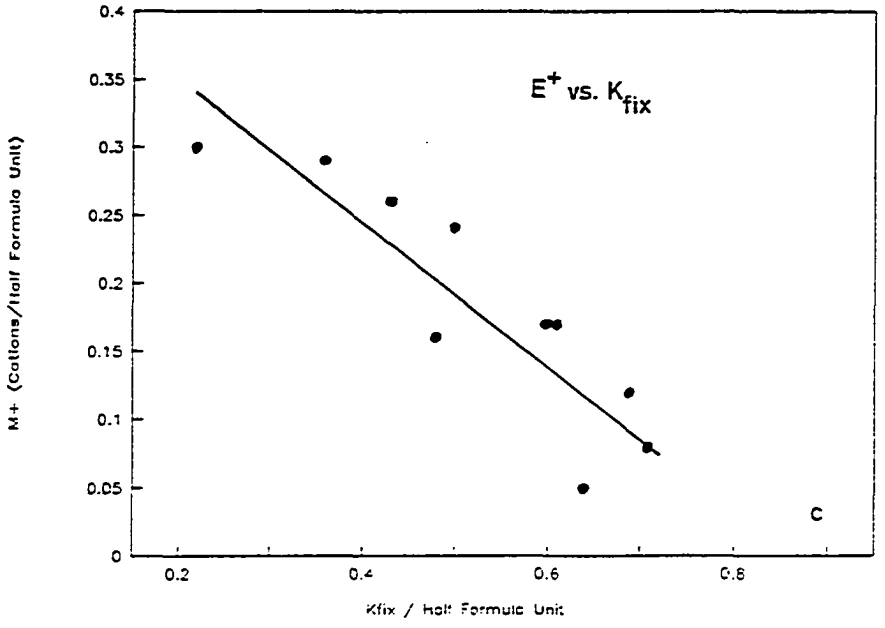

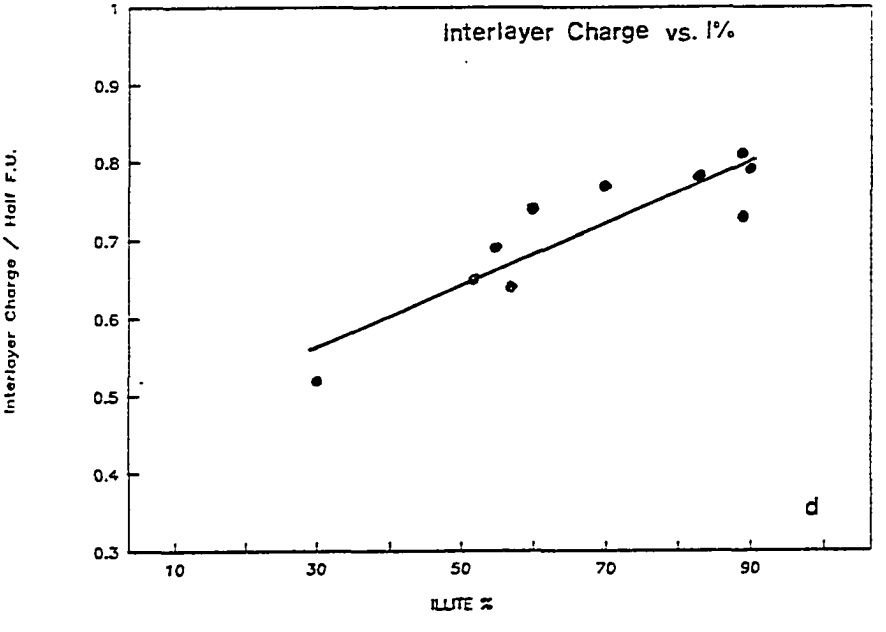

DISCUSSION

Proportion of illite as inferred from XRD and its relation to stacking order and diffracting domain thickness in I/S

XRD results for about 100 samples of Paleozoic K-bentonites from the U.K., 14 of which are detailed in the results section aove, show that the proportion of illite in I/S ranges from about 30% to >95%, and that I/S with higher proportions of illite generally exhibit a higher degree of stacking order. This relationship is well-established from previous studies of K-bentonites (i.e. **Huff and Türkmenoglu, 1981; Nadeau and Reynolds, 1981**).

In these bentonite samples, I/S having less than about 50% illite layers show principally random (R0) inter-stratification. I/S of even slightly higher illite content than 50% are best characterized as having either complete R1 or partial R1 (R=0.5) ordered domains, or both, in addition to random domains (Figs. 3-7). Although many samples have around 50% illite layers, none shows a complete, rectorite-like R1 order. Further increase of illite content up to about 65% generally increases the relative proportion of ordered I/S domains in the mixtures. Complete or near complete R1 order is observed in I/S containing 65-80% illite layers (the average for 18 samples is 72% ± 6). No sample is found to exhibit a complete R2 order similar to those from thermally altered bentonites

(**Bethke and Altaner, 1986; Bethke et al., 1986**). However, samples with partial R2 (R=1.5) as well as partial R3 (R=2.5) order are common in the range 80-90% illite layers. All samples with >90% illite layers exhibit R3 order. It should be noted that samples characterized here as partially ordered and designated by R=1.5 or R=2.5 are also closely modeled as mixtures of R1 and R2 or R1 and R3 ordered I/S, respectively (see Fig. 9). On this basis, it is believed that those samples with partial ordering closely resemble the samples of similar composition described as R1/R3 ordered by previous workers (**Brusewitz, 1986; Srodon et al., 1986**).

Modeling of XRD results show that the minimum diffracting domain thickness (N) is 3-7 layers thick (average=5) in random I/S while it is 3-14 layers thick (average≈9) in ordered I/S. Because thicker diffracting domain sizes are consistently associated with I/S of higher illite content as well as higher degrees of stacking order, it is concluded that illite clusters or domains within individual crystallites should also be thicker. This conclusion conforms with the observation of **Nadeau et al. (1984, 1985)** that illite particles get thicker during the conversion from random to ordered I/S. A diffracting crystallite domain thickness of 3-7 is consistently used to best model the random I/S samples of this study. Clearly,

crystallites 3-7 layers thick are significantly different from 1-3 layer thick crystallites (or particles) that **Nadeua et al. (1985)** suggests random I/S is built of. Simulation attempts using crystallite thickness ranges of 1-2, 1-3, and 2-3 in the NEWMOD program failed to produce realistic patterns for random I/S. This failure, however, can not be taken as a hardproof for the absence of 1-3 layer thick crystallites in I/S because the NEWMOD program allows only a crude specification of particle thickness distributions.

Estimation of proportion of illite layers in I/S

The proportion of illite layers in the samples was estimated from XRD as described in the experimental section above. In order to evaluate the relationship of the proportion of illite layers from XRD to the fixed-K content of the samples, the proportion of illite layers was also estimated from $K_{fix}/K_{fix/max}$ following the method of **Brusewitz (1986)**. $K_{fix/max}$ represents an extrapolated value of fixed-K per layer for the end member illite and is found to be 0.76 from Figure 14b (also in Fig. 17a). Because K_{fix} is the amount of the fixed-K per silicate layer in the structural formula, the ratio $K_{fix}/K_{fix/max}$ gives an estimate of the proportion of the illite for any given sample.

These estimates of proportion of illite by XRD and $K_{fix}/K_{fix/max}$ ratio (see Table 2) are generally comparable:

9 of the 14 XRD derived values are lower; 8 of the estimates are within ±5% of each other while 12 of them are within ±10% of each other. Two samples (WDH-25 and NI6) with over 95% illite layers by XRD estimates, however, are estimated by $K_{fix}/K_{fix/max}$ to have around 80% illite layers (Table 2). This disparity appears to result from an anomalously low amount of fixed-K in these two samples due to an analytical error, such as poor estimation of K_2O from XRF intensities. In deed, these samples, because of their greatly unbalanced structural charge and octahedral sums significantly different from 2.00, had been excluded from chemical data as noted earlier.

Alternatively, however, it could be argued that the disparity above is caused by overestimation by XRD of the proportion of illite layers in these highly illitic samples. **Eberl and Srodon (1988)**, for example, recently concluded that proportions of illite they estimated by the XRD peak-position method for highly illitic I/S are more than the proportions of illite measured by TEM. They attributed XRD overestimates to the presence of non-swelling surfaces at the ends of stacks of illite particles (short-stack effect), and proposed a correction technique for I/S with >90% illite. In the present data, however, the match between XRD and $K_{fix}/K_{fix/max}$ estimates for 5 other highly illitic I/S, including 4 samples with around 90%

illite layers, is excellent (Table 2). On this basis, it is believed that XRD estimates of proportion of illite presented here are realistic representations of sample compositions.

Initial Smectite and End-member Illite Compositions

The chemical data for I/S presented in several plots above can be extrapolated to characterize the compositions of the pre-diagenetic or "initial" smectite and end-member illite of the transition series (Table 3). Closely charge-balanced structural formulas, as well as substantially good agreement between the calculated and extrapolated values of net and interlayer charges of initial smectite and end-member compositions strongly suggest that the structural formulas in Table 3 and the chemical trends described in the results section are real.

The initial smectite clearly is montmorillonitic in composition rather than beidellitic as indicated by its Si≈4 content (Table 3). Si values for low- and high-charge beidellites typically vary between 3.7 and 3.3 cations per formula unit, respectively (**Velde, 1985**). More than 4.00 Si per half formula unit in extrapolated initial smectite composition probably indicates the presence of amorphous silica. In addition, extrapolated 0.03 fixed-K indicates about 5% pre-diagenetic illite layers. Exchangeable cations

equaling a maximum of 0.45 and a net negative charge of 0.48 also reveal a true smectitic nature when respectively compared to the 0.4 average charge of a "pure" smectite layer (**Weaver and Pollard, 1973**), and to 0.2-0.6, charge range accepted for smectites (**Brindley, 1980**).

The illite end-member of the series has an extrapolated fixed-K content of 0.76 and 0.05 equivalents of exchangeable cations, both summing to 0.81 total (net) charge density per layer. Virtually the same values were found for end-member illite, first by **Hower and Mowatt (1966)**, and more recently by **Srodon et al. (1986)** and **Velde and Brusewitz (1986)** in Paleozoic K-bentonites from various locations. The linear relationship between illite percent and fixed-K (Fig.17a) suggest that the 0.76 fixed-K obtained for the end-member illite is a constant value per illite layer throughout the I/S composition range. This result differs from that of **Srodon et al. (1986)** who, deducing from their expandability vs. fixed-K data, best fitted with two straight lines, suggested that 0.75 fixed-K is an average for two kinds of equally abundant layers containing 0.55 and 1.0 fixed-K. Nonetheless, these workers provided in a recent paper (**Eberl and Srodon, 1988**) a reinterpretation of their earlier data on the basis of TEM; they now think that the relationship between expandability and fixed-K is fitted by one straight line instead of two,

and that the second line in their earlier report was an artifact due to underestimation of expandability (=overestimation of illite percent) by XRD peak position method.

Previous chemical analyses of I/S, used in conjunction with the proportion of illite both from XRD and TEM particle thickness, indicated that K content per illite layer in I/S is lower than that of a true mica such as muscovite (i.e. **Srodon et al., 1986; Nadeau and Bain, 1986; Meuneir and Velde, 1989**). As noted above, end-member illite has about 0.76 fixed-K when I/S data are extrapolated to 100% illite (Fig. 17a). Nonetheless, I/S data extrapolates to 0.86 fixedK when no exchangeable cations are present (Fig. 17c, for E^{+}=0), a condition that better represents an ideal muscovite (E^{+}=0). Because in both cases fixed-K are less than ideal muscovite (the latter is closer to 1), it can be concluded from the present data that illite formed during bentonite diagenesis has less K than ideal muscovite.

The question, however, whether 0.76 or 0.86 is a better representation of the real amount of fixed-K in end-member illite still remains to be answered . It is important to note that the value of 0.86 for fixed-K represents the condition E^{+}= 0, a condition not observed in illitic clays from bentonites, not even in illites

Table 3: Initial smectite and end-member illite compositions (half formula unit) as extrapolated from I/S data.

Smectite			Illite
Tetrahedral			
[1]Si= 4.14	←	from Figure 14a	→ Si= 3.39
Al= 0.00			Al= 0.61
Charge= 0.00			Charge=-0.61
Octahedral			
Al= 1.41	←	[2](=2.00-Mg-Fe)	→ Al= 1.66
Mg= 0.49	←	from Figure 15b	→ Mg= 0.27
Fe= 0.10	←	from Figure 15c	→ Fe= 0.07
Charge=-0.49			Charge=-0.27
Net Charge=-0.49			Net Charge=-0.88
[3]Net Charge=-0.53	←	from Figure 16a →	Net Charge=-0.83
Interlayer			
K_{fix}= 0.03	←	from Figure 17a	→ K_{fix}= 0.76
E^{+}= 0.45	←	from Figure 17b	→ E^{+}= 0.05
Charge= 0.48			Charge= 0.81
[3]Charge= 0.53	←	from Figure 17c →	Charge= 0.81

[1]Extraneous Si (more than 4.00), not considered to be held structurally, does not contribute to the tetrahedral charge.

[2]Octahedral occupancy values for initial smectite and end-member illite are 2.10 and 2.11, respectively, when the extrapolated Al values of 1.51 and 1.77 obtained from the regression lines in Figure 15a are used. These values for octahedral occupancies clearly are too high for a dioctahedral structure and cause greatly unbalanced structural formulae for both. Therefore, octahedral Al was calculated by subtracting extrapolated Mg and Fe values from 2.00, ideal maximum dioctahedral occupancy, which lowers the octahedral Al by about 0.1 both in smectite and end-member illite. Substantially well-balanced structural formulae thereby obtained, however, suggest that 1.41 and 1.66 are better approximations for octahedral Al in initial smectite and end-member illite, respectively.

[3]Given for comparison with charges calculated from structural formulae .

reportedly neoformed from solution in sandstone pores (**Wilson and Pittman, 1977; McHardy et al., 1982; and Nadeau and Bain, 1986**). Rotliegend illite, for example (sample ROT,**Nadeau and Bain, 1986**), a well-known illite from sandstone pores, has 0.74 fixed-K, 0.03 NH_4^+ and 0.05 Ca in interlayer sites, summing to about 0.87 cations per illite interlayer (=interlayer charge density). Because the extrapolated end-member illite of the present study has practically the same K content (0.76, Table 3) as the Rotliegend illite, it is concluded that 0.76 better represents the real amount of K in illite than 0.86. The value 0.86, on the other hand, seems to represent a maximum for net layer charge for end-member illite (0.83-0.88, Table 3), rather than the amount of fixed-K. This argument is supported by solid solution considerations by **Meuneir and Velde (1989)** who showed that I/S compositions observed in several sequences merge toward an illite phase with a 0.87 layer charge. **Meuneir and Velde (1989)**, as well as data presented here, further suggest that this maximum layer charge (i.e layer charge deficiency) 0.86 is never satisfied fully by K^+ ions in illite during bentonite diagenesis.

A further feature of interest of the end-member illite in Table 3 is its phengitic rather than muscovitic

composition:

$K_{0.76}\ E^{+}_{0.05}(Si_{3.39}\ Al_{0.61})(Al_{1.66}\ Mg_{0.27}\ Fe_{0.07})\ O_{10}(OH)_2$.

Aside from its K content, this composition is in good agreement with an ideal phengite composition, recognized by an Si:Al ratio of 3.5:0.5 in tetrahedral sites and by substitution of R^{+2} cations, primarily Mg, in octahedral sites (**Velde, 1985**). Furthermore, there is a remarkable similarity between the composition above and the mica with maximum phengite substitution in burial metamorphic rocks (**Radoslovich, 1963**):

$K\ (Si_{3.40}Al_{0.6})(Al_{1.60}\ R^{+2}_{0.40})\ O_{10}(OH)_2$.

The phengitic character of several illitic clays from bentonites with a short and shallow burial history has been previously noted by **Hower and Mowatt (1966)** and **Nadeau and Bain (1986)**. The five most illitic samples of this study come from Dob's Linn in the central belt of the Southern Uplands of Scotland (Appendix C), where the rocks were subjected to high diagenetic or low anchizone metamorphism (**Kemp et al., 1985; Merriman and Roberts, 1990**). Therefore, it seems that the extrapolated end-member illite presented above with a phengitic tetrahedral and octahedral composition is a realistic representation of illite formed under predominantly diagenetic conditions.

Conversion of Smectite to Illite

A noteworthy aspect of the XRD results is the absence of complete R1 order near 50% illite layers. This feature, coupled with the observation that a strong R1 order develops only after the proportion of illite exceeds about 65%, is important in that it indicates a random-preferential rather than a pervasive illitization scheme during much of the bentonite diagenesis. The rationale for such a scheme involves the observation that most bentonitic smectites have randomly distributed interlayers of different charge densities (**Lagaly and Weiss, 1976; Stull and Mortier, 1974**). Also, there is convincing experimental evidence that high-charge smectites fixate K^+ ions more easily and in greater amounts than low-charge smectites (**Srodon and Eberl, 1984; Eberl et al. 1986**). These two observations together suggest: 1) that there is a strong relationship between the initial charge of smectite interlayers and their tendency to fixate K^+ ions - i.e. the higher the charge, the easier the fixation in an interlayer space; and 2) that a process that increases the layer charge is responsible for fixation of K ions. Thus, in a smectite with an initial random distribution of low-, intermediate-, and high-charge interlayers, the high-charge interlayers would preferentially incorporate and fix K^+ ions.

On the basis of above arguments and the chemical data presented earlier, illite layers in K-bentonites described here are thought to have formed from smectite by a transformation mechanism consisting of: 1) continuous tetrahedral Al^{+3} for Si^{+4} substitution throughout diagenesis, and 2) incorporation and fixation of K^{+} in the interlayer spaces. The relationship between the proportion of tetrahedral charge in the net negative layer charge and the proportion of illite (or fixed-K, Fig. 16b and 16c) is considerably better correlated than that of total (net) negative layer charge and the proportion of illite (Fig. 16a). This suggests that the increase in the negative tetrahedral charge in response to substitution of Al^{+3} for Si^{+4}, rather than the increase in negative net charge, is more directly related to the fixation of K^{+} ions in the interlayer spaces.

The scheme described above is essentially the same as the transformation model proposed by **Hower et al. (1976)** to explain illite formation in the Gulf Coast shales. Present scheme differs from that of **Hower et al. (1976)**, however, in its emphasis on the greater importance of the increase in negative tetrahedral charge as opposed to the increase in total (net) negative layer charge.

A neoformation mechanism for the formation of illite, involving dissolution of smectite layers, and precipitation

and subsequent growth of illite particles (**Nadeau et al. 1984, 1985; and Nadeau and Bain, 1986**), does not appear to be likely in I/S from K-bentonites because of the following considerations:

1) **Boles and Franks (1979)** showed that illitization in I/S from Wilcox sandstones/shales of Texas is better explained by a reaction in which Al is assumed immobile and thus conserved ("immobile Al reaction"), than by a reaction in which Al is assumed mobile and additive ("mobile Al reaction"). The immobile Al reaction differs from the other mainly in that it requires destruction of some smectite layers in order for Al to beutilized in producing illite layers. The immobile Al reaction also differs from the other reaction in releasing considerably more Si, H_2O, Mg, Fe, and exchangeable cations as reaction products. In terms of the conversion type, the immobile Al reaction describes a neoformation mechanism based on dissolution of smectite and reprecipitation of illite from solution. The mobile Al reaction, on the other hand, depicts a layer-by-layer transformation of smectite to illite.

The present data from K-bentonites show that Al (and/or Al_2O_3) is mobile and additive in the system. This is evidenced by the observation that the most important chemical changes and corresponding charge modifications in the silicate layer structure, both tetrahedral and

octahedral, are caused principally by the continuous addition of Al. Clearly, these observations support Al mobility and layer-by-layer transformation of smectite to illite.

2) As noted before, the present data indicates a constant K content of about 0.76 per illite layer throughout the entire smectite-to-illite transition. A recent AEM/TEM study of a highly illitic I/S from a K-bentonite bed (**Huff et al., 1988**) suggests practically the same K content per illite layer in analyzed illite packets, and provide independent support for a K content of 0.76 per illite layer in these clays.

On the other hand, the K content of highly illitic I/S clays from a well-known hydrothermal system in Japan is higher, consistently varying in the range 0.8-0.9 per illite layer, as determined both by XRF (**Inoue et al., 1988**), and by electron microprobe (**Veblen et al., 1990**). There seems to be sufficient evidence, principally from morphological and particle size studies of these clays, that suggests that these highly illitic I/S clays neoformed via dissolution of smectite, and precipitation and subsequent growth of illite particles (**Inoue et al., 1987; Inoue et al., 1988**). A higher K content of 0.85-0.9 is also suggested by solution equilibration studies for a phase (i.e. illite or K-deficient muscovite) that crystallizes

at elevated temperatures (**McDowell and Elders, 1980; Sass et al., 1987; Rosenberg and Kittrick, 1990**), conditions similar to those of a hydrothermal system. These studies collectively suggest that illite formed by precipitation and/or subsequently grown by addition of layers from solution have a K content of 0.8-0.9. If this conclusion about the K content of neoformed illite in hydrothermal deposits is accurate, then the formation of illite layers with less K in bentonites is difficult to explain by the same process. In other words, these two different mechanisms seem to produce two different types of illite.

3) XRD suggests that I/S interstratification is virtually random up to about 50% illite layers. If a neoformation process were responsible for the formation of illite layers, some XRD detectable short-range order - produced by the formation of ordered domains composed mainly of 2-3 layers thick illite particles - would be expected in this range. XRD detectability of minor amounts of ordered domains does not seem to be a factor for the observed lack of ordering because XRD would detect such small ordered domains even if they compose only 10% of an I/S clay (see Fig. 4). Total randomness of the interstratification in the <50% illite range, therefore, can bebetter explained by layer-by-layer mechanism in which the randomness of the charge distribution in pre-diagenetic

smectite is the most important control for the K-fixation process to form illite layers.

CHAPTER 2 : ALKYLAMMONIUM ION CHARACTERIZATION OF I/S CLAYS

INTRODUCTION

Interstratification and interlayer stacking order in I/S minerals are currently explained on the basis of two models (Fig. 1; section 1). The Markov model **(MacEwan, 1956, 1958; Reynolds and Hower, 1970; Reynolds, 1980)** postulates that I/S is composed of silicate layers about 10Å thick that are separated by K-fixed illite and hydrous smectite interlayers. The interlayers are stacked in the c-axis direction to form crystallites (also called MacEwan crystallites) of various ordering types. MacEwan crystallites are commonly considered to consist of 5-15 silicate layers (50-150Å thick). In contrast, the fundamental particle model **(Nadeau et al., 1984, 1985; Nadeau, 1985)**, based on TEM observations of dispersed I/S, proposes that I/S is composed of fundamental particles that are mainly 10-50Å thick, considerably smaller than crystallite thicknesses inferred from XRD, and that these particles can hydrate at their interfaces and act as smectite interlayers. In effect, the fundamental particle model implies that materials yielding XRD patterns of I/S do not necessarily contain chemically distinct illite and smectite layers.

A direct way of testing whether or not the expanding, smectite-like component of I/S clays is actually smectite is to determine the magnitude and distribution of the layer

charge of this component. Determining the layer charge is essential because smectite is defined, and distinguished from other expanding 2:1 clay minerals on the basis of its layer charge. Past studies indicate that the mean layer charge of "pure" smectite varies around 0.4 per half formula unit (**Weaver and Pollard, 1973**), and that a great majority of them have heterogeneous charge distributions across their silicate layers (**Lagaly and Weiss, 1976; Lagaly, 1981**). Principally due to this demonstrated heterogeneity, the Nomenclature Committee of AIPEA (Association Internationale pour l'Etude des Argiles) accepts a charg range of 0.20-0.60 equivalents per half formula unit for smectite (**Bailey, 1980**). Despite this definition of smectitic charge, however, layer charge characterization of the expanding, smectite-like component of I/S minerals is to a great degree lacking.

The layer charge of monomineralic clays may be estimated from structural formulas that are based on total elemental analyses or measured directly by various absorption methods. Due to the interstratified nature of I/S minerals, however, these methods provide average results that contribute little information about the layer charge of individual mineral components. Thus, other methods of characterizing the layer charge of I/S minerals have been sought. One that has received particular

attention with expanding layer silicates has been the alkylammonium exchange method **(Lagaly and Weiss, 1969)**. The attraction of this method is due primarily to its effectiveness in the presence of non-expanding components such as kaolinite or micas in treated samples. **Lagaly (1979)** was the first to demonstrate that the alkylammonium ion exchange method is capable of determining the interlayer charge of the expanding component in regularly interstratified minerals with mica-like (i.e. illite) and smectitic or vermiculitic interlayers in a 1:1 ratio. He speculated, however, that in randomly interstratified minerals, layer charge determinations might be difficult.

This section presents the results of alkylammonium exchange experiments conducted on a suite of I/S clays whose XRD characteristics demonstrate widely varying expandability and interstratification ranging from random (R0) to long-range ordered (R3). The theoretical basis for studying the interlayer charge of the expanding, smectite-like component of I/S by the alkylammonium exchange is that smectites exchange quantitatively their interlayer cations within several hours of saturation by alkylammonium ions whereas mica-like interlayers react very slowly over periods of days, or even weeks **(Lagaly, 1979)**. Thus, an I/S with both smectite and mica-like illite interlayers would exchange only the cations in smectite interlayers if

treated for a short period of time. This would allow the interlayer charge density and its distribution for the expanding, smectite-like component of the mineral to be estimated. The results presented here show that the method is applicable to randomly interstratified minerals, despite the concerns raised by **Lagaly (1979)**.

EXPERIMENTAL PROCEDURE

Samples

A suite of fourteen interstratified I/S clays from lower Paleozoic K-bentonites, ranging from randomly interstratified (R0) to long-range ordered (R3), and containing between 30% and >95% illite layers was used in this study (Table 1). Details on the mineralogy and composition of the I/S clays are presented in Chapter 1.

Methods

The preparation of alkylammonium chloride solutions and the treatment of clay samples with these solutions were conducted according to the procedure of **Rüehlicke and Köhler (1981)**. For alkylammonium treatments, 300 mg of <0.2μm fraction of clays were first Na-saturated with 5N NaCl solution and then washed free of excess salt. The Na-clay was then dispersed in distilled water to give a suspension concentration of about 10 mg clay/ml water. 2 ml of this clay suspension was poured into small glass tubes

TABLE 1: Samples selected for alkylammonium exchange experiments. Values for R, I, and N are based on comparison of XRD patterns with computer simulated patterns generated by the NEWMOD program (**Reynolds, 1985**).

Sample	R Value	I%	N*	Other Minerals
SI-59	0	30	3-7	I (5%), K (3%)
SI-64	0	45	3-7	I (4%), K (3%), Q (2%)
SI-55	0/1	52	3-5/3-14	I (8%), K (7%)
SI-44	0/1	55	3-5/3-14	K (7%)
SI-53	0/0.5	57	3-14/3-14	K (trace)
SI-9	0/0.5/1	60	3-7/3-14/3-14	
MLH	1	70	3-14	
SI-47	1.5	83	3-14	K (trace)
WDH-62	2.5	89	3-14	
WDH-64	3	89	3-14	
WDH-60	3	90	3-14	
WDH-68	3	90	3-14	
WDH-25	3	95	3-14	C (trace)
NI6	3	97	3-14	C (3%), Q (1-2%)

* Number of silicate layers in refracting crystallite domain.

I: Discrete Illite, K: Kaolinite, C: Chlorite, Q: Quartz.

and mixed with 4 ml of alkylammonium chloride solutions of different carbon chain length (Nc=6-18, Nc being the number of carbon atoms in the alkyl chain). Solution tubes were stoppered, shaken vigorously, and kept at 60°C for 24 hours with occasional shaking. The suspensions were then repeatedly washed with 95% ethanol until the supernatant solution was free of silver nitrate-detectable chloride ions. After the supernatant from the final wash was discarded, the sample was ultrasonically dispersed in 2 ml ethanol for about half a minute. About 1 ml of clay-ethanol suspension was uniformly spread on a glass slide, air-dried, and kept at 60°C in a desiccator under vacuum until X-rayed. A Siemens D-500 3kW powder x-ray diffractometer using monochromated Cu-Kα radiation was used to record the XRD patterns (between 2 and 32° 2θ) of 13 separate alkylammonium derivatives (Nc=6-18) of each sample.

The interlayer charge density of the expanding, smectite-like component in the samples was determined as follows: In samples where the expanding component displayed a clear mono-to-bilayer transition between 13.7 and 17.7 Å, the method of **Lagaly (1981)** was used, in which the transition Nc's are converted to layer charges. A detailed description of the rationale behind this method is given in Appendix A.

For samples in which the monolayer and bilayer

plateaus were not obvious, the transition Nc's at which mono-to-bilayer transition would take place were calculated, using smectite percentages determined by XRD. Consider, for example, an I/S sample which has an expandability of 50% (=smectite %). When each smectite interlayer in this clay has alkylammonium ions arranged in monolayers, the average basal spacing for this monolayer alkylammonium-smectite/illite complex would be:

$$d = 11.8 Å = (13.6 Å)*(50\% S) + (10.0 Å)*(50\% I)$$

Similarly, the average basal spacing for a bilayer alkylammonium-smectite/illite complex would be:

$$d = 13.8 Å = (17.7 Å)*(50\% S) + (10.0 Å)*(50\% I)$$

The basal spacings between these two values would represent the mono-to-bilayer transition. The Nc's that correspond to 11.8 and 13.8 Å can be converted to layer charges and then the mean layer charge and the distribution of charge can be determined as in **Lagaly (1981)**.

For samples in which the expanding component did not display a mono-to-bilayer transition and basal spacings increased more or less linearly with the alkyl chain length, the method of **Ghabru et al. (1989)** was used. This method, which determines the mean layer charge as a function of the tilt angle of alkylammonium ions in the

interlayers, is a modification of the method of **Lagaly and Weiss (1969)** for estimating layer charge in high-charge smectites and vermiculites. A more complete account of the procedures used for the determination of the mean layer charge by this method is also presented in Appendix A.

RESULTS

The powder XRD patterns of fourteen I/S clays, each treated with alkylammonium ions of various chain length (Nc=6-18) are presented in Appendix B. Sample SI-47, which has an expandability of 17%, and 7 other samples of higher expandability (Table 1) are different in their XRD behavior from the 6 saples having 11% or lower expandability. For convenience, the relevant XRD characteristics of the samples are described below after the samples are grouped into two sets choosing 15% expandability as an arbitrary value between 11 and 17% expandabilities.

I/S with >15% expandability: The XRD patterns of I/S samples with >15% expandability show:

1) a peak that migrates from the 13-10.5Å region in the short-chain alkylammonium derivatives (Nc=6-8) to the 18.0-11.5Å region in the longer-chain alkylammonium derivatives (Nc=10-14). Both the range of peak migration and the values of basal spacing between which the peak migration takes place get smaller with decreasing

expandability (increasing proportion of illite) in the samples. For example, the peak migration takes place from 13Å to about 18Å in 70% expandable sample SI-59 whereas it takes place between 11.3Å a 12.3Å in 30% expandable sample MLH. Clearly, these observed changes in XRD behavior are caused by the increase in the proportion of non-expanding illite interlayers relative to the proportion of expandable interlayers; and

2) an additional low angle peak in the region 22Å-34Å, that becomes apparent only in long-chain alkylammonium derivatives (Nc=12,13-18). Because this low angle peak has spacings mostly 10Å or larger than those at higher 2θ positions, it is interpreted to be aused by diffraction from packets containing illite and smectite layers with incomplete ordering. Additional support for this interpretation is provided by the lack of XRD evidence from glycolated samples for a mineral phase that would produce such large spacings upon alkylammonium treatment. Nevertheless, why this low angle peak is present only with long chain alkylammonium derivatives is not fully understood. However, the presence of the low angle peak does not inhibit a clear observation of the relationship of the basal spacing (d) to alkylammonium chain length (Nc) in the 10-18Å region, which is presented in Figure. 1.

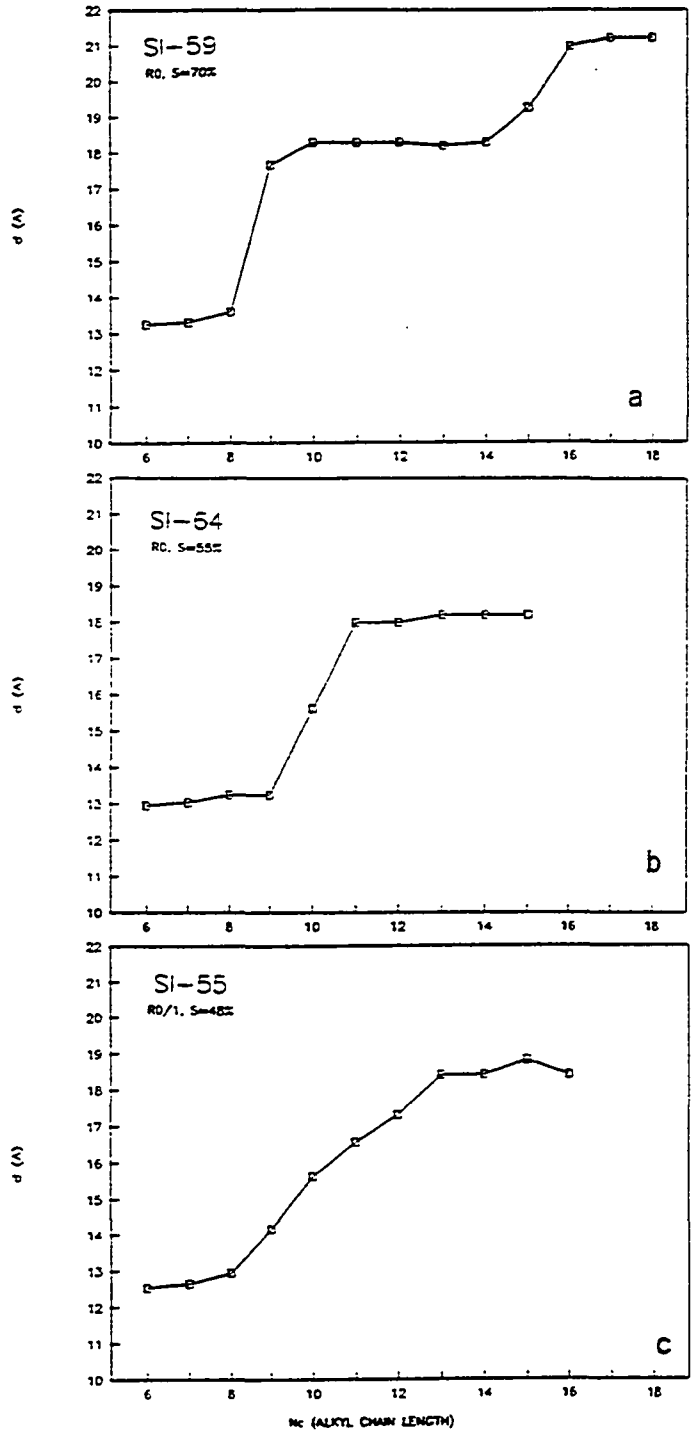

Figure 1: Variation of basal spacing (d) in eight I/S clays with more than about 15% expandabilities, treated with alkylammonium chloride ions of various chain length (Nc).

(Figure 1 continued next page)

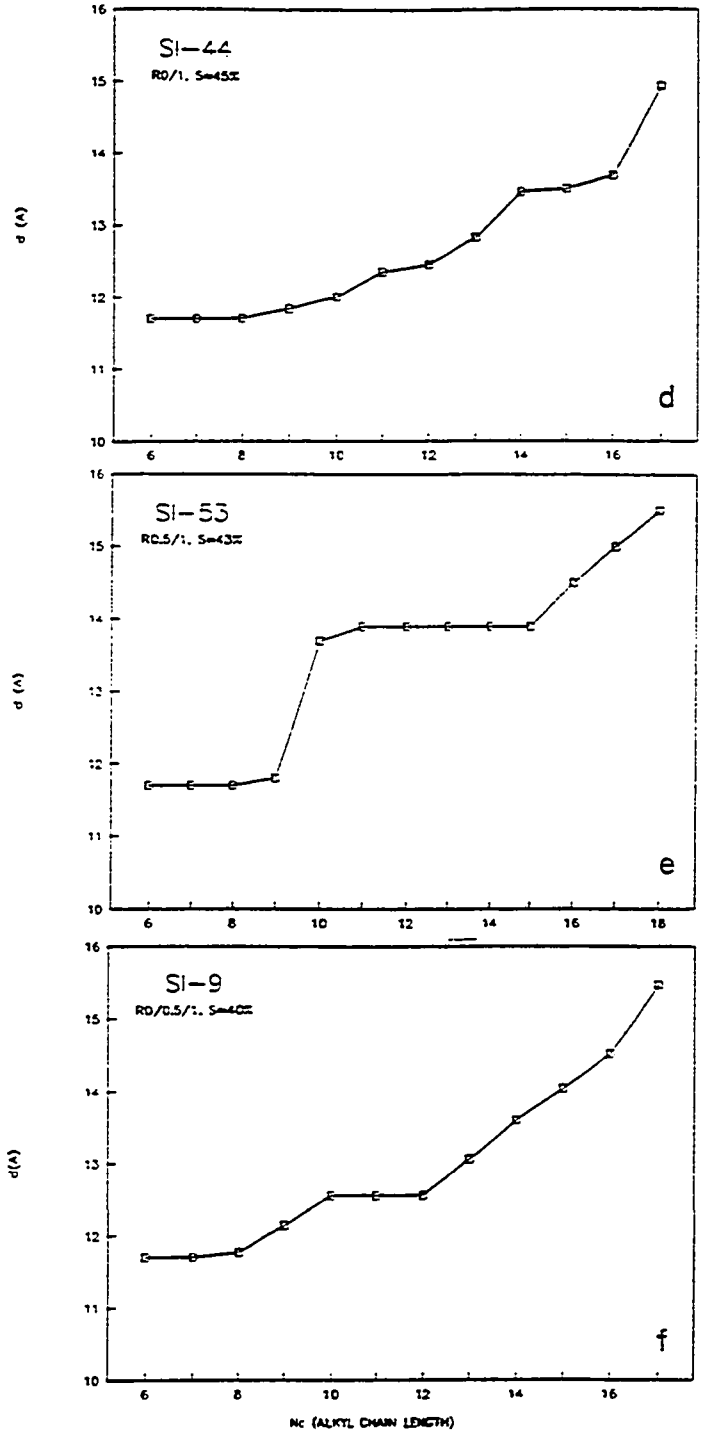

(Figure 1 continued next page)

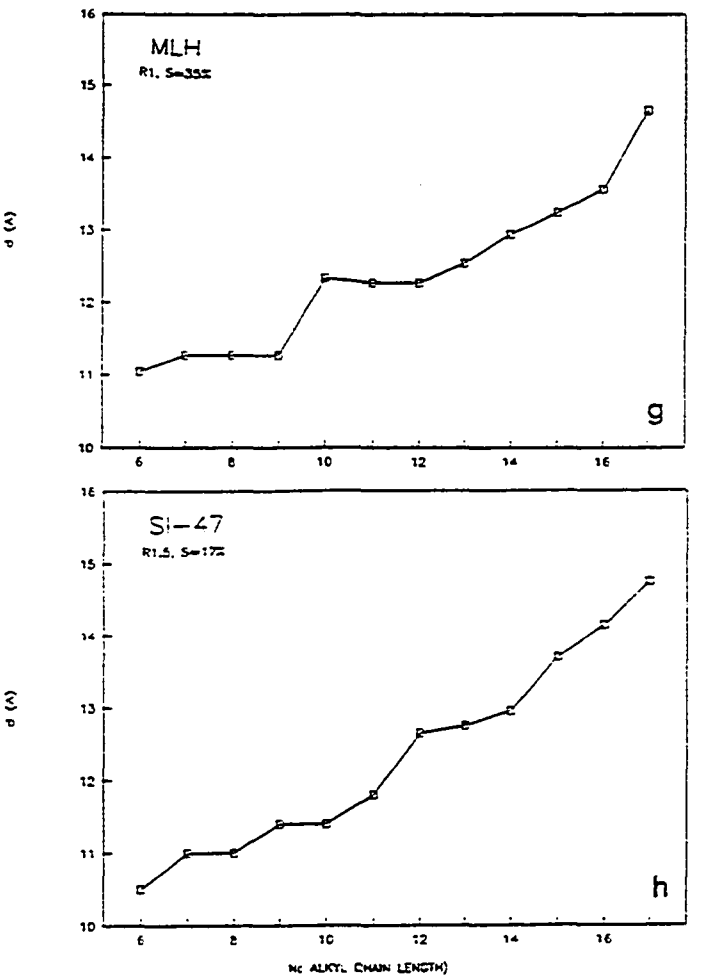

Alkylammonium derivatives of the randomly interstratified samples SI-59, SI-64, and SI-55 exhibit distinct mono-to-bilayer transitions similar to that of smectite (Fig. 1a, b, and c). Two or more basal reflections are observed for the monolayer and bilayer arrangements at about 13Å and 18Å, respectively. Transition samples are distinguished by spacings between 13Å and 18Å. For sample SI-59, the transition starts at Nc>7, and is completed at Nc=10 as indicated by the plateaus for monolayer and bilayers arrangement at about 13Å and 18Å, respectively (Fig. 1a). From these transition points, it can be calculated (**Lagaly, 1981**) that layer charge density in the expanding interlayers of this sample varies between 0.36 and 0.46 equivalents per formula unit. The mean layer charge is calculated to be 0.40 equivalents per formula unit (see Appendix A for a detailed account of the determination of charge density limits, and the mean layer charge density). The lower and upper charge density limits, and the mean layer charge densities for samples SI-64 and SI-55 are similarly calculated from mono-to-bilayer transitions. The results clearly show that both samples, plus SI-59, have heterogeneous and smectitic interlayer charge densities (Table 2).

In samples SI-44, SI-53, SI-9, MLH, and SI-47, the monolayer and bilayer arrangements produce basal spacings

in the ranges 12-10Å and 14-12Å, respectively. These values are smaller than the values that are obtained for pure smectites. The spacings are smaller for I/S, however, because the total average contribution from the expanded layers to the diffracted x-ray beam is smaller at higher illite proportions. The short-chain derivatives of SI-44, SI-53, and SI-9 are characterized by basal spacings of about 11.7Å, forming plateaus in Nc-d(001) plots (Figs. 1d, 1e and 1f). In order to determine whether 11.7Å represents a monolayer arrangement of alkylammonium ions in the expandable layers, percent expandability (=percent smectite) was used to calculate a basal spacing for an I/S minerl that has alkylammonium ions arranged in monolayers in its expandable interlayers. Calculated powder XRD patterns indicate that samples SI-44, SI-53, and SI-9 have between 45 and 40% expandability (see Figs. 5, 6, and 7; Chapter 1). If and when all the expandable interlayers are occupied by alklylammonium ions arranged in monolayers, the basal reflections for the expandability range 45-40% would have spacings of 11.62Å

=(45%S*13.6Å+55%I*10Å)/100

and 11.45Å

=(40%S*13.6Å+60%I*10Å)/100.

Because the difference between the observed and calculated basal spacings falls within the confidence level

with which smectite percent can be estimated in I/S by XRD methods (±5 for most I/S) it is likely that 11.7Å plateau is in deed due to monolayer arrangement of alkylammonium ions. The 13.5Å, 13.9Å, and 12.6Å plateaus observed in the respective Nc-d(001) plots of SI-44, SI-53, and SI-9 are believed to represent formation of bilayers in the expandable layers as the following basal spacings calculated for a bilayer arrangement using smectite percentages are similar to the observed basal spacings:

13.5Å = (45%S*17.7Å+55%I*10Å)/100,

13.3Å = (43%S*17.7Å+57%I*10Å)/100, and

13.1Å = (40%S*17.7Å+60%I*10Å)/100.

For sample MLH, which contains 30% smectite layers, the plateaus that form at 11.3Å and 12.3Å are considered to represent monolayer and bilayer arrangements, respectively, as they are in very good agreement with the calculated values of 11.1Å and 12.3Å. The sharp mono-to-bilayer transition taking place over only one chain length category between Nc=9 and Nc=10 (Fig. 1g) suggests a homogeneous layer charge distribution for this sample. Sample SI-47, which has only about 17% smectite according to XRD, produces even smaller spacings (Fig. 1h). The Nc=6, and Nc=9-10 derivatives of this sample with 10.5Å and 11.4Å basal reflections represent monolayer and bilayer formations in the expandable interlayers, respectively.

Calculated basal spacings for an I/S with 17% smectite are 10.6Å for a monolayer arrangement and 11.3Å for a bilayer arrangement, and are in good agreement with the observed values. The transitions taking place over two or more chain length categories, and the calculated values of mean layer charge ranging between 0.32 and 0.45 (Table 2) indicate that the expandable interlayers in samples SI-44, SI-53, SI-9, and SI-47 are also smectitic and possess a heterogeneous charge distribution. Only sample MLH, which also has a smectitic charge, possesses a homogeneous charge distribution.

I/S with <15% expandability: All six I/S samples with <15% expandabilities respond to the alkylammonium treatment in a similar fashion. The XRD patterns of alkylammonium derivatives of these samples (Appendix B) show:

1) an illite peak at about 10Å, persistent over the whole range of alkylammonium ion chain lengths; and

2) an expanded component that becomes apparent with long-chain alkylammonium derivatives, and expands with increasing chain length.

The expanded component is present over a wider range of alkylammonium chain lengths in the derivatives of WDH-60, WDH-25, and NI-6 than in those of WDH-62, WDH-64, and WDH-68. Because the continuous and more or less linear increase of spacing with increasing chain length of the

expanded component (Fig. 2) is indicative of a high-charge, vermiculite-like mineral (**Lagaly, 1981; Ghabru et al., 1989**), its layer charge density can be estimated using the empirical relationship of **Ghabru et al.(1989)**, developed for quantitatively estimating the layer charge density in vermiculites (see Appendix A for a detailed account of this procedure). The estimated layer charge densities (Table 3) show that the expanded component in samples WDH-25, WDH-60, WDH62, and WDH-68 are indeed vermiculitic. In sample NI-6, however, the charge density of the expanded component is even higher than that of a vermiculite, and very close to that of an ideal dioctahedral mica (**Bailey, 1980**).

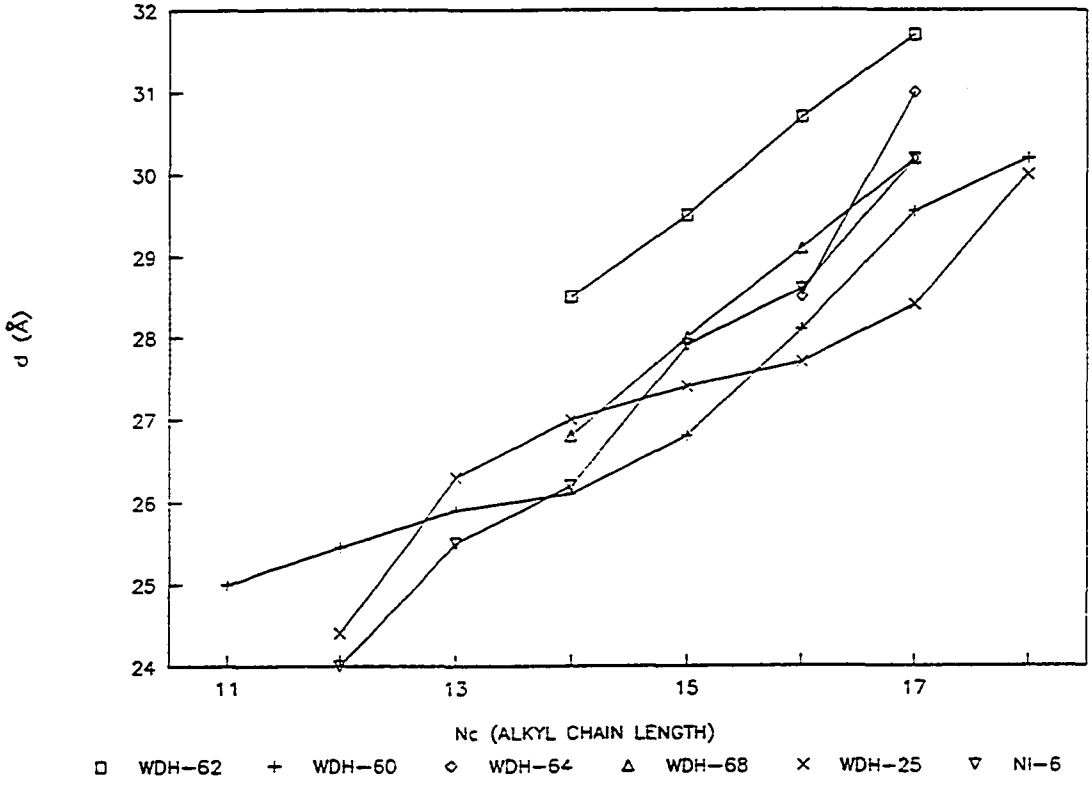

Figure 2: Variation of basal spacing (d) with alkylammonium chain length (Nc) of the expanded component observed in six I/S samples with <15% expandabilities.

Table 2: Interlayer charge density and its distribution in I/S minerals with expandabilities between 70% and 15%.

Sample	Transition range (Nc Classes)	Charge Range*	Mean Charge*	Nature
SI-59	7-10(3)	0.46-0.36	0.40	Heterogeneous
SI-64	7-11(3)	0.46-0.34	0.37	"
SI-55	7-13(6)	0.46-0.29	0.36	"
SI-44	8-14(6)	0.42-0.28	0.32	"
SI-53	8-11(3)	0.42-0.29	0.37	"
SI-9	7-10(3)	0.46-0.29	0.39	"
MLH	9-10(1)	0.40-0.35	0.38	Homogeneous
SI-47	6-9(2)	0.51-0.36	0.45	Heterogeneous
		Average=	0.38±0.04	

*Expressed as equivalents per formula unit.

Table 3: Estimated layer charge of the expanded component observed in six I/S samples with <15% expandabilities.

Sample	Layer Charge[1]
WDH-62	0.812
WDH-60	0.695
WDH-64	NE
WDH-68	0.812
WDH-25	0.694
NI-6	0.926

[1] Estimated using the linear regression expression of **Ghabru et al. (1989).**

NE : Layer charge is not estimated due to few data points.

DISCUSSION

The results demonstrate that treatment of I/S minerals with >15% expandabilities with alkylammonium ions of various chain lengths allows charge density in their expandable interlayers to be quantitatively estimated.

Good agreement between observed and calculated basal spacings indicate that all samples with expandabilities >15% have a monolayer configuration of short-chain alkylammonium ions (Nc=6-7) in their expandable interlayers. Furthermore, the start of monolayer-to-bilayer transition in these samples is clearly observed, and takes place mostly at Nc=7 and Nc=8 (Table 2).

The formation of monolayers with short-chain alkylammonium ions, rather than bilayers or pseudo-trimolecular layers, or paraffin type structures, provides compelling evidence of interlayer charge densities of <0.5 equivalents per unit formula. In other words, these charge densities are characteristic of smectitic clays. Several workers have previously observed that short-chain alkylammonium ions form bilayers and pseudotrimolecular layers with high-charged smectites (0.5-0.6), and paraffin type structures with vermiculites (0.6-0.9) (**Lagaly and Weiss, 1969; Lagaly, 1982; Ghabru et al., 1989; Olis et al., 1990**). Therefore, it would appear that expandable interlayers in I/S with >15% expandability range are

smectitic in terms of their charge.

The average interlayer charge density estimated by alkylammonium ion exchange method for the eight I/S samples with >15% expandabilities is 0.38% ± 0.04 (Table 2). This value is about 15 to 30% lower than the total (net) layer charge density of initial smectite composition determined by extrapolation of structural formula data, about 0.5 equivalents per half formula unit (Table 3, Chapter 1). This result conforms to the observation that the alkylammonium exchange method estimates interlayer charge density which, for smectites, represents about 80% of the total charge as inferred from structural formula (**Lagaly, 1981**). Also **Laird et al. (1989)** showed that alkylammonium exchange values are 20 to 30% lower than structural formula values for monomineralic smectites and vermiculites. This apparent discrepancy is due mainly to cations adsorbed on the lateral edges of the clay particles (broken-bond effect) which are accounted for by the structural formula method. The alkylammonium ion exchange method accounts for the exchanged cations only in the interlayer sites.

On the other hand, interlayer charge densities determined by alkylammonium exchange of these same eight I/S samples are, on average, about 45% lower than the total layer charge densities determined by the structural formula method (Table 4). Such low values by the alkylammonium

exchange method obviously cannot be a result of the broken-bond effect only, but a combination of the broken-bond effect plus an averaging effect of the structural formula method for two-component (bimineralic) minerals such as I/S. On this basis, it is believed that the large differences of charge densities observed between the values from the two methods reflect the presence of a chemically distinct smectite component in I/S and confirm the two-component (bimineralic) nature of I/S clays with >15% expandabilities.

As shown above, expandable interlayers in I/S with >15% expandabilities, even if disturbed and resedimented, retain a smectitic character regardless of the proportion of illite. An important implication of this result, with regard to the mechanism by which smectite is converted to illite during bentonite diagenesis, is that it supports a layer-by-layer transformation mechanism (**Hower et al., 1976; Srodon et al., 1986**) rather than a neoformation mechanism (**Nadeau et al., 1985**).

Nadeau and coworkers viewed the expandability in I/S minerals as a result of interparticle diffraction without considering the surface charge of what they termed illite particles. The new layer charge data presented here do not preclude the existence of the interparticle diffraction, rather they establish the smectitic character of the illite

particle surfaces of Nadeau and coworkers in the >15% expandability range. Thus, a layer-by-layer transformation of I/S, in which the interlayer charge characteristics of a precursor smectite is inherited, seems more likely than a neoformation mechanism because neoformation requires precipitation of illite particles with surface charges significantly higher than that of smectite.

Table 4: Interlayer charge densities determined from structural formula based on total elemental analyses (SF) and alkylammonium ion exchange method (AE) of eight I/S samples with >15% expandability.

		Interlayer Charge		
Sample	I%	SF[1]	AE	%(SF-AE/SF)
SI-59	30	0.52	0.28	23
SI-64	45	(0.88)?	0.37	(58)?
SI-55	52	0.65	0.36	45
SI-44	55	0.69	0.32	54
SI-53	57	0.64	0.37	40
SI-9	60	0.74	0.39	48
MLH	70	0.77	0.38	51
SI-47	83	0.78	0.45	42
			Average=	45.1% ±10.8

[1] Because structural formulae for most samples are well-balanced, interlayer charge are considered equal to total charge (see Table 2, Section 1).

In the XRD patterns of the samples with <15% expandability, the persistence of an illite peak (10Å) throughout the entire range of alkylammonium chain length, even after a week of treatment in some samples, indicates that most illite interlayers are non-expandable. These interlayers must be more or less completely filled with K as such non-expansion behavior is observed only in biotite (**Ghabru et al., 1989**), and muscovite (**Vali and Köster, 1986**).

However, the appearance of a low angle peak in the patterns of the long-chain alkylammonium derivatives of these same samples suggests that packets (or domains) f an expandable, vermiculitic component are present, in addition to illite. This observation, as inferred from XRD, that expanding layers exist in packets, is most notable in that it conflicts with the current models of I/S. For illite-rich I/S, both the MacEwan crystallite and the fundamental particles models predict only a small number of expandable interlayers separated by illite packets (or particles), but not packets of expandable interlayers (**Altaner and Bethke, 1988; Nadeau et al., 1984**).

An alternative explanation to account for the presence of these packets of expandable layers is an exchange reaction between K^+ and long-chain alkylammonium

ions. K^+/alkylammonium ion exchange has been observed in some micas (**MacIntosh et al., 1971**), and also illites from soils (**Laird, 1987**). Because of the following observations, however, this process does not seem likely to have taken place in the I/S samples used in this study:

1) the XRD patterns presented in Appendix B reflect the effects of alkylammonium exchange on the samples after 12 to 24 hours of treatment. Portions of several samples exhibiting a low angle peak in addition to the illite peak also were subjected to a week of treatment, during which sample suspensions were vigorously shaken daily, following addition of fresh alkylammonium solutions. These prolonged treatments produced no detectable change in the XRD characteristics of the samples. If the low angle peaks were due to a K^+/alkylammonium ion exchange reaction in some interlayers, one would have expected low angle peaks to increase in intensity and/or shift to lower angle positions due to the prolonged reaction times. Such changes, however, are not observed (also **Lagaly, 1979**).

2) It is difficult to explain the appearance of the low angle peaks by K^+/alkylammonium exchange while no appreciable change in the intensity of the 10Å illite peaks can be observed (see, for example, patterns for sample NI6, p. 198, Appendix B).

It should be noted that the present XRD data do not

preclude the presence of smectite-like expandable interlayers between illite packets. Nevertheless, the similarity of charge densities estimated for the expanding component by the alkylammonium ion exchange method and the total charge values calculated from structural formulas (Table 5) suggests that a vermiculite-like component is the only expandable component. Therefore, it may be that the expandable interlayers isolated between illite clusters also have a vermiculitic charge, but cannot be detected separately by XRD because of their minor contribution to the overall expandability. If that is the case, then the highly illitic samples described here as illite/smectite with <15% expandability can better be characterized as interstratified illite/vermiculite. Here, the term vermiculite is used strictly in the sense of the layer charge of the expanding phase. HRTEM lattice-fringe imaging of alkylammonium-treated derivatives of these illite-rich clays should provide a better insight into these uncertainties about the nature of layer charge density in expandable interlayers and particle interfaces.

Table 5: Interlayer charge density of the expanding component in six highly illitic clays as determined by the alkylammonium ion exchange method (AE). Interlayer charge density of the samples as determined by structural formula method (SF) are also provided.

		Interlayer Charge	
Sample	I%	SF	AE
WDH-62	89	0.81	0.82
WDH-64	89	0.73	ND
WDH-60	90	0.79	0.70
WDH-68	90	0.83	0.81
WDH-25	95	0.69	0.70
NI6	>95	0.94	0.93

Note: Interlayer charge density and total charge by the structural formula method can be considered equal for samples WDH-62,64,60, and 68 for which charge balance is very good.

ND - Not determined because of too few data points.

CHAPTER 3: CHARACTERIZATION OF UNTREATED AND ALKYLAMMONIUM ION EXCHANGED ILLITE/SMECTITE BY HIGH RESOLUTION TRANSMISSION ELECTRON MICROSCOPY

INTRODUCTION

Illite/smectite (I/S) is a clay mineral that exhibits properties of both illite and smectite, and thus has long been referred to as an interstratified or mixed-layered mineral. The structure of interstratified minerals in general, and that of I/S in particular, has been widely investigated (for example **Nadeau et al., 1984, 1985; Srodon et al., 1986; Eberl and Srodon, 1988; Veblen et al., 1990**). Much of the recent discussion stems from the apparent discrepancies between the interpretation of I/S structure according to x-ray diffraction (XRD) and transmission electron microscope (TEM) data. Models of interstratification based on XRD (**Reynolds, 1980**) suggest that I/S is composed of crystallites containing two types of layers, expanding smectite and non-expanding illite layers. One-dimensional XRD coherent domain size considerations further suggest that I/S crystallites, also referred to as MacEwan crystallites, are predominantly 5 to 15 silicate layers (50-150Å) thick.

TEM observations, on the other hand, reveal that I/S, after being completely dispersed, is composed of extremely small particles, only one to a few silicate layers thick (**Nadeau et al., 1984, 1985; Nadeau, 1985**). Nadeau and coworkers termed these particles "fundamental particles" and interpreted them as individual, primary particles

rather than fragments of larger crystals. They further proposed that interparticle x-ray diffraction effects between these particles account for what was generally interpreted as interstratification. An important implication of the concept of fundamental particles and interparticle diffraction is that clays producing XRD patterns of interstratified I/S do not necessarily contain chemically distinct illite and smectite layers.

Transmission electron microscopy (TEM), and in particular, high resolution transmission electron microscopy (HRTEM) has been the preferred analytical method of numerous workers attempting to resolve the discrepancies outlined above. HRTEM studies of dispersed I/S (for example **Bell, 1986; Klimentidis and Mackinnon, 1986; Vali and Köster, 1986**) appear to indicate the presence of MacEwan crystallites as they show R1-ordered packets of I/S that are thicker than fundamental particles. These studies were not fully conclusive, however, because they could not demonstrate whether the observed packets were parts of the same single crystal or different crystals which, during sample preparation, became stacked by chance.

After studying ion-thinned chips of shales, **Ahn and Peacor (1986)** stated that I/S are discrete megacrystals of illite and smectite tens of silicate layers thick. They interpreted interstratification as an artifact resulting

from the disintegration of megacrystals in the course of x-ray sample preparation. Recently, Ahn and Peacor reinterpreted their observations (**Ahn and Peacor, 1989**) on the basis of computer simulations of **Guthrie and Veblen (1989a)**, and they now recognize megacrystals as ordered I/S crystals.

Huff et al. (1988), using analytical transmission electron microscopy (ATEM), showed that illite and partially collapsed smectite layers are intimately associated in a K-bentonite sample although they could not demonstrate ordering unambiguously. **Ahn and Buseck (1990)**, who used ultra-high resolution TEM imagery of ion thinned chips of shale and bentonite samples, showed coherently diffracting sample domains that are thicker than fundamental particles. They concluded that the smectite interlayers, being loosely bonded, are more easily cleaved than illite interlayers, and that thin flakes similar in thickness to fundamental particles can be derived during sample preparation. **Ahn and Buseck (1990)** as well, however, could not differentiate illite and smectite layers unambiguously. **Veblen et al. (1990)**, **Srodon et al. (1990)**, and **Lindgreen and Hansen (1991)** reported that illite/smectite ratios in undisturbed I/S as determined from HRTEM images are consistent with those from XRD. These workers deduced, as did **Ahn and Buseck (1990)**, that

fundamental particles are secondary crystallites that are separated along smectite interlayers of larger crystals.

In summary, most of the HRTEM data accumulated recently appear to provide support for the existence of MacEwan crystallites in I/S clays. However, none of these studies provides a clear understanding of whether or not the expanded interlayers in ordered I/S domains (or interfaces of fundamental particles) are smectitic. This is central to the controversy between the fundamental particle and the MacEwan crystallite models because ordered I/S is a single phase (i.e. illite) according to the fundamental particle model.

This chapter reports the results of an HRTEM study performed on dispersed portions of three, highly illitic, I/S samples treated with alkylammonium chloride ions whose XRD characteristics are reported in Chapter 2. Alkylammonium ion treatment has proven to provide a stable expansion of expandable interlayers under HRTEM conditions (**Rühlicke and Niederbudde, 1985; Bell, 1986; Klimentidis and Mackinnon, 1986; Vali and Köster; Marcks et al. 1989; Ghabru et al., 1989**) even though it causes some disruption of the original clay fabric in the process (**Lee and Peacor, 1986**). Stable expansion of expandable interlayers is vital since positive differentiation of illite and smectite layers is very difficult otherwise, even if ultra-high

resolution TEM is used (**Ahn and Buseck, 1990**). Furthermore, the type of structural arrangement adsorbed alkylammonium ions adopt can be inferred from the thickness of expanded interlayers on HRTEM images which, in turn, can be used to estimate whether the layer charge density of the expandable layers is smectitic or vermiculitic (**Marcks et al., 1989; Olis et al., 1990**). The results reported here demonstrate that alkylammonium expansion coupled with the dispersion technique used provides an excellent tool for the HRTEM characterization of the physical nature of the dispersed I/S.

EXPERIMENTAL PROCEDURE

Samples

Three highly illitic samples were selected for study by high resolution transmission electron microscopy (HRTEM). Sample SI-47 has incomplete R2 (R=1.5) ordering with about 83% illite layers (Figs. 9a and b; Chapter 1). This sample has also been modeled as a mixture of R1 and R2 (R1/R2) or R1 and R3 (R1/R3) ordered I/S with around 77% illite layers (Figs. 9c and d; Chapter 1), and so will simply be referred to as sample R>1 in the following discussion. According to XRD, both of the other two samples, WDH-68 and NI6, are long-range ordered (R3), and have 90% and >95% illite layers, respectively (Figs. 12c and d; Chapter 1).

These samples were selected for TEM study because of the following characteristics:

1) Their <0.2μm fractions are essentially pure I/S with only a trace of chlorite in sample NI6.

2) They form a series of increasing illite content from around 80% to >95% as well as increasing degree of ordering, and thus provide an opportunity to study and document the nature of different I/S ratios at high resolution.

3) As shown in Chapter 2, the XRD characteristics of sample WDH-68 and NI6 indicate the presence of vermiculite-

like domains when treated with long-chain alkylammonium chloride ions. TEM images of alkylammonium-treated portions of these samples have the potential of not only showing whether or not such domains exist as structural entities, but also of revealing the layer charge nature of the illite particle interfaces.

The chemical compositions of these three samples are presented in Table 2, Chapter 1. The trends in interlayer occupancy of K based on these analyses are consistent with the proportions of illite as determined by computer modeling of XRD data, and indicate a K content of about 0.75 cations per illite interlayer. Sample R>1 is studied by HRTEM both untreated as wellas after alkylammonium ion exchanged.

Sample preparation

Samples for TEM were prepared by a technique modified from those of **Vali and Köster (1986)** and **Marchs et al. (1989)**. The technique is designed to minimize the formation of aggregates or clumps so that the primary intracrystallite (or intraparticle) features of dispersed sample domains could be observed without ambiguity. In view of some studies that conclude that interstratification in I/S is merely an artifact due to aggregation of fundamental particles during XRD sample preparation (**Nadeau et al., 1984; 1985**), an HRTEM study of I/S clays in a dispersed and

aggregate-free system seems to be as important as, and complementary to, the HRTEM studies of I/S processed to preserve the original clay fabric (**Ahn and Buseck, 1990; Srodon et al., 1990**). An outline of the procedure is as follows:

1) The <0.2μm fractions of the samples were obtained as overflow suspensions by centrifugation of coarse, Na-saturated sample suspensions using a Sharples supercentrifuge.

2) Sample suspensions of the <0.2μm fractions were concentrated by repeated settling and decantation, and treated with long-chain alkylammonium ions: Sample R>1 treated with hexadecylammonium chloride ions (Nc=16), one R3 sample (WDH-68) with heptadecylammonium ions (Nc=17), and the other R3 sample (NI6) with hexadecylammonium ions. The alkylammonium treatment method follows essentially that of **Rühlicke and Köhler (1981)**, and is described in Chapter 2.

3) 20 to 30 mg of each sample suspension was ultrasonicly agitated for 1-2 minutes to ensure a homogeneous dispersion.

4) The ultrasonically-treated suspension was mixed in a ratio of about 1:5 by volume with epoxy resin (London-White) in a glass tube. The tube was closed with a stopper, and agitated for 1 minute in an ultrasonic bath, and then

left at room temperature overnight. Because suspended particles settle to the lower half of the tube after about 12 hours, the resin/water mixture in the upper half was readily decanted and fresh resin added before another ultrasonic treatment. This procedure was repeated 2-3 times until water bubbles, indicating the presence of water in the mixture, can not be detected following an ultrasonic treatment. In other words, ultrasonic treatment produces a homogeneous mixture of resin and suspended material provided little or no water is present.

5) About 5 ml of resin/sample suspension was poured into a mold and left to polymerize in an oven for 24 hours at 70°C. Polymerization was generally complete after about 15 hours.

6) The solid polymerized resin block was trimmed, and a pyramid tip was shaped (Fig. 1). Ultrathin sections <500Å thick were then cut from this pyramid shaped tip (Fig. 1) by ultramicrotomy.

7) Ultrathin sections were mounted on nickel/copper TEM grids and carbon coated.

The technique described above differs from previously reported techniques of dispersed sample preparation for TEM in that during the entire process clay particles are not allowed to dry into aggregates. In addition, other techniques involve centrifugation of the resin/sample mold

to obtain oriented aggregates of materials at the base of the resin block. The technique described here maintains a good degree of dispersion of particles. Moreover, the ultrathin sections have been cut from a part of the resin block (Fig. 1) where particle concentrations are lower as compared to the base of the block where particles are more likely to form aggregates due to settling. The principal advantage of imaging dispersed particles by TEM as opposed to imaging aggregates is that one can observe unambiguously 1) the size range of the dispersed particles, and 2) whether or not the discrete clay particles are interstratified (i.e. capable of intracrystalline expansion).

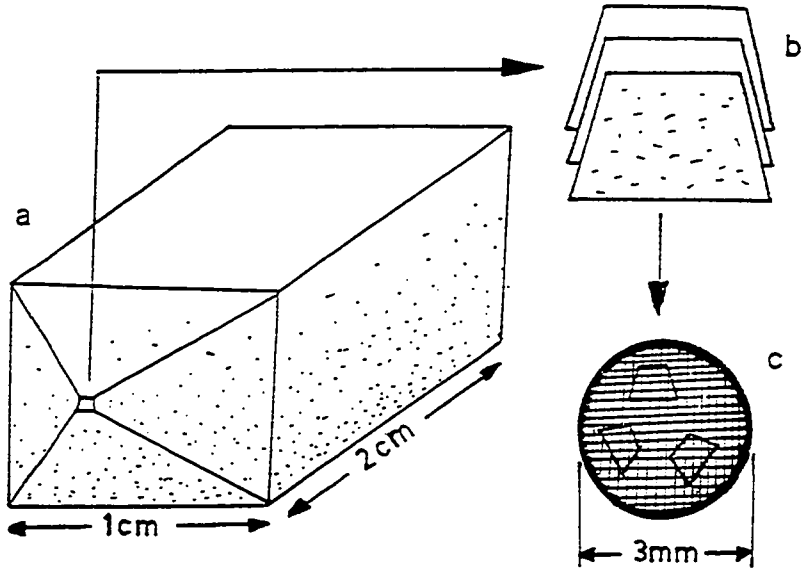

Figure 1: Trimmed resin block (a), and ultrathin microtome sections cut from the pyramid shaped tip before (b) and after mounting on a TEM grid (c).

Electron Microscopy

Electron microscopy was performed with a Philips CM20 transmission electron microscope (TEM). The microscope was operated at an accelerating voltage of 120 kV, and bright field (BF) images were obtained at various magnifications ranging from 10,000X to 300,000X. Most images, however, were obtained at a magnification of 115,000X using small size apertures (Objective Aperture=50 μm, Condenser Aperture=100 μm) to limit the image-forming beams to the 001 lattice fringes. The purpose of using smaller apertures was to suppress potentially confusing cross-fringes arising from hkl reflections. The extremely small size of particles on ultrathin sections, coupled with the high rate of beam damage of hydrous layer silicates, greatly impeded formation of selected area diffraction (SAD) patterns; only a few were obtained from rare large sample regions.

Lattice-fringe imaging was performed on numerous regions of ultrathin sections of each sample. Image contrast consistent with I/S ordering was best observed at relatively large values of overfocus, a result supported both by computer simulations and experimental studies (**Guthrie and Veblen, 1989a, 1989b; Veblen et al., 1990; Jiang et al., 1990**). These studies demonstrated that certain overfocus conditions enhance the lattice fringe contrast and make it possible to distinguish the illite and

smectite layers which, under optimum focus or underfocus conditions, show no significant contrast differences. Thus, most images were exposed at overfocus conditions in order to obtain enhanced lattice fringe contrast.

Tens of electron micrographs of several sample regions on ultrathin sections were obtained. Measurements such as lattice fringe counts and crystallite thicknesses were made directly on the image negatives by means of a Minolta RP605Z microfilm viewer with a magnification range of 13-27X.

RESULTS

Untreated, dispersed sample R>1

Figure 2 is a low-magnification TEM image showing an overwiew of the texture in the untreated, dispersed sample R>1. The region shown displays wavy, sub-parallel and closely spaced crystallites with lens-shaped openings in between them. Crystallites are mostly <0.2μm in their smallest dimension whereas they are as large as 2μm parallel to the direction of preferred orientation. The contrast variations over these crystallites, however, reveal that even the smallest crystallites are composed of smaller, closely attached crystallites with different orientations as well as thicknesses. These aggregates are most likely the portions of clay material that were not completely dispersed despite vigorous ultrasonic treatment.

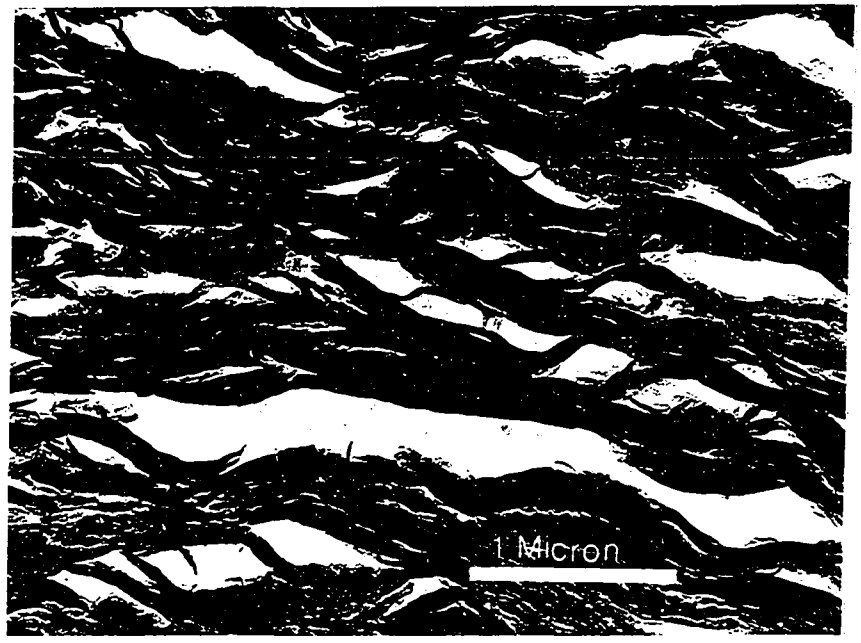

Figure 2: Low-magnification TEM micrograph of sample R>1 showing the texture in a localized aggregate of I/S crystallites. The variable contrast over individual crystallites reveals the presence of smaller crystallites.

The bulk of the sample is represented by individual crystallites or particles that are mostly <1000Å in their longest dimension, thus requiring HRTEM magnification for details of their extremely fine structure. BF lattice fringe images of sample R>1 obtained under HRTEM conditions are shown in Figures 3-6.

Three principal modes of occurrence of silicate ayers have been observed in the lattice fringe images:

1) Packets of straight, 10Å thick light fringes that alternate with thin, dark fringes (Fig. 3). These packets, which usually have >4 layers, are bordered by heavier dark fringes, and are interpreted to consist of illite layers. It is possible, however, that some of the layers are collapsed smectite.

2) Packets in which somewhat wavy, light fringes about 12Å thick alternate with heavier dark fringes (Fig. 3). These are interpreted as packets of partially collapsed smectite. They are much less common than illite packets.

3) Packets or units only 2, 3, or 4 illite fringes thick that are separated by smectite fringes. Figure 3 shows two such units composed of one illite fringe (20Å thick). Sample areas dominated by these smaller units are interpreted as ordered I/S domains. The units displaying the sequences ...SIS..., ...SIIS..., and ...SIIIS... are designated as R1, R2, and R3, respectively, where S

Figure 3: HRTEM image showing all three modes of occurence of silicate layers in sample R>1 : 1) An illite packet (arrows on the left) consisting of six layers (number of interlayers + 1). The average distance between the dark fringes in the packet is 10Å; 2) A smectite packet (arrows on the right) consisting of eight layers. The average distance between the dark fringes in the packet is about 12Å; and 3) Two fairly obvious, ordered I/S units, each 20Å thick. Also shown are a 12Å silicate unit and a low-angle crystallite boundary (arrow on top).

corresponds to heavier dark smectite fringes and I to less intense (thinner) dark fringes of illite (Figs. 4a and b). These interpretations are consistent with computer simulations of **Guthrie and Veblen (1989a, 1989b)** who showed that heavier dark fringes correspond to smectite interlayers while less intense dark fringes correspond to illite interlayers.

Most of the imaged sample regions are composed of mixtures of ordered I/S units similar to those shown in Figure 4. Sample R>1 thus does not appear to have a perfectly ordered structure, consistent with XRD characteristics of the sample.

Larger and possibly slightly thicker regions of sample R>1 also display periodicities due to various modes of ordering. Figure 5 is an overview of such an area which also illustrates that some of the layers bend or terminate, producing a ropy texture; non-imaged portions of the sample are probably due to non-alignment of the beam and to radiation damage.

In addition to basal lattice fringes arising from 001 reflections, some images show 4.5Å cross-fringes formed by hkl reflections. Figure 6 shows 4.5Å cross-fringes in an image obtained under overfocus conditions to enhance contrast of basal fringes. **Veblen et al. (1990)** showed that images with the clearest cross-fringes do not display

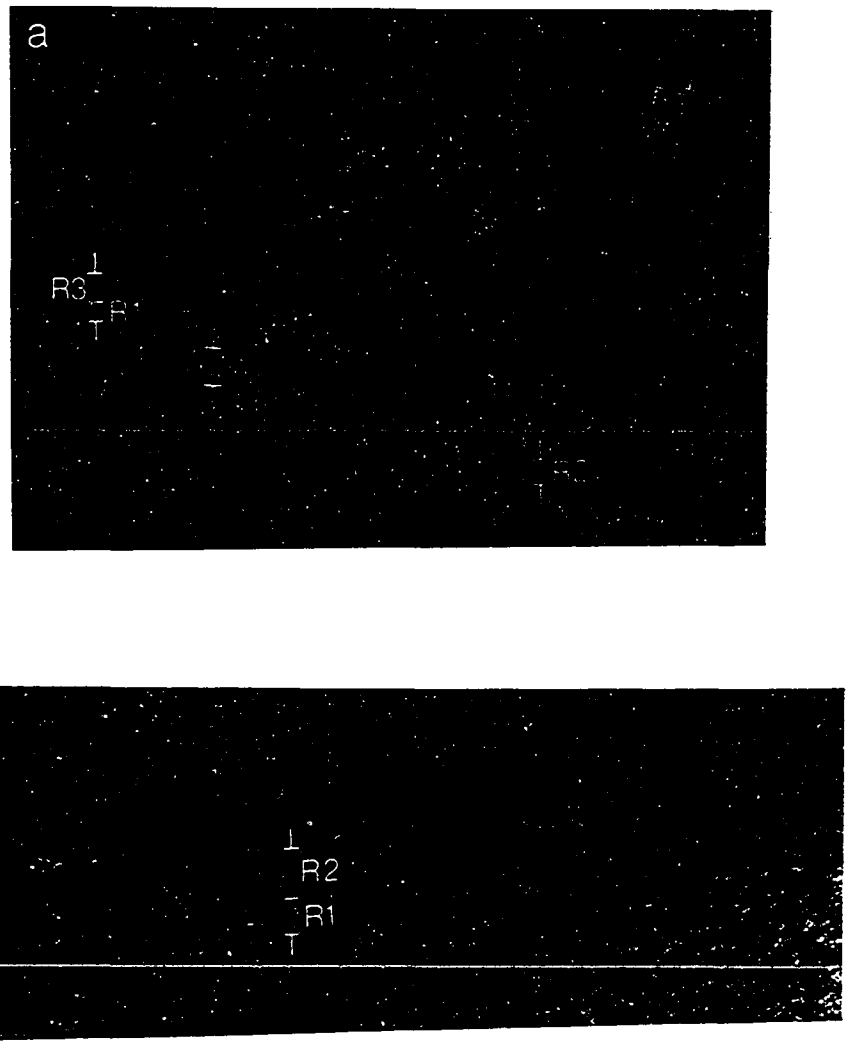

Figure 4: HRTEM image obtained near a crystallite edge in sample R>1. a) Ordered R1, R2 and R3 sequences (see text for discussion) . A single layer unit (S) and a 60Å thick, apparently coherent packet of illite layers are also shown. b) Enlargement of a region near the lower left corner of (a) showing adjacent R1 (20Å) and R2 (30Å) units not apparent in (a).

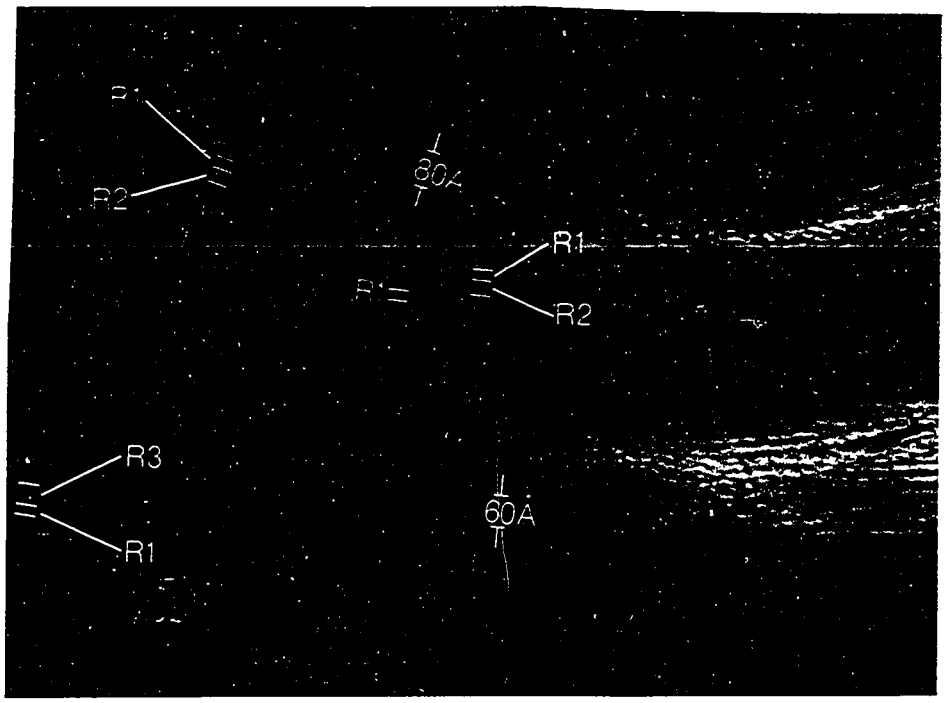

Figure 5: An overview of a relatively large and thicker area in sample R>1 showing R1, R2, and R3 units. A few thicker illite packets are also shown. Note bending and layer terminations, producing a ropy texture.

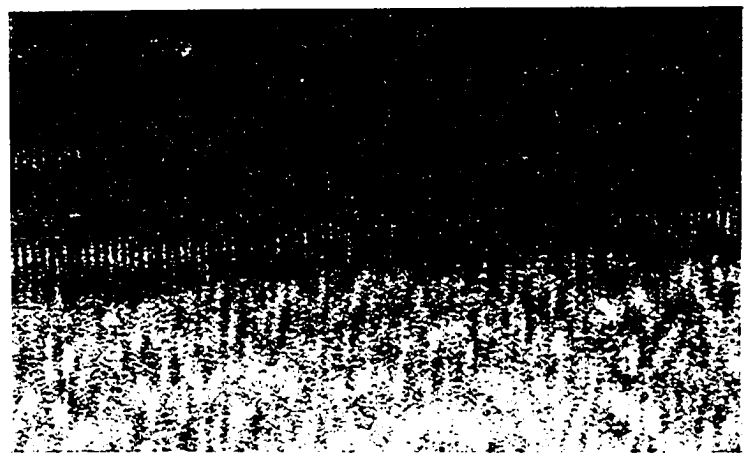

Figure 6: Enlargement of a HRTEM image from sample R>1 showing 4.5Å cross-fringes. Poorly defined basal fringes of an 30Å unit are also indicated. Note that cross-fringes are well over ten 2:1 silicate layers thick. Basal fringes become less apparent toward the top margin of the image due to underfocus.

basal fringes. The highly enhanced contrast of the 4.5Å cross-fringes in Figure 6 coupled with poorly developed basal fringes (i.e 30Å periodicity shown) suggest that this region of the sample was slightly underfocused, most likely due to warping or twisting. Nevertheless, the extent of cross-fringes, however obtained, can be used to asses the nature of stacking of silicate layers (**Veblen et al., 1990**). Most of the cross-fringes observed in sample R>1 extend over several 2:1 layers (well over ten layers in Fig. 6), and demonstrate coherent stacking of ordered domains.

Alkylammonium ion-treated, dispersed I/S

As noted before, portions of sample R>1, SI-47, as well as two, R3 ordered samples, WDH-68 and NI6, were also prepared for study with TEM after they were treated with long-chain alkylammonium chloride ions. XRD patterns of the alkylammonium treated portions of these samples are shown in Figure 7.

Ultrathin sections of these three samples are dominated by extremely small, isolated particles, mostly several hundred angstroms thick parallel to the c^*-axis, indicating a good degree of dispersion. Because of the extremely small particle size and thickness, imaging was performed at high magnifications, usually over 115,000X.

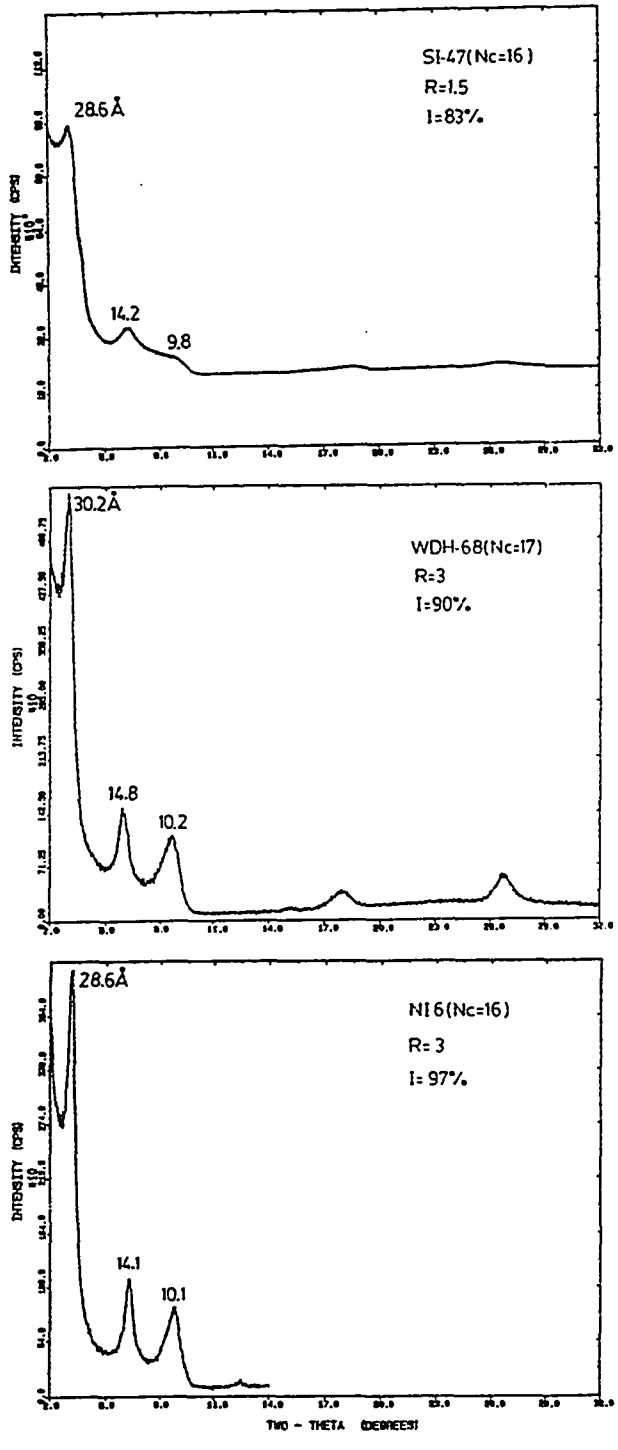

Figure 7: XRD patterns of alkylammonium ion-treated samples used for TEM study. a) Sample R>1 (SI-47) treated with hexadecylammonium chloride ions; b) R3 ordered sample WDH68 treated with heptadecylammonium ions; c) R3 ordered sample NI6 treated with hexadecylammonium ions.

Sample R>1: Figure 8 shows a relatively low-magnification image (88,000X) of two clay particles from sample R>1 that are 300-350Å thick parallel to c^*-axis. This image also shows that these two particles tend to part orseparate into smaller packets or units that are mostly 20, 30, or 40Å thick from one edge to the other (Fig. 9). Although particles consisting of several of these packets are common, single dispersed packets are not encountered in any of the ultrathin sections imaged here.

Higher magnification images and enlargements of low-magnification images reveal that the light fringes which define packet boundaries within larger crystallites or particles represent alkylammonium expanded interlayers. They are mostly 15-16Å thick (Fig. 10) in more stable crystallite interiors and tend to be larger (as large as 20Å) near crystallite edges (Figs. 8, 9 and 10).

An important observation made for alkylammonium treated sample R>1 is that no area recorded on any of the images shows 10Å periodicity, like those shown in Figures 3 and 4, typical of illite layers. Computer simulations of **Guthrie and Veblen, 1989a, 1989b**) showed that sequences of I and S can be observed only under special conditions of crystal thickness, crystal orientation, and microscope focus. Thus, several attempts using various crystal

Figure 8: HRTEM image of hexadecylammonium chloride-treated sample R>1 showing clay particles composed of expanded interlayers (light fringes indicated by arrows) and packets of clay.

Figure 9: HRTEM image of an isolated crystallite or particle and measured packet thicknesses in hexadecylammonium chloride-treated sample R>1. Despite alkylammonium exchange and vigorous ultrasonic treatment, disintegration of crystallites into packets along expanded interlayers are apparent only near particle edges (arrows).

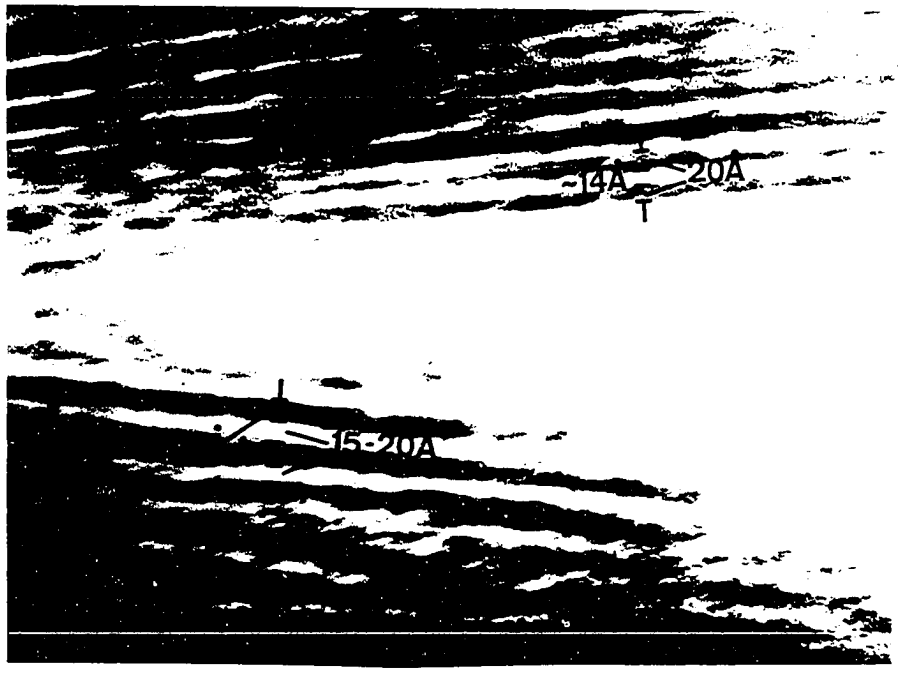

Figure 10: Enlargement of an HRTEM image from hexadecylammonium chloride-treated sample R>1 showing thickness of interlayers (light fringes) and clay packets.

orientations and microscope focus conditions were made. These failed to produce a 10Å periodicity, even though the thickness of the tens of measured packets consistently were integral multiples of 10 (i.e. 20Å, 30Å, 40Å, etc.). It, therefore, seems likely that microtome sections of sample R>1 were not thin enough to render properly oriented crystallites capable of producing a 10Å periodicity.

The XRD pattern of alkylammonium-treated sample >1 (Fig. 7a) exhibits a reflection at about 30Å which to a first approximation suggests the presence of expanded layers of a similar periodicity. In TEM images of sample R>1, however, a 30Å periodicity (i.e a 10Å silicate layer + a 15-20Å expanded interlayer=25-30Å) is not seen. On this basis, it appears that the few packets of smectite-like layers observed in sample R>1 prior to alkylammonium treatment, such as the one shown in Figure 3, must indeed comprise a very small volume in the bulk sample.

R3 ordered samples: HRTEM images of two, R3 ordered samples, WDH-68 and NI6, treated with heptadecylammonium and hexadecylammonium ions, respectively, are in general similar to those of alkylammonium treated sample R>1. However, the R3 samples have several distinct characteristics (Figs. 11, 12, and 13):

1) The intraparticle clay packets measured are mostly over 40Å, thicker than those of R>1 sample. These packets

are apparently coherently stacked, though some pinch out or terminate (Fig. 11b).

2) Alkylammonium expanded interlayers are less variable, with a spacing around 20Å. This spacing suggests a more homogeneous cation density in the interlayers. Expanded interlayers >20Å as well as only 10Å, however, are also observed (Fig. 13).

3) In contrast to sample R>1, both a 10Å single layer periodicity and a 30Å expanded layer periodicity are observed in both R3 samples (Figs. 12 and 13). In deed, several images contain comparatively large sample regions of 30Å lattice fringe periodicity (Fig. 12). This observation is important because it confirms the presence of 30Å expanded layers inferred from XRD.

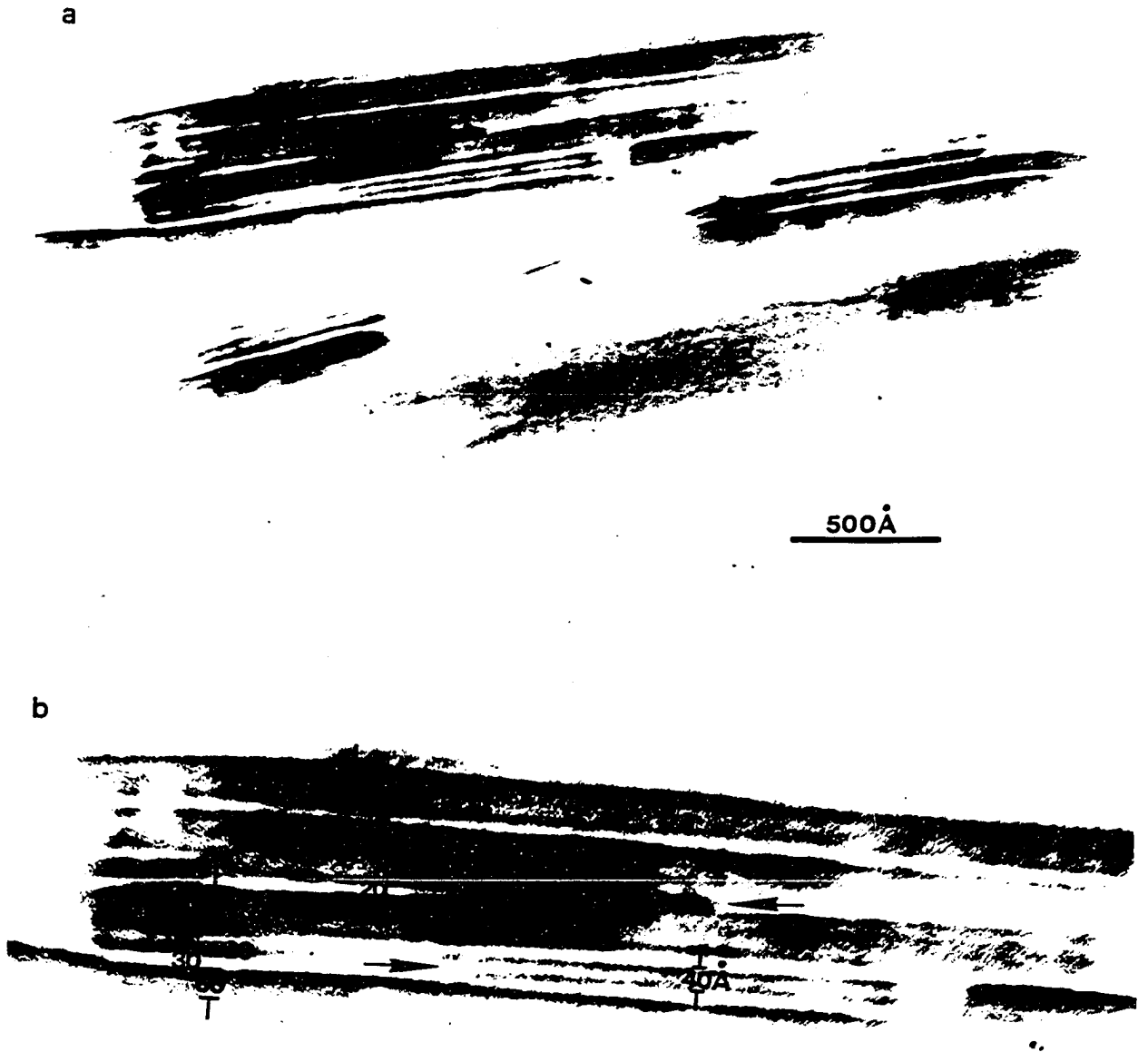

Figure 11: a) TEM image of heptadecylammonium chloride-treated R3 ordered sample WDH-68 showing dispersed crystallites that contain expanded interlayers. b) Enlargement of part of (a) showing the thickness of illite packets and expanded interlayers. Note irregularities in the stacking such as subparallelism or termination of packets (shown by arrows).

Figure 12: HRTEM image of heptadecylammonium-treated R3 ordered sample WDH-68 showing a region with 30Å lattice fringe periodicity in addition to thicker illite packets with 20Å expanded interlayer in between them.

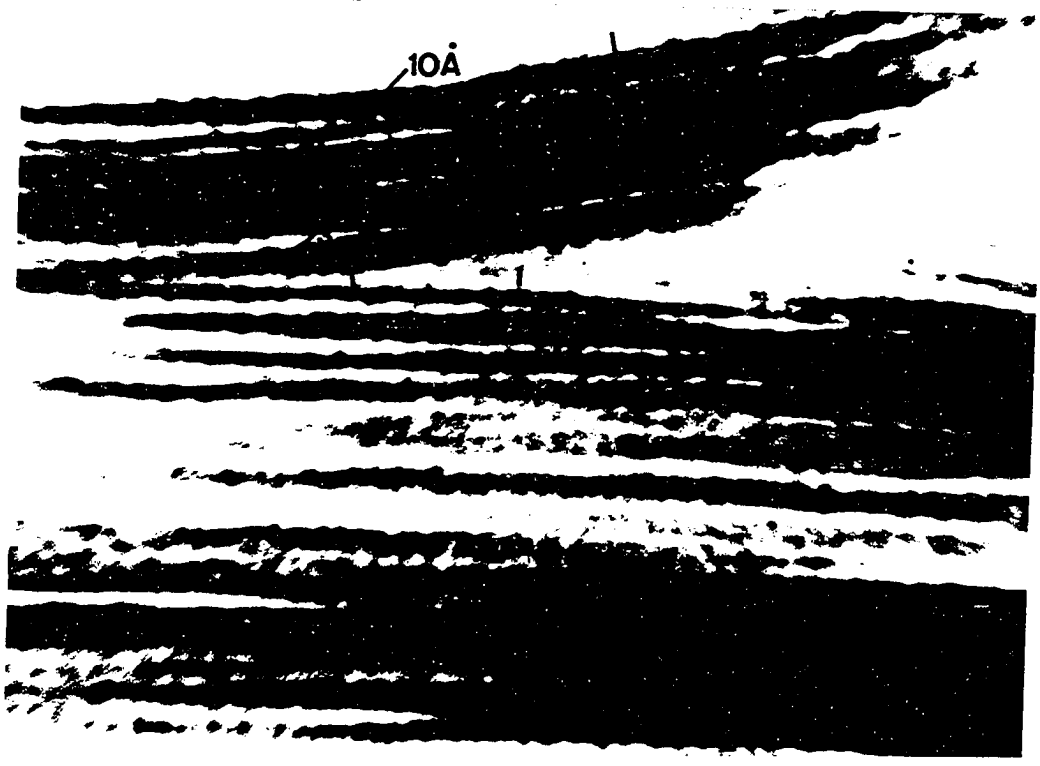

Figure 13: HRTEM image of hexadecylammonium chloride-treated R3 ordered sample NI6 showing two clay particles in contact. Note the presence of expanded layers giving rise to 20-30Å periodicity in addition to rather regular stacks of mostly 40Å thick illite packets.

DISCUSSION

Interpretation of HRTEM images and their implications for the structure of illitic I/S

HRTEM images of sample R>1 are dominated by crystallites showing 20Å, 30Å, and 40Å lattice fringe contrast, interpreted to correspond to R1, R2, and R3 ordered I/S units, respectively (Figs. 4, and 5). This interpretation, in which heavier dark fringes are viewed as smectite interlayers (Figs. 3, 4, and 5), is in accordance with computer simulations (**Guthrie and Veblen, 1989a, 1989b**). It is also supported by HRTEM images of hexadecylammonium chloride-treated portions of sample R>1 which show expanded interlayers in crystallites built mostly of 20, 30, and 40Å thick units (Figs. 8, 9, and 10).

There are, however, two other possibilities for interpretation of these observations. The first possibility involves the results of **Iijima and Buseck (1978)**, who showed that lattice fringes with 20Å and 30Å periodicities may also result from polytypic periodicities in 2M and 3T mica polytypes, respectively. However, because the XRD pattern obtained for the <0.5μm fraction of sample R>1 does not show either 2M or 3T reflections (Fig. 13, Chapter 1), these polytypes cannot be responsible for all 20Å and 30Å periods observed on the TEM images. Furthermore, small objective aperture size used for microscopy minimizes

multiple diffraction caused by hkl reflections, which is the main source of polytypic TEM periods (**Iijima and Buseck, 1978**). Finally, it is difficult to attribute the extensive presence of 20Å, and 30Å periods to polytypes as such polytypic periods require tilting around a specific crystallographic axis with respect to the electron beam (**Iijima and Buseck, 1978**).

The second possibility is that lattice fringes with 20-40Å periodicities, or measured units or packets of similar thicknesses in alkylammonium-treated samples may be due to stacked illite particles (**Nadeau et al. 1984, 1985**). This possibility is also considered unlikely because of the considerations presented below.

Several images containing 4.5Å cross-fringes in sample R>1 (Fig. 6) suggest that the range of coherent stacking across silicate layers is invariably larger than the illite particle thicknesses observed in I/S of similar composition (see particle distributions reported in **Nadeau et al., 1985**). This observation is in agreement with the recent studies of **Ahn and Buseck (1990)** and **Veblen et al. (1990)** which also indicated that the range of coherent stacking exceeds the size of fundamental particles.

The longest dimension of most crystallites observed on images of all three samples are <1000Å, significantly smaller than the average particle lengths observed in

highly illitic, completely dispersed I/S samples (about 3000Å; Table 2; **Nadeau, 1985**). This suggests that the degree of dispersion achieved in the present samples is very good. Despite this, however, discrete particles similar in thickness to the particles reported for highly illitic I/S (50-90Å thick; Table 2; **Nadeau, 1985**) are not observed. Instead, dispersed particles appear to consist of several units or packets very similar in thickness to the illite particles that **Nadeau (1985)** observed (Figs. 8, 9, 11, and 13). The thickness of these dispersed particles coupled with their intraparticle expansion behavior (i.e. in Fig. 11) strongly suggest that fundamental particles are secondary, not primary, crystallites produced by disintegration of larger crystallites along smectite interlayers.

Nadeau et al. (1984, 1985) attributed the interstratified XRD behavior of I/S clays to interparticle diffraction effects of fundamental particles whose interfaces adsorb ethylene glycol. On the basis of the dominating intraparticle expansion behavior of dispersed particles, it is concluded that intraparticle or intracrystalline expansion, rather than interparticle diffraction (or expansion) is largely responsible for the interstratified XRD behavior of the highly illitic I/S minerals studied.

Layer charge density as inferred from alklyammonium expanded interlayer thicknesses on HRTEM images

The alkylammonium ions in the expanding interlayers of 2:1 layer silicates can be arranged in monolayers (≈4Å), bilayers (≈8Å), pseudotrimolecular layers (≈12Å) and paraffin type structures (12-25Å) (**Lagaly and Weiss, 1969, 1976**). Weiss and coworkers showed that adsorption of alkylammonium ions by 2:1 expanding silicates proceeds by a cation exchange reaction, and developed the alkylammonium ion exchange method (Appendix A). This method allows both the magnitude and the distribution of layer charge density to be determined using the relationship between the type of alkylammonium arrangement as inferred by XRD basal spacings and the alkylammonium chain length.

An extensive determination of the distribution of layer charge in bulk samples requires preparation of complexes from several alkylammonium ions. However, a practical estimation of the range of layer charge density is possible by inferring the type of alkylammonium arrangement fro expanded interlayer thicknesses on HRTEM images. Several recent HRTEM studies have indeed proven the utility of such a technique by confirming the XRD basal spacings observed for monomineralic smectite and vermiculite directly on high resolution images (**Vali and Köster, 1986; Rühlicke and Niederbudde, 1985; Ghabru et al., 1989; Marcks**

et al., 1989). In the present study, hexadecylammonium (Nc=16) and heptadecylammonium (Nc=17)ions have been used to form expanded complexes of I/S. Both XRD and HRTEM spacings for long-chain alkylammonium (Nc=16-18) complexes of smectite and vermiculites of the previously cited studies have been utilized to serve as quidelines.smectites and vermiculites have been utilized to serve as guidelines.

Tens of measurements on TEM images show that the expanded interlayer thicknesses observed for sample R1 are predominantly 15-16Å thick in more stable crystallite interiors, indicating bilayer to pseudotrimolecular arrangement of alkylammoniums. Such arrangements have previously observed for natural high-charge smectite (0.45-0.60) and low-charge vermiculite (0.50-0.70) samples (Lagaly and Weiss, 1976; Lagaly, 1982). On the other hand , expanded interlayers as large as 20Å are also observed near crystal edges. Because many crystallites exhibit a dispersion-related "loose" texture near their edges whether or not these 20Å interlayers represent high charge vermiculitic interlayers can not be determined with certainty.

The expanded interlayers observed in the two R3 ordered samples are predominantly 20Å or thicker, strongly suggesting the presence of high-tilt paraffin type structures typically observed in monomineralic high charge

vermiculites (0.7-0.9; **Ghabru et al., 1989; Marcks et al., 1989**). The R3 ordered samples also show domains with 30Å lattice fringe contrast due to 20Å expanded interlayers alternating with 10Å thick silicate layers. This result is consistent with XRD data which suggested the presence of segregated vermiculite-like domains in highly illitic I/S samples (Fig. 7; see also Chapter 2).

On the basis of the present results, it appears that the layer charge density of what has been characterized as a smectite component in R3 ordered interstratified I/S minerals is actually vermiculitic. It is important to note that this distinction is made strictly with regard to the layer charge density. In other words, a vermiculitic charge is not intended to imply a trioctahedral structure, customarily assumed for vermiculites, in the highly illitic samples studied.

CONCLUSIONS

A suite of fourteen samples of Paleozoic K-bentonites, which effectively spans the entire range of commonly occurring illite/smectite (I/S) compositions and ordering types, has been characterized by x-ray diffraction (XRD), x-ray fluorescence spectroscopy (XRF), high resolution transmission electron microscopy (HRTEM), and alkylammonium ion exchange. The conclusions drawn from the data presented and discussed in the foregoing chapters are as follows:

1) In K-bentonites, I/S clays with less than about 50% illite occur principally as randomly (R0) interstratified mixtures. I/S clays in the composition range 50-85% illite are mostly mixtures either of randomly interstratified and short-range (R1) ordered domains or of intermediate-range (R2) and long-range (R3) ordered I/S domains. I/S clays with 100% rectorite-like R1 ordering and complete R2 ordering, such as those observed in hydrothermally altered bentonites (**Bethke and Altaner, 1986**), are not found in nearly 100 Paleozoic K-bentonite samples that have been studied. I/S clays with ≥90% illite occur as long-range (R3) ordered mixtures.

2) A progressive sequence of illite polytypes from $1M_d$ to 1M to $2M_1$ is observed in the range R0 to R3. 1Md is the prevailing illite polytype during much of the smectite-to-

illite conversion. 1M and $2M_1$ become the dominant polytypes after the proportion of illite exceeds about 80%,

3) The increases in the amount of tetrahedral Al^{+3} for Si^{+4} substitution and the amount of K are the principal controlling factors responsible for the increases in the proportion of illite and the degree of ordering in I/S.

4) On the basis of chemical analyses and XRD data, the illite component of I/S is found to have a fixed-K content of about 0.76 cations per layer. Extrapolation of these data point to a precursor smectite, montmorillonitic in composition, and to an end-member ilite, phengitic in composition.

5) The chemical and XRD data are consistent with a layer-by-layer transformation mechanism of smectite to illite in which randomly distributed high-, intermediate-, and low-charge interlayers of a precursor smectite preferentially incorporate K^+ ions in response to an increasingly negative tetrahedral charge.

6) The alkylammonium ion exchange method of layer charge characterization is applicable to a wide range of I/S compositions. The charge densities and distributions in I/S with >15% expandabilities are characteristic of smectite. This result provides compelling evidence for the two-

component nature of I/S in this range; it also provides strong support for the layer-by-layer transformation mechanism in which the expandable layers in I/S retain their smectitic charge. The neoformation mechanism proposed for the formation of illite in bentonites(**Nadeau et al., 1985; Nadeau and Bain, 1986**) appears to be unlikely because such a mechanism requires precipitation of illite particles with surface charges significantly higher than that of a typical smectite.

7) The XRD data for alkylammonium exchanged I/S with <15% expandabilities indicate the presence of domains of expandable layers with charges between 0.6 and 0.9 equivlents, characteristic of vermiculite. In deed, the presence of such domains has been confirmed by the HRTEM images of these clays. Also, the expandable interlayers between the illite packets or surfaces of illite particles (**Nadeau et al. 1985**) have, as inferred from their alkylammonium expanded thicknesses on HRTEM images, a vermiculitic rather than smectitic charge. Therefore, what has been frequently described as highly illitic I/S both in the literature and in this dissertation can actually be better and more correctly characterized as illite/vermiculite, the term vermiculite being applied strictly in the sense of layer charge density.

8) The HRTEM observations suggest that the fundamental particles postulated by Nadeau and coworkers are predominantly, if not all, secondary crystallites produced by disintegration of interstratified crystallites along the expandable interlayers.

REFERENCES CITED

Aagaard, P. and Helgeson, H.C. (1983) Activity composition relations among silicates and aqueous solutions: II. Chemical and thermodynamic consequences of ideal mixing of atoms on homological sites in montmorillonites, illites, and mixed-layer clays. Clays and Clay Minerals, 31, 207-217.

Ahn, J.H. and Buseck, P.R. (1990) Layer-stacking sequences and structural disorder in mixed-layer illite/smectite: image simulations and HRTEM imaging. American Mineralogist, 75, 267-275.

Ahn, J.H. and Peacor, D.R. (1986) Transmission and analytical electron microscopy of the smectite-to-illite transition. Clays and Clay Minerals, 34, 165-179.

Ahn, J.H. and Peacor, D.R. (1989) Illite/smectite from Gulf Coast shales: A reappraisal of transmission electron microscope images. Clays and Clay Minerals, 37, 542-546.

Altaner, S.P., Hower, J., Whitney, G. and Aronson, J.L. (1984) Model for K-bentonite formation: evidence from zoned K-bentonites in the disturbed belt, Montana. Geology, 12, 412-415.

Altaner, S.P. and Bethke, C.M. (1988) Interlayer order in illite/smectite. American Mineralogist, 73, 766-774.

Altaner, S.P., Weiss, C.A.Jr. and Kirkpatrick, R.J. (1988) Evidence from ^{29}Si NMR for the structure of mixed-layer illite/smectite clay minerals. Nature, 331, 699-702.

Austin, G.S., Glass, H.D. and Hughes, R.E. (1989) Resolution of polytype structure of some illitic clays minerals that appear to be 1Md. Clays and Clay Minerals, 37, 128-134.

Bailey, S.W. (1980) Summary of recommendations of AIPEA Nomenclature Committee. Clays and Clay Minerals, 28, 73-78.

Beawers, A.H. and Larsen, B.L. (1953) Electrophoresis of clays by the Schlieren moving boundary procedure. Soil Sci. Soc. Ame. Proc., 17, 22-25.

Bell, T.E. (1986) Microstructure in mixed-layer illite/ smectite and its relationship to the reaction of smectite to illite. Clays and Clay Minerals, 34, 146-154.

Bethke, C.M. and Altaner, S.P. (1986) Layer-by-layer mechanism of smectite illitization and application to a new rate law. Clays and Clay Minerals, 34, 136-145.

Bethke, C.M., Vergo, N. and Altaner, S.P. (1986) Pathways of smectite illitization. Clays and Clay Minerals, 34, 125-135.

Boles, J.R. and Franks, S.G. (1979) Clay diagenesis in Wilcox Sandstones of southwest Texas: implications of smectite diagenesis on sandstone cementation. J. Sed. Petrol., 49, 55-70.

Brindley, G.W. and Hoffman, R.V. (1962) Orientation and packing of aliphatic chain molecules on montmorillonite. Clays and Clay Minerals, 9, 546-556.

Brusewitz, A.M. (1986) Chemical and physical properties of Paleozoic potassium bentonites from Kinnekule, Sweden. Clays and Clay Minerals, 34, 442-454.

Brusewitz, A.M. (1988) Asymmetric zonation of a thick Ordovician K-bentonite bed at Kinnekule, Sweden. Clays and Clay Minerals, 36, 349-353.

Burthner, R.L. and Warner, M.A. (1986) Relationship between illite/smectite diagenesis and hydrocarbon generation in Lower Cretaceous Mowry and Skull Creek Shales of the northern Rocky mountain area. Clays and Clay Minerals, 34, 390-402.

Burst, J.F. (1969) Diagenesis of Gulf Coast clayey sediments and its possible relation to petroleum migration. American Association of Petroleum Geologists Bulletin, 53, 73-93.

Byrne, R.J.S. (1954) Some observations on montmorillonite-organic complexes. Clays and Clay Minerals, 2, 241-253.

Carter, D.L., Heilman, M.D. and Gonzales, L.L. (1965) Ethylene glycol monoethyl ether for determining surface area of silicate minerals. Soil Science, 100, 356-360.

Dunoyer de Segonzac, G. (1970) The transformation of clay minerals during diagenesis and low-grade metamorphism: A review. Sedimentology, 15, 281-346.

Dyal, R.S. and Hendrics, S.B. (1950) Total surface of clays in polar liquids as a characteristic index. Soil Science, 69, 421-432.

Eberl, D.D. (1978) Reaction series for dioctahedral smectite. Clays and Clay Minerals, 26, 327-340.

Eberl, D.D. and Hower, J. (1976) Kinetics of illite formation. Geol. Soc. Ame. Bull., 7, 1326-1330.

Eberl, D.D. and Srodon, J. (1988) Ostwald ripening and interparticle-diffraction effects for illite crystals, American Mineralogist, 1335-1345.

Eberl, D.D., Srodon, J. and Northrop, H.R. (1986) Potassium fixation in smectite by wetting and drying. In Geochemical processes at mineral surfaces, J.A. Davis and K.F. Hayes (Eds.), American Chemical Society Symposium Series, 323, 296-326.

Eslinger, E. and Savin, S.M. (1973) Mineralogy and oxygen isotope geochemistry of the hydrothermally altered rocks of the Ohaki-Broadlands, New Zealand geothermal area. Ame. J. Sci., 273, 240-267.

Gibbs, R.J. (1968) Clay mineral mounting techniques for x-ray diffraction analysis. J. Pet. Sed., 38, 242-244.

Garrels, R.M. (1984) Montmorillonite/illite stability diagrams, Clays and Clay Minerals, 32, 161-166.

Ghabru, S.K., Mermut, A. and Arnaud, R.J.S. (1989) Layer charge and cation-exchange characteristics of vermiculite (weathered biotite) isolated from a gray luvisol in northeastern Saskatchewan. Clays and Clay Minerals, 37, 164-172.

Goulding, K.W.T. and Talibudeen, O. (1980) Heterogeneity of cation-exchange sites for K-Ca exchange in aluminosilicates. J. Colloid Interface Sci., 78, 15-24.

Grim, R.E., Bray, R.H. and Bradley, W.F. (1937) The mica in argillaceous sediments. American Mineralogist, 22, 813-829.

Günal, A. (1986) Clay mineralogy, petrography, chemical composition and stratigraphic correlation of some middle Ordovician K-bentonites in the eastern midcontinent. Ph.D. thesis, University of Cincinnati.

Guthrie, G.D. and Veblen, D.R. (1989) High-resolution transmission electron microscopy of mixed-layer illite/smectite: Computer simulations. Clays and Clay Minerals, 37, 1-11.

Guthrie, G.D. and Veblen, D.R. (1990) Interpreting one-dimentional high-resolution transmission electron micrographs of sheet silicates by computer simulation. American Mineralogist, 75, 276-288.

Harward, M.E., Carstea, D.D. and Sayegh, A.H. (1969) Properties of vermiculites and smectites: Expansion and collapse. Clays and Clay Minerals, 16, 437-447.

Hausler, W. and Stanjec, H. (1988) A refined procedure for the determination of layer charge with alkylammonium ions. Clay Minerals, 23, 333-337.

Hendricks, S.B. and Teller, E. (1942) X-ray interference in partially ordered layer lattices. J. Chemical Physics, 10, 147-167.

Hoffman, J. and Hower, J. (1979) Clay mineral assemblages as low-grade metamorphic geothermometers: Application to the thrust faulted disturbed belt of Montana, USA. Soc. Econ. Paleont. Mineral., Special Paper 26, 55-79.

Horton, D.G. (1985) Mixed-layer illite/smectite as a paleotemperature indicator in the amethyst vein system, Creede district, Colorado, USA. Contributions to Mineralogy and Petrology, 91, 171-179.

Hower, J. and Mowatt, T.C. (1966) The mineralogy of illites and mixed-layer illite/montmorillonites. American Mineralogist, 51, 825-854.

Hower, J., Eslinger, W.V., Hower, M., and Perry, E.A. (1976) Mechanism of burial metamorphism of argillaceous sediments: 1. Mineralogical and chemical evidence. Geol. Soc. Ame. Bull., 87, 725-737.

Hsieh, Y.D., Tsui, P.P. and Hsu, P.H. (1984) Expansion of smectites as a function of vapor pressure of ethylene glycol. Soil Sci. Soc. Ame. J., 48, 935-938.

Huff, W.D. and Türkmenoglu, A.G. (1981) Chemical characteristics and origin of Ordovician K-bentonites along the Cincinnati arch. Clays and Clay Minerals, 29, 113-123.

Huff, W.D., Whiteman, J.A. and Curtis, C.D. (1988) Investigation of a K-bentonite by x-ray diffraction and analytical electron microscopy. Clays and Clay Minerals, 36, 83-93.

Huff, W.D. and Morgan, D.J. (1990) Stratigraphy, mineralogy and tectonic setting of Silurian K-bentonites in southern England and Wales. Proceedings of the 9th International Clay Conference, Strasbourg, 1989, V.C. Farmer and Y.Tardy (Eds.), Sci. Géol. Mém., 88, 33-42, Strasbourg, 1990.

Inoue, A., Minato, H., and Utada, M. (1978) Mineralogical properties and occurrence of illite/montmorillonite mixed-layer minerals formed from Miocene volcanic glass in Wago-Omano district. Clay Science, 5, 123-136.

Inoue, A. and Utada, M. (1983) Further investigations of a conversion series of dioctahedral mica/smectites in the Shinzan hydrothermal alteration area, northeast Japan. Clays and Clay Minerals, 31, 400-412.

Inoue, A., Kohyama, W., Kitagaura, R., and Watanabe, T. (1987) Chemical and morphological evidence for the conversion of smectite to illite. Clays and Clay Minerals, 35, 111-120.

Inoue, A., Velde, B., Meuneir, A., and Touchard, G. (1988) Mechanism of illite formation during smectite-to-illite conversion series by scanning and transmission electron microscopes. American Mineralogist, 73, 1325-1334.

Jagodzinski, H. (1949) One-dimensional disorder in crystals and their influence on x-ray interferences: I. Calculation of the degree of disorder from the x-ray intensities. Acta Crystallographica, 2, 201-207.

Jiang, W.T., Peacor, D.R., Merriman, R.J. and Roberts, B. (1990) Transmission and analytical electron microscopic study of mixed-layer illite/smectite formed as an replacement of diagenetic illite. Clays and Clay Minerals, 38, 449-468.

Jonas, E.C. and Roberson, H.E. (1966) Structural charge density as indicated by montmorillonite hydration. Clays and Clay Minerals, 13, 223-230.

Jordan, J.W. (1949a) Organophilic bentonites: I. Swelling in organic fluids. J. Phys. Colloid Chem., 53, 294-306.

Jordan, J.W. (1949b) Alteration of the properties of bentonite by reaction with amines. Mineral Magazine, 28, 598-605.

Kakinoki, J. and Komura, Y. (1965) Diffraction by a one-dimensional disordered crystal. I. The intensity equation. Acta Crystallographica, 19, 137-147.

Keller, W.P. (1945) Calculating formulas for fine grained minerals on the basis of chemical analysis. American Mineralogist, 30, 1-26.

Keller, W.P. (1955) Interpretation of chemical analysis of clays. Clays and Clay Minerals, 1, 92-94.

Kemp, A.E.S., Oliver, G.J.H. and Baldwin, J.R. (1985) Low grade metamorphism and accretionary tectonics: Southern Uplands terrane, Scotland. Mineralogical Magazine, 49, 335-344.

Kittrick, J.A. (1984) Solubility measurements of phases in three illites. Clays and Clay Minerals, 32, 115-124.

Klimentidis, R.E. and Mackinnon, I.D.R. (1986) High-resolution imaging of ordered mixed-layer clays. Clays and Clay Minerals, 34, 155-164.

Lagaly, G. (1979) The layer charge of regular interstratified 2:1 clay minerals. Clays and Clay Minerals, 27, 1-10.

Lagaly, G. (1981) Characterization of clays by organic compounds. Clay Minerals, 16, 1-21.

Lagaly, G. (1982) Layer charge heterogeneity in vermiculites. Clays and Clay Minerals, 30, 215-222.

Lagaly, G. and Weiss, A. (1969) Determination of layer charge in mica-type layer silicates. Proceedings of the International Clay Conference, Tokyo, Japan, L. Heller (Ed.), 61-80.

Lagaly, G. and Weiss, A. (1976) The layer charge of smectitic layer silicates. Proceedings of the International Clay Conference, Mexico City, Mexico, 1975, 157-172.

Lagaly, G., Gonzales, M.F. and Weiss, A. (1976) Problems in layer-charge determination of montmorillonites. Clay Minerals, 11, 173-187.

Lee, J.H. and Peacor, D.R. (1986) Expansion of smectite by laurylamine hydrochloride: Ambiguities in transmission electron microscopy results. Clays and Clay Minerals, 34, 69-73.

Levinson, A.A. (1955) Studies in the mica group: Polytypes among illites among illites and hydrous micas. American Mineralogist, 40, 41-49.

Lindgreen, H. and Hansen, P.L. (1991) Ordering of illite-smectite in upper Jurassic claystones from the North Sea. Clay Minerals, 26, 105-125.

MacEwan, D.M.C. (1956) Fourier transform methods for studying scattering from lamellar systems: I. A direct method for analyzing interstratified mixtures. Kolloidzeitscrift, 149, 96-108.

MacEwan, D.M.C. (1958) Fourier transform methods for studying scattering form lamellar systems: II. The calculation of x-ray diffraction effects for various types of interstratification. Kolloidzeitschrift, 156, 61-67.

MacHardy, W.J., Wilson, M.J. and Tait, J.M. (1982) Electron microscope and x-ray diffraction studies of filamentous illitic clay from sandstone of the Magnus field. Clay Minerals, 17, 23-39.

Mackintosh, E.E., Lewis, D.G. and Greenland, D.J. (1971) Dodecylammonium-mica complexes: I. Factors affecting the exchange reaction. Clays and Clay Minerals, 19, 209-218.

Marcks, CH., Wachsmuth, H. and Reichenbach, H.G.V. (1989) Preperation of vermiculites for HRTEM. Clay Minerals, 24, 23-32.

Merriman, R.J., Roberts, B. (1990) Metabentonites in the Moffat Shale Group, Southern Uplands of Scotland: Geochemical evidence for ensialic marginal basin volcanism. Geological Magazine, 127, 259-271.

McAtee, J.L., Jr. (1958) Heterogeneity in montmorillonite. Clays and Clay Minerals, 5, 279-288.

McDowell, D.S. and Elders, W.A. (1980) Authigenic layer silicate minerals in borehole Elmore 1, Salton Sea geothermal field, California, USA. Contributions to Mineralogy and Petrology, 74, 293-310.

Meuneir, A. and Velde, B. (1989) Solid solutions in I/S mixed-layer minerals and illite. American Mineralogist, 74, 1106-1112.

Méring, J. (1949) L'intérference des rayons x dans les systems à stratification dé sordonnée. Acta Crystallographica, 2, 371-377.

Moore, D.M. and Reynolds, R.C.,Jr. (1989) X-ray diffraction and the identification and analysis of clay minerals, 332 p., Oxford University Press.

Mortland, M.M. (1970) Clay-organic complexes and interactions: In Brady, N.C.(Ed.), Advances in Agronomy. Academic Press, New York, 75-117.

Nadeau, P.H. (1985) The physical dimensions of fundamental clay particles. Clay Minerals, 20, 499-514.

Nadeau, P.H. and Reynolds, R.C., Jr. (1981) Burial and contact metamorphism in the Mancos shale. Clays and Clay Minerals, 29, 249-259.

Nadeau, P.H. and Bain, D.C. (1986) Compositions of some smectites and diagenetic illite clays and implications for their origin. Clays and Clay Minerals, 34, 455-464.

Nadeau, P.H., Tait, J.M., McHardy, W.J., and Wilson, M.J. (1984) Interstratified XRD characteristics of physical mixtures of elementary clay particles. Clay Minerals, 19, 67-76.

Nadeau, P.H., Wilson, M.J., MacHardy, W.J., and Tait, J.M. (1985) The conversion of smectite to illite during diagenesis: Evidence from some illitic clays from bentonites and sandstones. Mineralogical Magazine, 49, 393-400.

Newman, A.C.D. (1983) The specific surface of soils determined by water sorption. J. Soil Sci., 34, 23-32.

Olis, A.C., Malla, D.B. and Douglas, L.A. (1990) The rapid estimation of the layer charges of 2:1 expanding clays from a single alkylammonium ion expansion. Clay Minerals, 25, 39-50.

Perry, E.A. and Hower, J. (1970) Burial diagenesis in Gulf Coast pelitic sediments. Clays and Clay Minerals, 18, 165-177.

Philen, O.D., Jr., Weed, S.B. and Weber, J.B. (1971) Surface charge characterization of layer silicates by competitive adsorption of two organic divalent cations. Clays and Clay Minerals, 19, 295-302.

Radoslovich, E.W. (1963) The cell dimensions and symmetry of lattice layer silicates: 5. Composition limits. American Mineralogist, 46, 348-367.

Reynolds, R.C.,Jr. (1980) Interstratified clay minerals. In G.W. Brown and G. Brown (Eds.), Crystal structure of clay minerals and their x-ray identification, 249-303, Mineralogical Society, London.

Reynolds, R.C., Jr. (1985) NEWMOD: A computer program for the calculation of one-dimensional diffraction patterns of mixed-layer clays. R.C. Reynolds, 8 Brook Rd., Hanover, NH, 24p.

Reynolds, R.C., Jr. and Hower, J. (1970) THe nature of interlayering in mixed-layer illite-montmorillonites. Clays and Clay Minerals, 18, 25-36.

Rosenberg, P.E., Kittrick, J.A. and Sass, B.M. (1985) Implications of illite/smectite stability diagrams: A discussion. Clays and Clay Minerals, 33, 561-562.

Ross, C.S. and Hendricks, S.B. (1945) Minerals of the montmorillonite group, their origin and relation to soils and clays. U.S. Geol.Survey Prof. Paper, 205B, 23-79.

Rühlicke, G. and Köhler, E.E. (1981) A simplified procedure for determining layer charge by the n-alkylammonium method. Clay Minerals, 16, 305-307.

Rühlicke, G. and Niederbudde, E.A. (1985) Determination of layer-charge density of expandable 2:1 clay minerals in soils and loess sediments using the alkylammonium method. Clay Minerals, 20, 291-300.

Sakharov, B.A. and Drits, V.A. (1976) Mixed-layer kaolinite-montmorillonite. A comparison of observed and calculated diffraction patterns. Clays and Clay Minerals, 21, 15-17.

Sass, B.A., Rosenberg, P.F. and Kittrick, J.A. (1987) The stability of illite/smectite during diagenesis: An experimental study. Geochimica et Cosmochimica Acta, 51, 2103-2115.

Sawhney, B.L. (1967) Interstratification in vermiculite. Proceedings of 15th National Clay Conference, Pittsburgh, PA, 1966, S.W. Bailey (Ed.), 75-84.

Scharpf, D.C. (1990) Stratigraphy and associated faunas of the Middle Ordovician (Rocklandian) Millbrig K-bentonite in central Kentucky. Unpublished M.S. thesis, University of Cincinnati.

Shimoda, S. (1970) A hydromuscovite from the Shakanai mine, Akita prefecture, Japan. Clays and Clay Minerals, 18, 269-274.

Srodon, J. (1984a) Illite/smectite in low-temperature diagenesis: data from the Miocene of the Carpathian Foredeep. Clay Minerals,

Srodon, J. (1984b) X-ray powder diffraction identification of illitic materials. Clays and Clay Minerals, 32, 337-349.

Srodon, J. and Eberl, D.D. (1984) Illite. In Micas, S.W. Bailey (Ed.), Mineralogical Society of America Reviews in Mineralogy, 13, 495-544.

Srodon, J., Morgan, D.J., Eslinger, E., Eberl, D.D., and Karlinger, M.R. (1986) Chemistry of illite/smectite and end-member illite. Clays and Clay Minerals, 34, 368-378.

Srodon, J., Andreoli, C., Elsass, F., and Robert, M. (1990) Direct high-resolution transmission electron microscopic measurement of expandability of mixed-layer illite/smectite in bentonite rock. Clays and Clay Minerals, 38, 373-379.

Sutherland, H.H. and MacEwan, D.M.C. (1961) Organic complexes of vermiculite. Clay Minerals Bull., 4, 229-233.

Stull, M.S. and Mortier, W.J. (1974) The heterogeneity of the charge density in montmorillonites. Clays and Clay Minerals, 22, 391-396.

Talibudeen, O. and Goulding, K.W.T. (1983) Charge heterogeneity in smectites. Clays and Clay Minerals, 31, 37-42.

Theng, B.K.G., Greenland, D.J., and Quirk, J.P. (1967) Adsorption of alkylammonium cations by montmorillonites. Clay Minerals, 7, 1-17.

Vali, H. and Köster, H.M. (1986) Expanding behavior, structural disorder, regular and random irregular interstratification of 2:1 layer silicates studied by high-resolution images of transmission electron microscopy. Clay Minerals, 21, 827-859.

Vali, H. and Hesse, R. (1990) Alkylammonium ion treatment of clay minerals in ultra-thin sections: A new method for HRTEM examination of expandable layers. American Mineralogist, 75, 1445-1448.

Vali, H., Hesse, R. and Köhler, E.E. (1991) Combined freeze-etched replicas and HRTEM as tools to study fundamental particles and multi-phase nature of 2:1 silicates. American Mineralogist (preprint).

Veblen, D.R., Guthrie, G.D., Kenneth, J.T.L., Jr., and Reynolds, R.C., Jr. (1990) High-resolution transmission electron microscopy and electron diffraction of mixed-layer illite/smectite: Experimental results. Clays and Clay Minerals, 38, 1-13.

Velde, B. and Brusewitz, A.M. (1982) Metasomatic and nonmetasomatic low-grade metamorphism of Ordovician meta-bentonites in Sweden. Geochimica et Cosmochimica Acta, 46, 447-452.

Velde, B. (1985) Clay Minerals: A physico-chemical explanation for their occurrence. Elsevier, Amsterdam, 425p.

Velde, B. and Brusewitz, A.M. (1986) Compositional variation in component layers in natural illite/ smectite. Clays and Clay Minerals, 34, 651-657.

Walker, G.F. (1967) Interactions of n-alkylammonium ions with mica-type layer silicates. Clay Minerals, 7, 129-143.

Warren, B.E. and Averbach, B.L. (1950) The effect of cold-work distortion on x-ray patterns. J. Appl. Phys., 21, 595-599.

Weaver, C.E. and Beck, K.C. (1971) Clay water diagenesis during burial: How much mud becomes gneiss. Geol. Soc. Ame. Spec. Pap., 134, 96p.

Weaver. C.E. and Pollard, L.D. (1973) The chemistry of clay minerals. Elsevier, Amsterdam, 250pp.

Weiss, A. (1963) Mica-type layer silicates with alkylammonium ions. Clays and Clay Minerals, 10, 191-204.

Weiss, A. and Kanther, I. (1960) Uber eine einfache Mglichkeit zur Abshatiung der schicht ladung glimmeragtiger schicht sili-
cate. Z. Naturforsch, 15b, 804-807.

Wilson, M.D. and Pittmann, E.D. (1977) Authigenic clays in sandstones: Recognition and influence on reservoir properties and paleoenvironmental analysis. Journal of Sedimentary Petrology, 47, 3-31.

Yoder, H.S. and Eugster, H.P. (1955) Synthetic and natural muscovites. Geochemica et Cosmochemica Acta, 8, 225-280.

APPENDIX A

Alkylammonium Ion Exchange Method

Alkylammonium ion exchange is a method that allows layer charge density and its distribution in mica-like layer silicates to be determined. The method is presented in this appendix for future reference, and follows essentially the original procedure of **Lagaly and Weiss (1969)**, except for a modification suggested by **Ghabru et al.(1989)** involving the procedure of determination of layer charge in vermiculites.

General: Alkylammonium chloride ions may form either a monolayer (13.6Å), a bilayer (17.7Å), a pseudo-trimolecular layer (21.7Å), or a paraffin-type (>21.7Å) structure in the interlayer spaces of smectites and vermiculites (Fig. 1): the different structures can be determined from measurements of basal spacings. The occurrence of these different structures in interlayer spaces depends upon the ratio A_c/A_e. A_c is the area which is occupied by a flat-lying alkylammonium ion. With Nc carbon atoms in the alkyl chain

$$A_c = 1.26 * 4.5 * Nc + 14 \quad (Å^2).$$

where 1.26 is the carbon bond length (in Å), 4.5 is the ion width (in Å), and 14 is the area occupied by the NH_4^+ group of the alkylammonium ion. The equivalent area, A_e, is the area which is available for each flat-lying, monovalent cation in the interlayer space . It is therefore

$$A_e = ab/2\epsilon$$

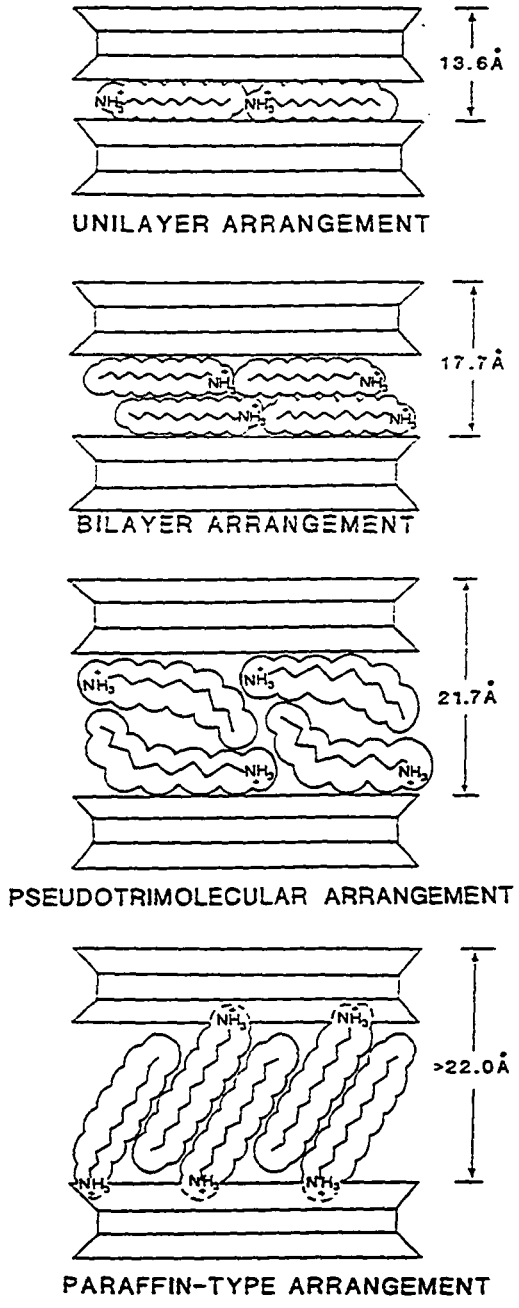

Figure 1: The four major configurations alkylammonium chloride ions may adopt in the interlayer spaces of 2:1 layer silicates.

where **a** and **b** are the unit-cell dimensions of smectite and ϵ is the cation density per half unit cell. For dioctahedral smectite **ab**≈ **46.5** Å², and therefore

$$A_e = 23.3/\epsilon.$$

When A_e is greater than A_c, the alkylammonium ions form monolayers (Fig. 2). With longer chain alkyls, A_c becomes greater than A_e and alkylammonium ions rearrange in bilayers. During this transition from monolayers to bilayers (Fig. 2), where A_c becomes equal to A_e, the following relationship is established: **1.26 * 4.5 * Nc + 14** $= 23.3/\epsilon$, and ϵ becomes

$$\epsilon = 23.3 / (5.67 * Nc + 14)$$

The layer charge ϵ can then be calculated for the values of **Nc** that mark the start and end of the transition, which represent the upper and lower limits of the charge density, respectively. The upper and lower limits of charge density can also be calculated from the bilayer-to-pseudotriomolecular layer transition that occurs when $A_c/A_e \approx 2$ with longer chain lenghts. Cation densities calculated using **Nc** values that mark the bilayer-to-pseudotrimolecular layer transition should be multiplied by two in order to account for the presence of two monovalent cations in the interlayers during this transition.

Paraffin-type structures are formed when the ratio A_c/A_e is greater than 2. this is commonly the case with

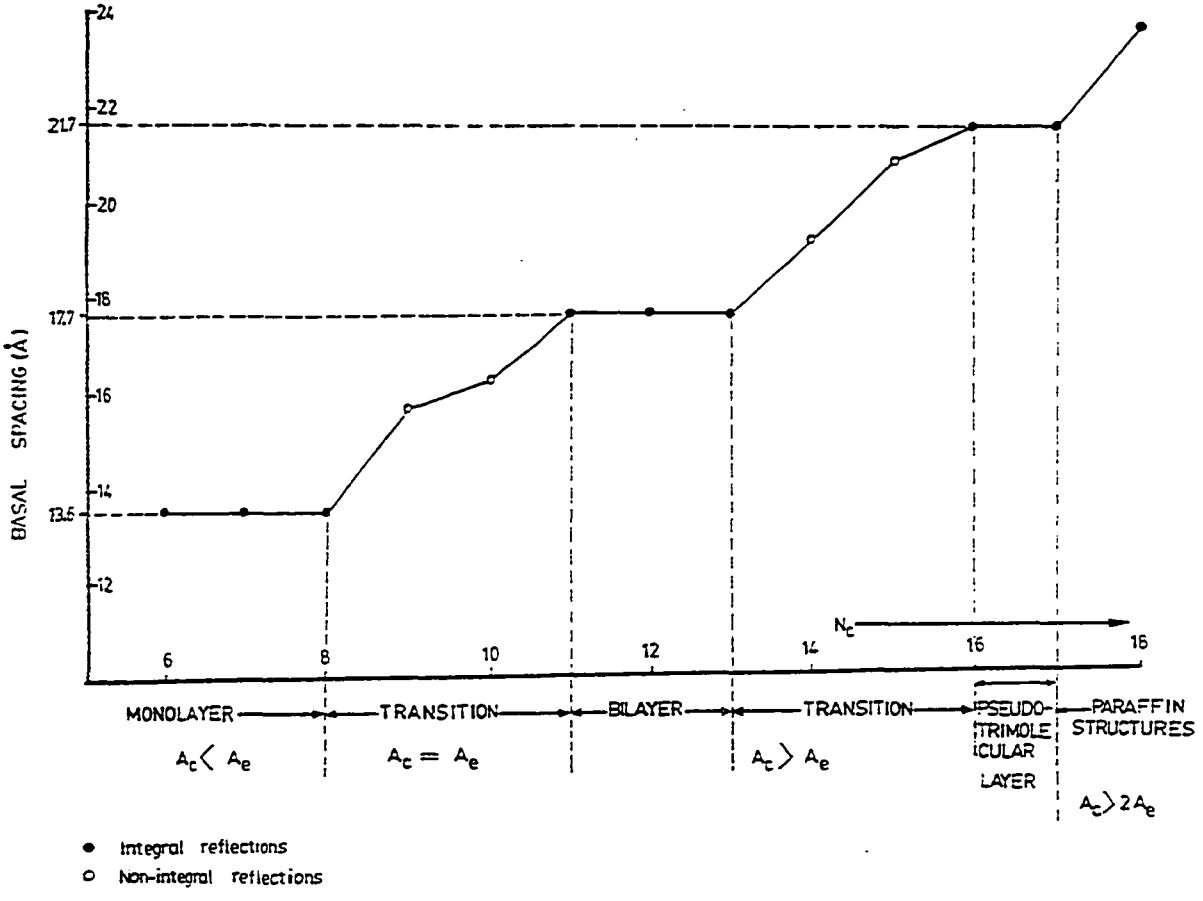

Figure 2: Variation of basal spacing of both low- and high-charged smectites due to formation of monolayers, bilayers, and pseudotrimolecular layers of alkylammonium ions in the interlayer spaces.

with long-chain alkylammonium derivatives of high-charged minerals in which A_c is large due to the long chains, and A_e is small because of high ϵ.

Determination of layer charge density and its distribution in smectite: The mean interlayer cation density (≈interlayer charge) and its distribution in alkylammonium exchanged smectite are commonly determined from the mono-to-bilayer transition. The upper and lower limits of the layer charge density are calculated using the **Nc** values that mark the start and end of the mono-to-bilayer transition.

If a smectite has a homogeneous charge distribution, mono-to-bilayer transition would take place as a sharp jump from 13.6Å to 17.7Å between two successive values of **Nc**. Consider, for example, the homogeneously-charged smectite shown in Figure 3a, showing a sharp mono-to-bilayer transition between **Nc=8** and **Nc=9**. A mean layer charge of 0.405 is assigned for the chain-length category defined between **Nc=8** and **Nc=9** (Table 1). This assigned value is the aritmethic average of the layer charge values calculated for **Nc=8** and **Nc=9**, which represent the upper and lower limits of layer charge for the sample, respectively.

Layer charge of smectite usually varies between interlayers such that mono-to-bilayer transitions occur over a range of **Nc** values (Fig. 3b). In other words, layer

charge heterogeneity in smectite leads to an interstratification of monolayers and bilayers in the interlayers, and thus gives rise to non-integral spacings between 13.6Å and 17.7Å during the transition. The mean layer charge of the heterogeneously-charged smectite shown in Figure 3b is calculated as follows: The **Nc=8** and **Nc=11** derivatives of this mineral mark the start and the end of the transition where 0% and 100% of the alkylammonium ions are arranged in bilayers, respectively. The fraction of bilayers that form in each of the three transition categories (**Nc**=8-9, 9-10, and 10-11) are calculated by proportioning the increases in basal spacing from 8 to 9, 9 to 10, and 10 to 11 with the total increase in basal spacing during the transiton (e.g. what fraction of bilayer formation would an increase of 0.9Å from 13.6Å to 14.5Å represent if a complete bilayer formation is represented by an increase of 4.1Å from 13.6Å to 17.7Å). The fraction of bilayers for transition categories 8-9, 9-10, and 10-11 are thus calculated to be 22% (=0.9*100%/4.1), 12% (=0.5*100%/4.1), and 66% (=2.7*100%/4.1), respectively. The layer charge densities corresponding to the same categories are 0.405, 0.375, and 0.350, respectively (Table 1).

The distribution of the layer charge densities are, by convention, shown in histograms as a function of

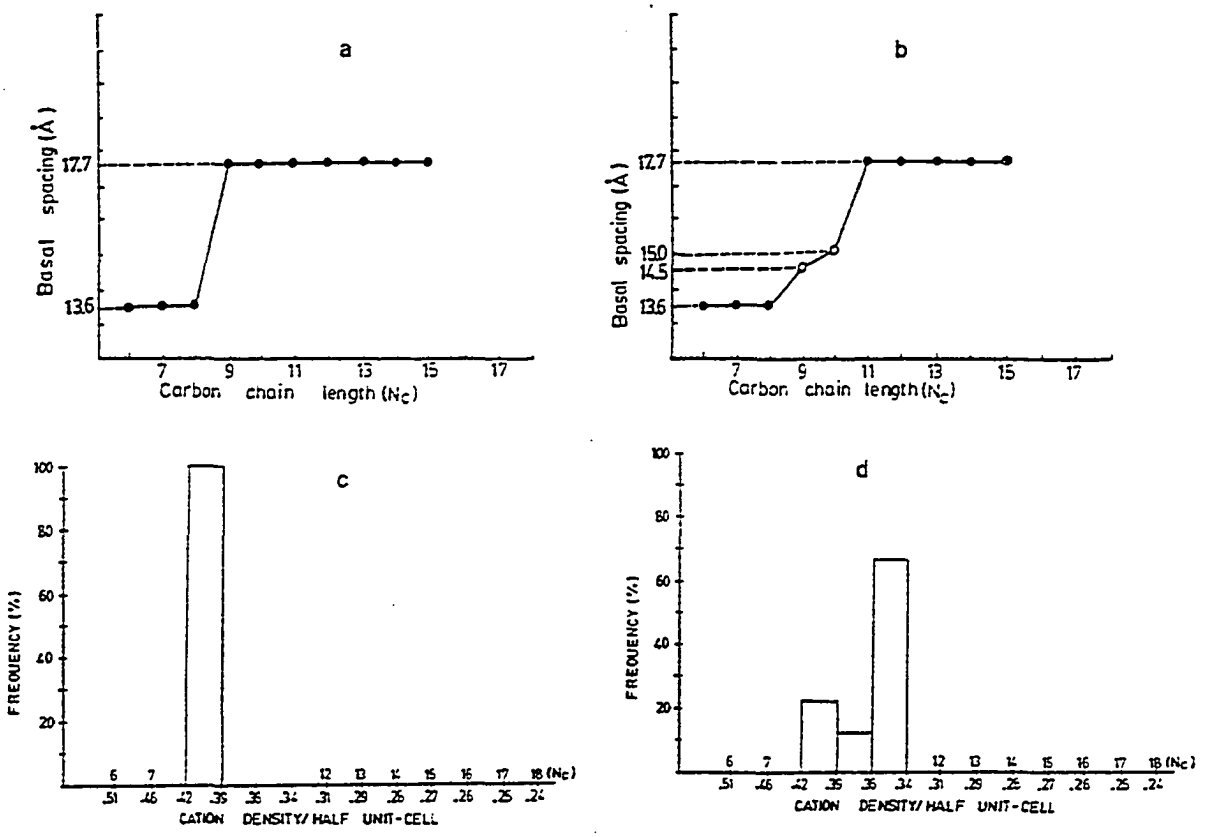

Figure 3: Variation of basal spacing of alkylammonium-exchanged smectites with alkyl chain length for different charge distributions: (a) homogeneous charge distribution; (b) heterogeneous charge distribution; (c) and (d) charge distribution histograms for alkylammonium-smectites shown in (a) and (b), respectively.

fraction of bilayers (Figs. 3c and 3d). The histogram in Figure 3d, for example, shows that 22% of the interlayers in the sample have a layer charge density of around 0.405, 12% of around 0.375, and 66% of around 0.350. The mean layer charge density can be calculated by taking a weighted

fraction of bilayers as weight factors. The mean layer charge density of the mineral is thus calculated to be 0.365 from

$$\epsilon = (22\%*0.405 + 12\%*0.375 + 66\%*0.350) / 100).$$

Table 1: Interlayer cation densities calculated for chain length catergories, assuming an average particle diameter of 400Å (from **Lagaly, 1981**).

Chain Length Category	Charge Density/half unit-cell
6-7	0.485
7-8	0.440
8-9	0.405
9-10	0.375
10-11	0.350
11-12	0.325
12-13	0.300
13-14	0.285
14-15	0.275
15-16	0.263
16-17	0.251
17-18	0.241

Determination of layer charge density and its distribution in vermiculite: As noted before, alkylammonium ions form paraffin-type structures in the interlayers of high-charged 2:1 layer silicates. This is particularly true of vermiculite, even with short-chain alkylammoniums. In the paraffin-type structure, the angle at which the alkylammoniums stand, tilt angle, is controlled by the layer charge density and increases to a maximum of 90° for a layer charge of 1.0 per half unit-cell (Fig. 4). The tilt angle, α, is calculated from the mean increase in basal spacing, δd, which is caused by an increase from one to the next higher (and/or longer) alkylammonium chain:

$$\alpha = \mathrm{Sin}^{-1}\, \delta d \,/\, 1.26$$

This is an empirical relationship, originally developed by **Lagaly and Weiss (1969)** and recently modified by **Ghabru et al. (1989)**, between the tilt angle and layer charge density for paraffin-type structures and has been adopted in this study to estimate layer charge density.

This empirical relationship illustrated in Figure 5, suggests a linear increase of the tilt angle α with layer charge density ϵ for values ≥ 0.65. In order to calculate the layer charge density, the following linear regression equation presented in **Ghabru et al. (1989)** is used:

$$\alpha = -47.82 + 137.82\ \epsilon$$

The equation is solved for a given calculated tilt angle α

to calculate ϵ.

Consider, for example, the mineral shown in Figure 6, exhibiting a linear increase of basal spacing upon treatment with alkylammonium ions of chain length **Nc**=9 through **Nc**=18. The mean increase in basal spacing δ**d** is 1.20 Å (= (30.8-20.0)/9) and tilt angle α is about 72° (= Sin^{-1} (1.20/1.26)) for this mineral. The mean layer charge density ϵ is therefore 0.87 from ϵ= (72° + 47.82) / 137.82.

Because neither mono-to-bilayer nor bilayer-to-pseudtrimolecular transitions are observed with vermiculites, the homogeneity or heterogeneity of the layer charge density across the interlayers can be expressed only qualitatively by the degree of linearity of the relationship between basal spacing and alkyl chain length. A perfectly linear relationship indicates a homogeneously-charged mineral. Deviations from linearity indicate the presence of interlayers with layer charge densities different from the mean layer charge density of the mineral.

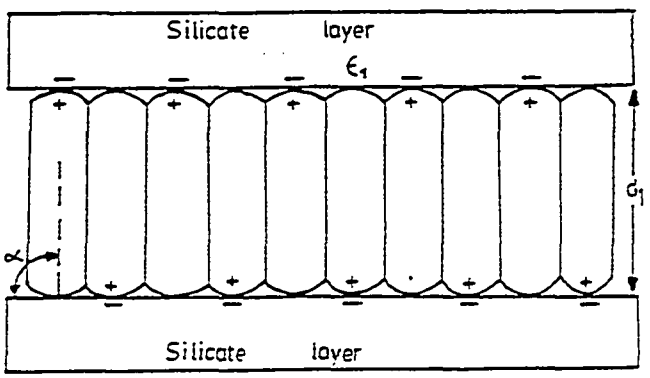

a) Tilt angle (α)=90°

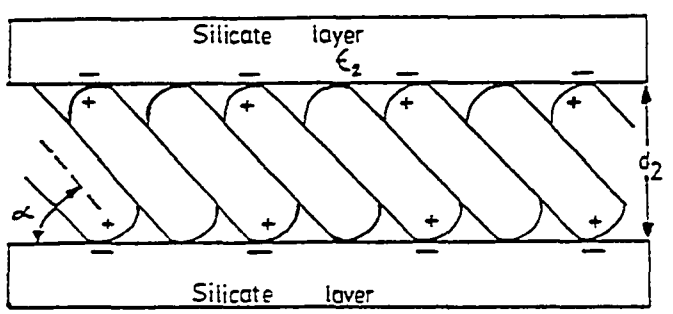

b) Tilt angle (α)=45°

Figure 4: Schematic illustration of idealized paraffin-type arrangement of alkylammonium cations in the interlayer space of a high-charge, 2:1 layer silicate at different angles. α = 90° (a) and α = 45° (b) represent different charge densities: $d_1 > d_2$, thus $\epsilon_1 > \epsilon_2$. Modified from **Ghabru et al., 1989.**

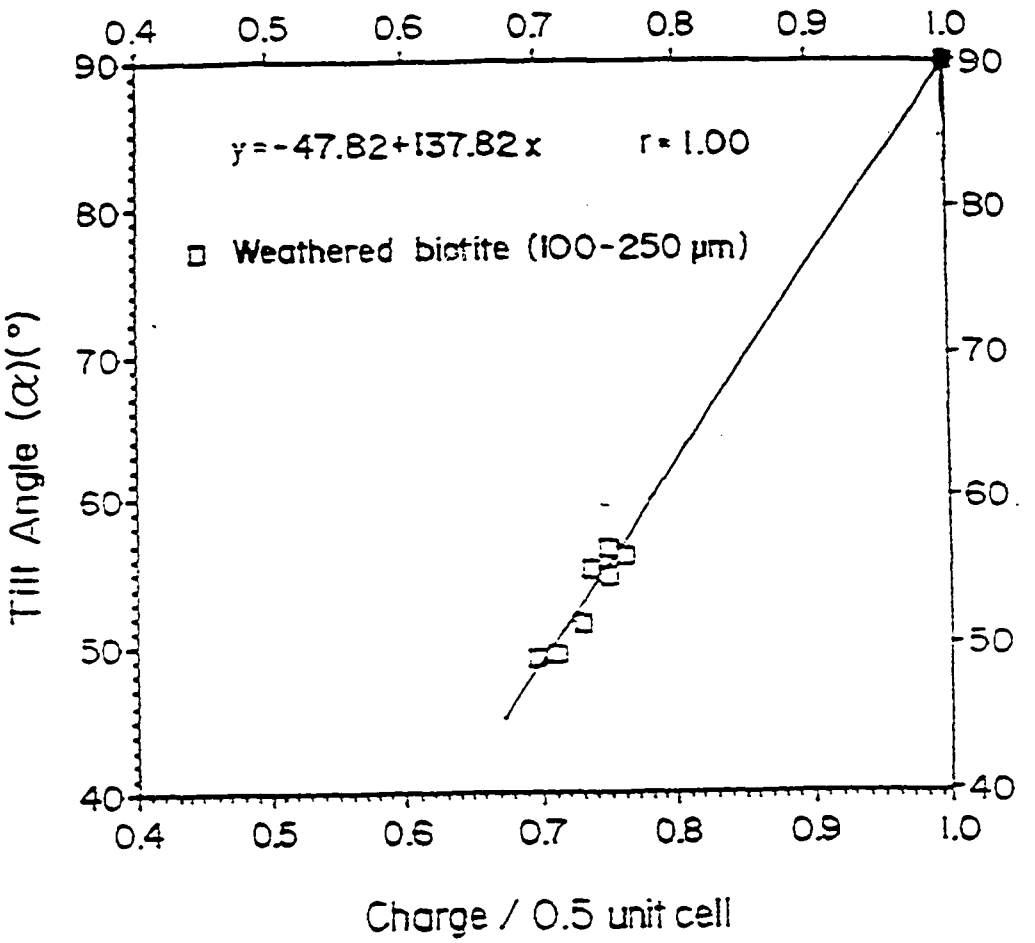

Figure 5: Dependence of tilt angle (α, in degrees) of alkylammonium cations on layer charge density of high-charge 2:1 layer silicates: regression line represents data points shown for a sand-size (100-250 μm) weathered biotite plus the theoretical maximum of 1 for a tilt angle of 90°. Modified from **Ghabru et al., 1989.**

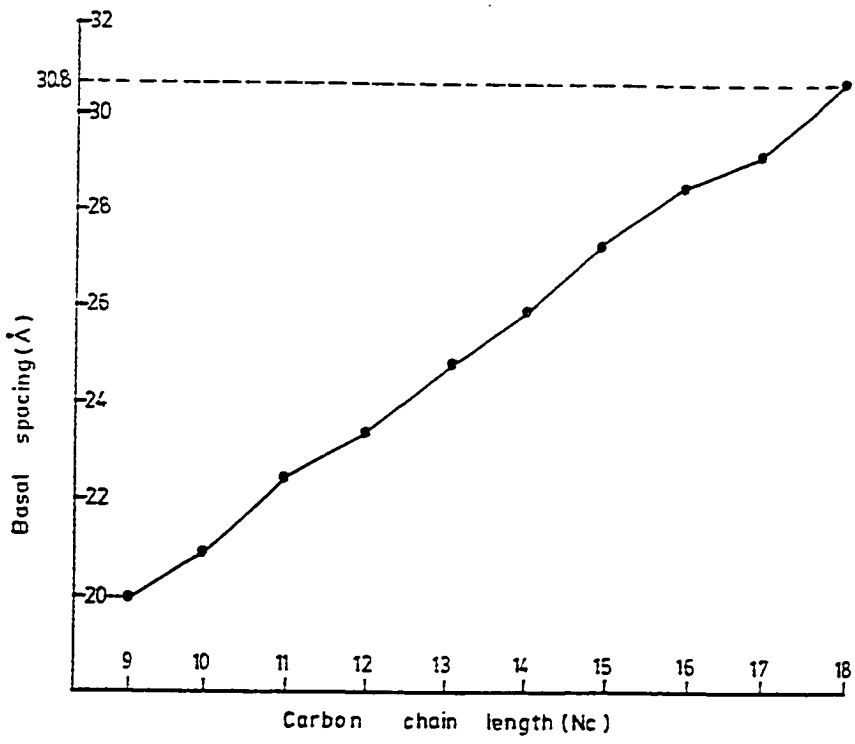

Figure 6: Typical linear variation of basal spacing in a high-charge vermiculite upon alkylammonium ion exchange of chain length Nc=9 through 18.

APPENDIX B

XRD patterns of Alkylammonium treated I/S clays

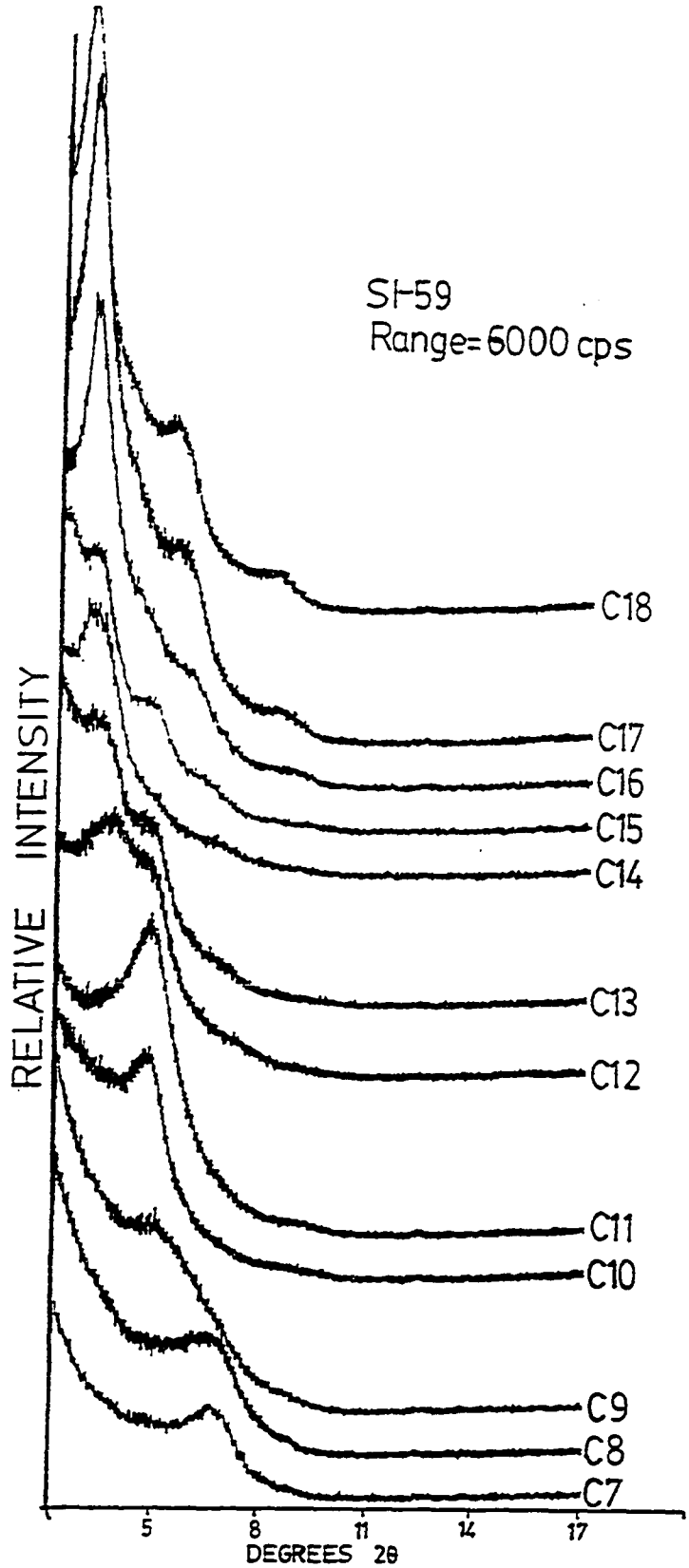

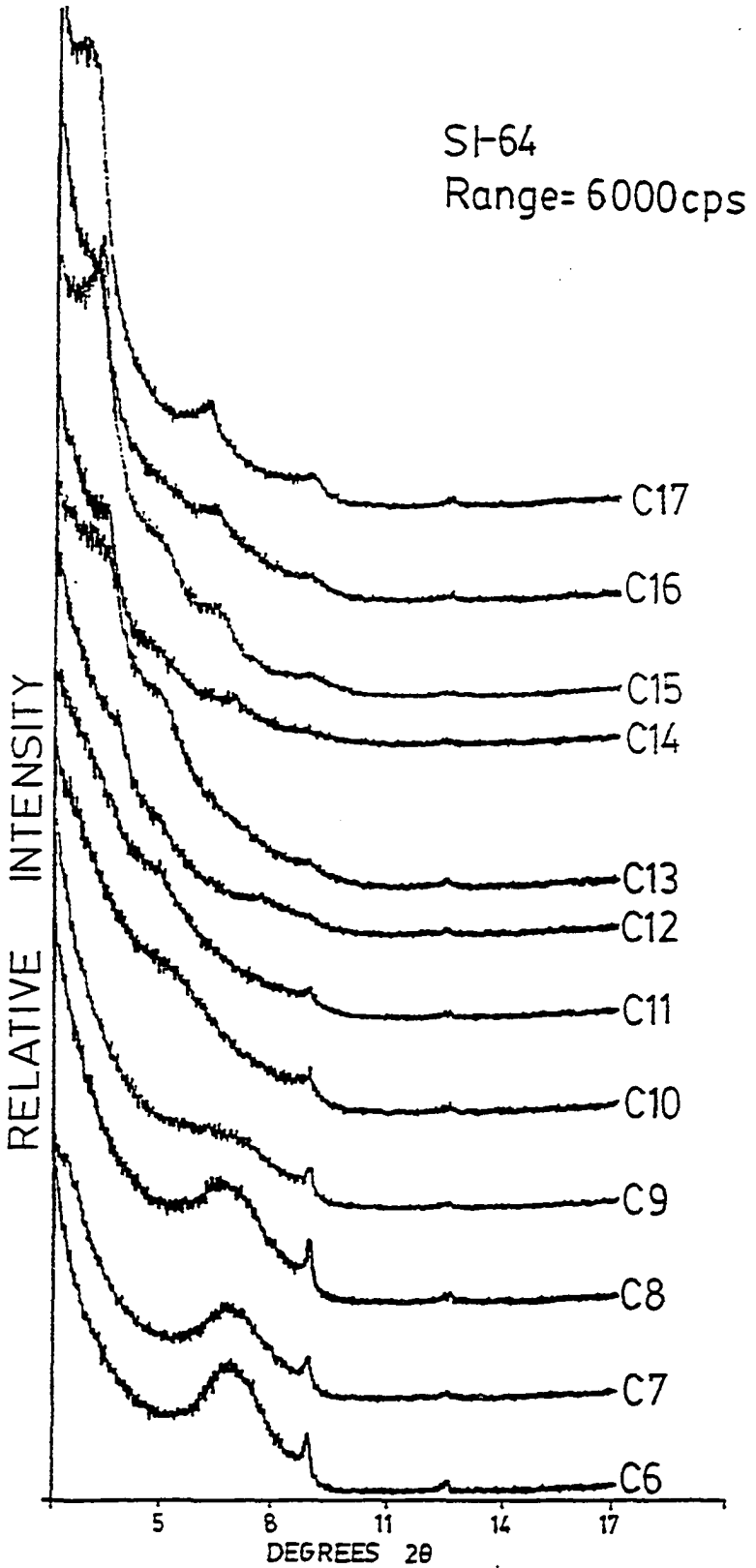

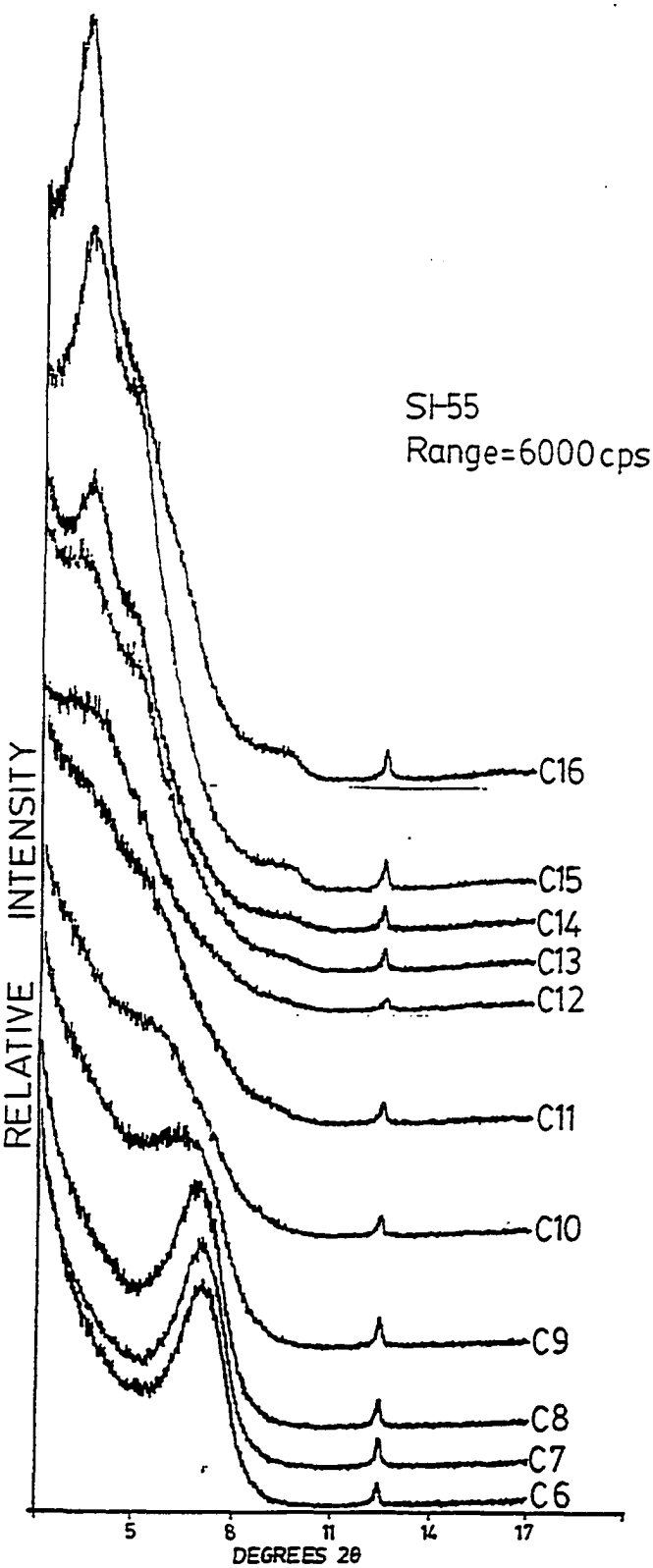

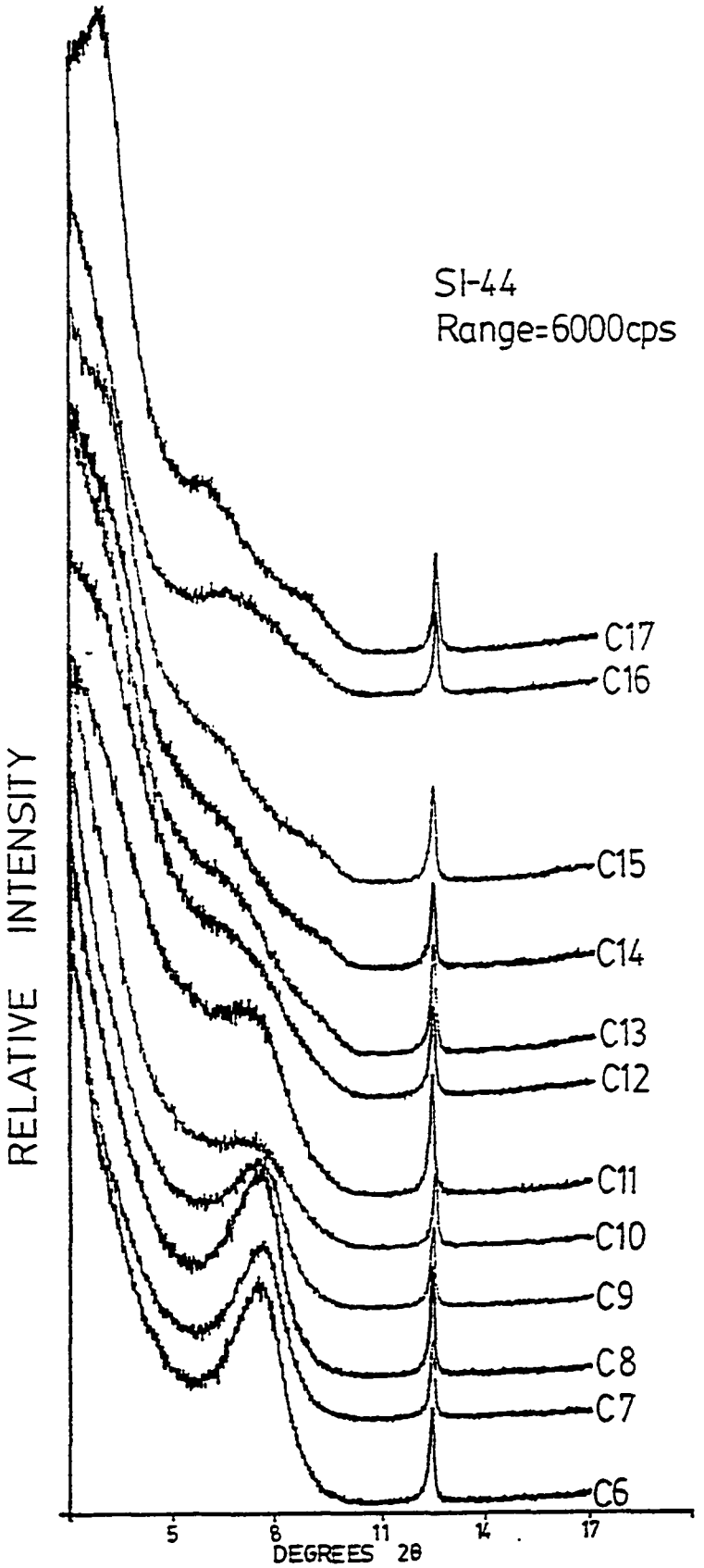

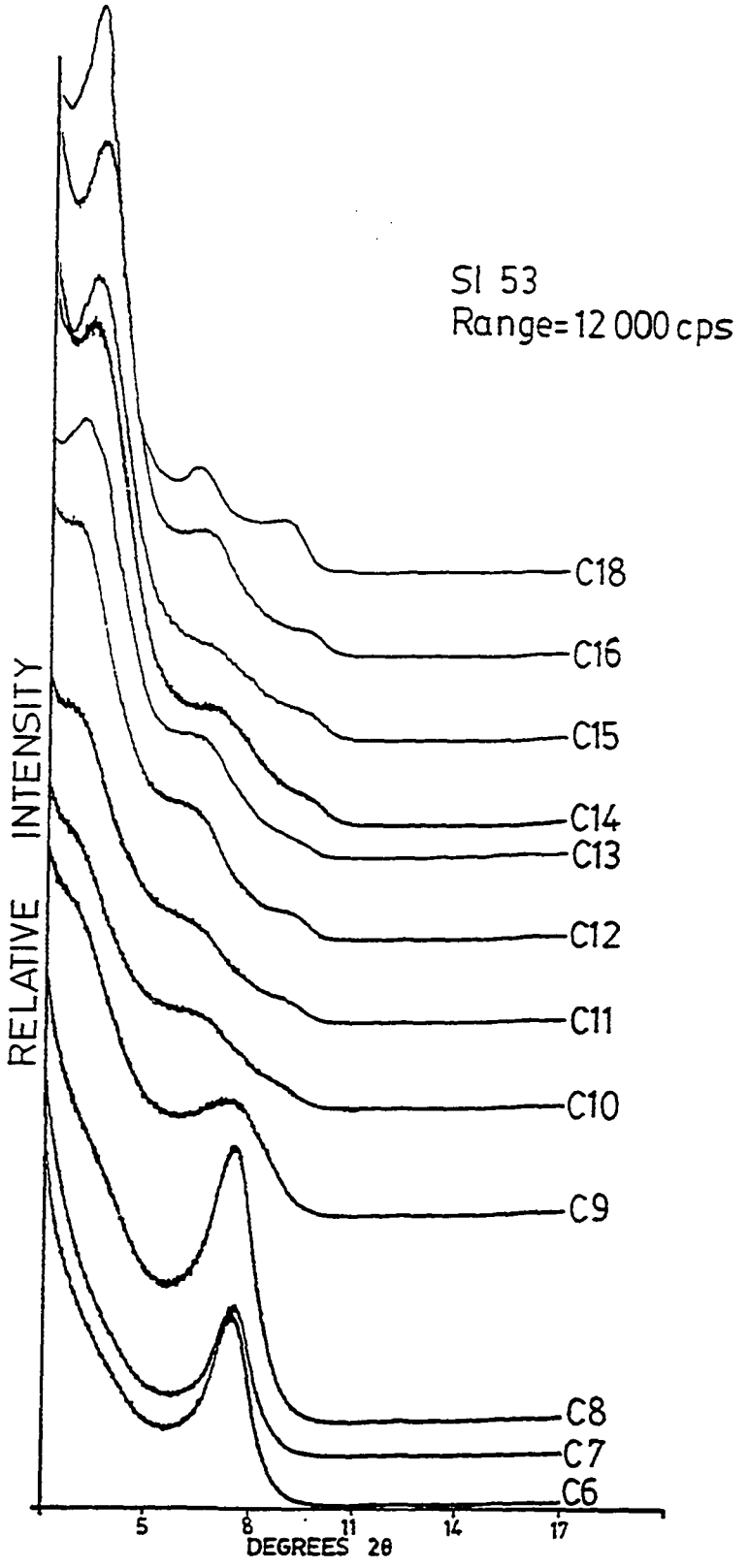

188

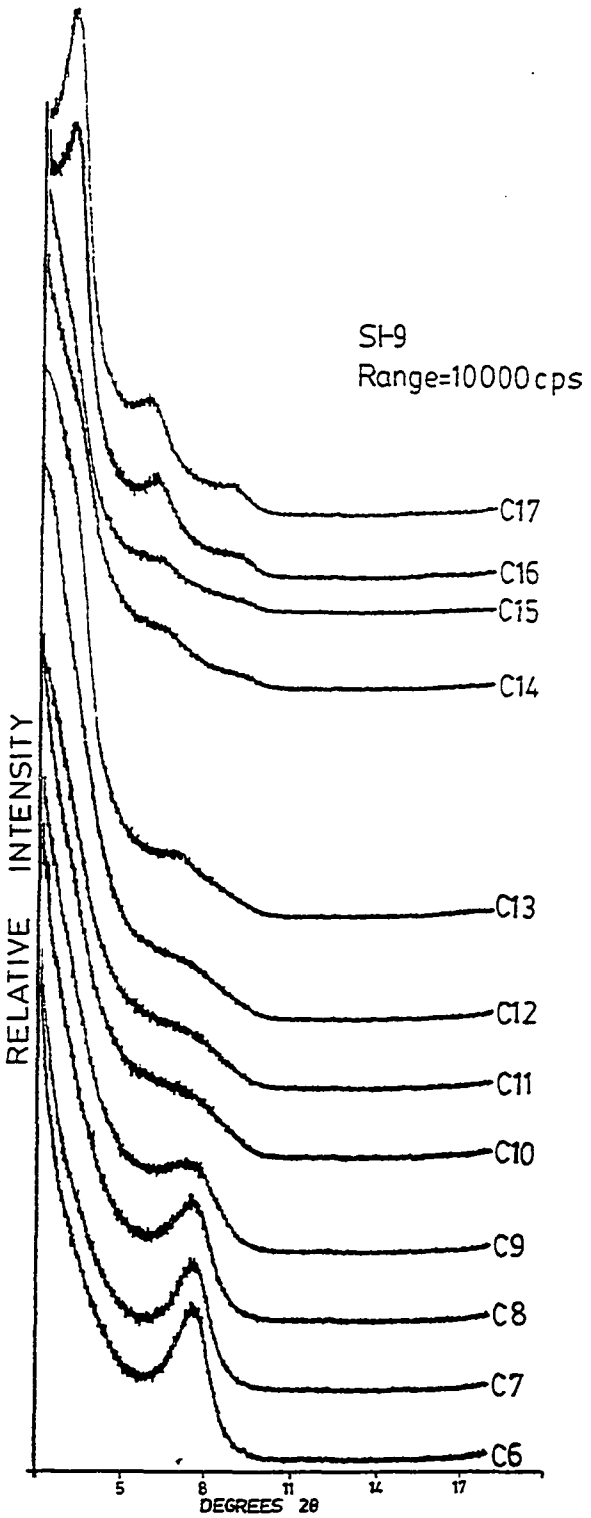

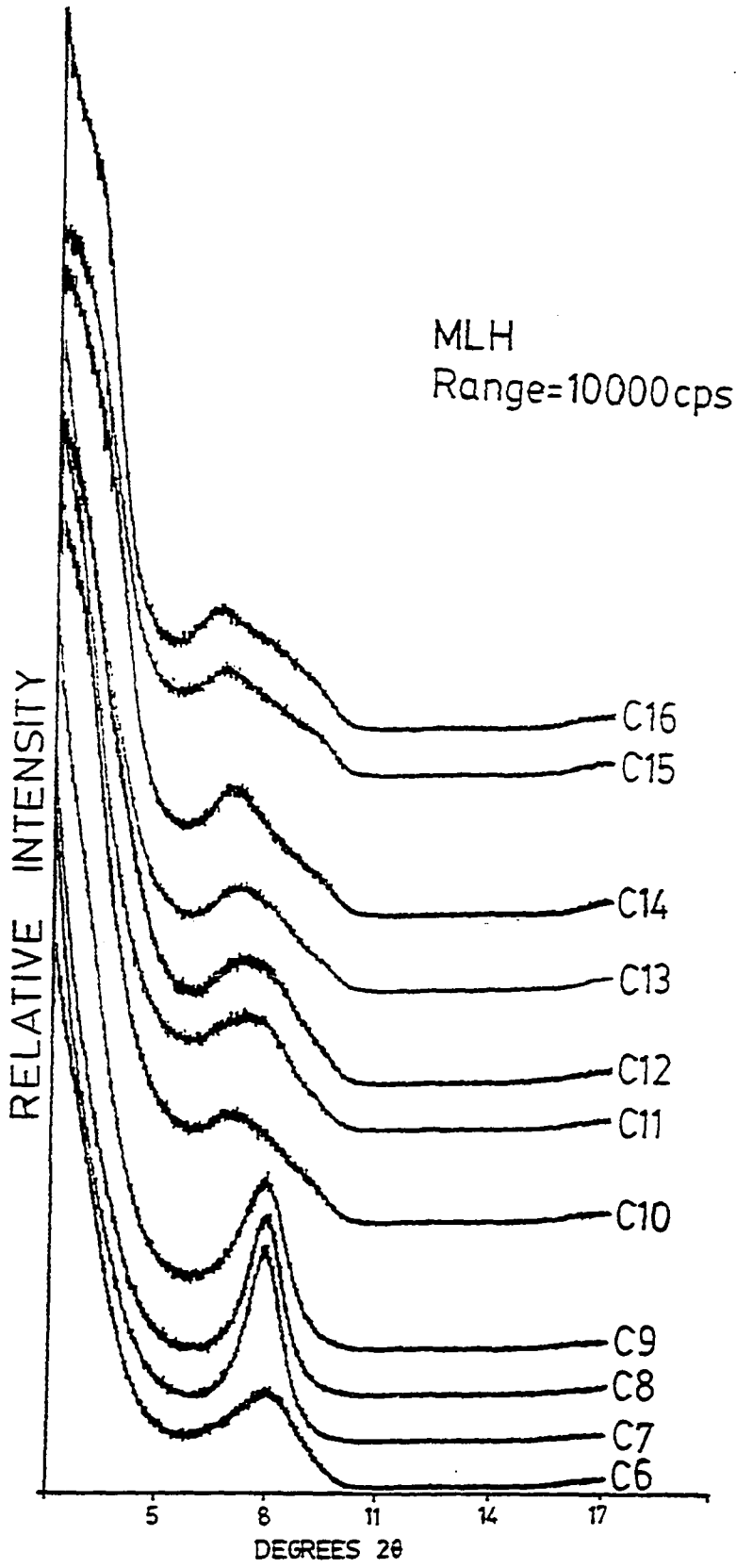

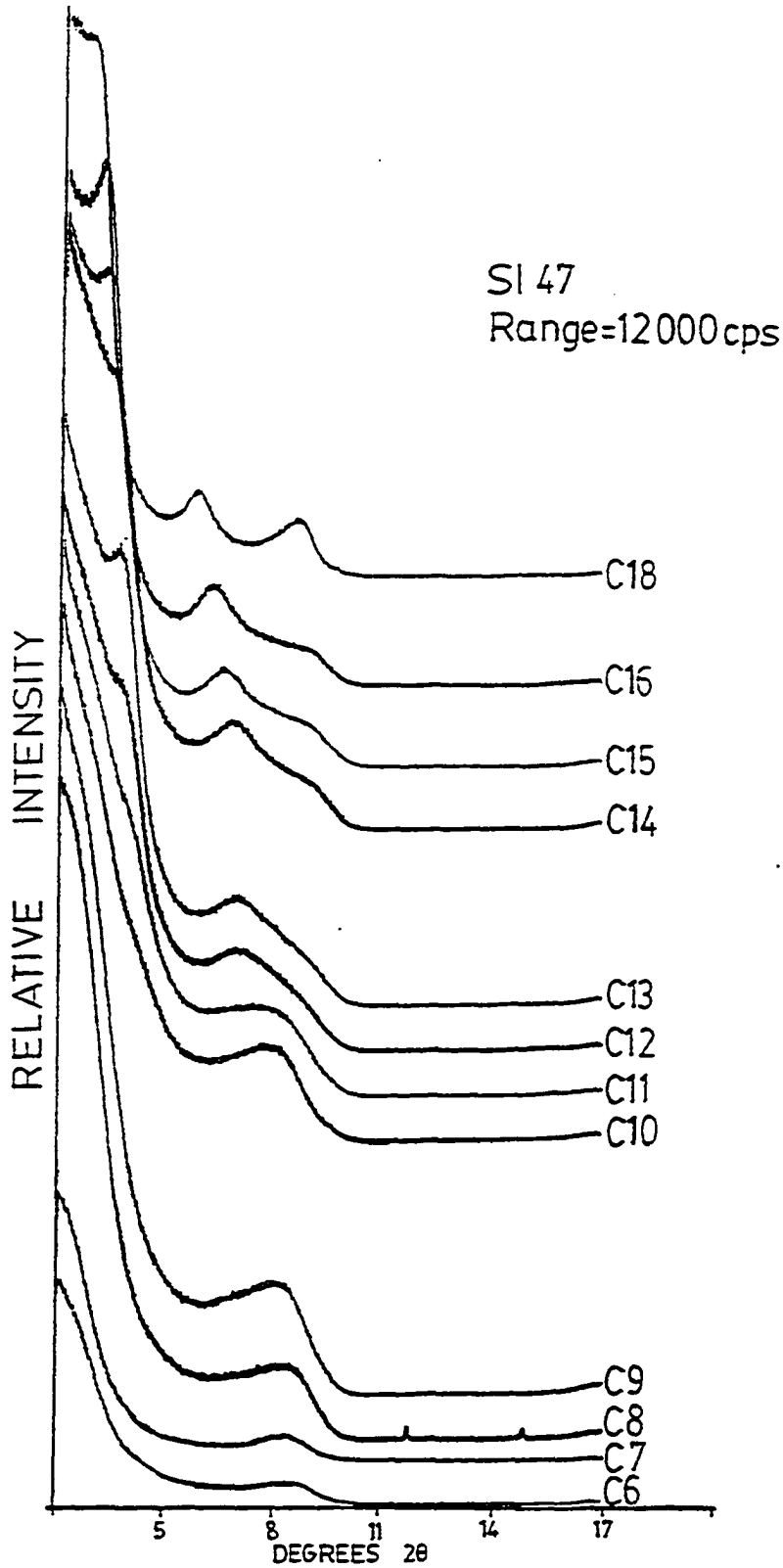

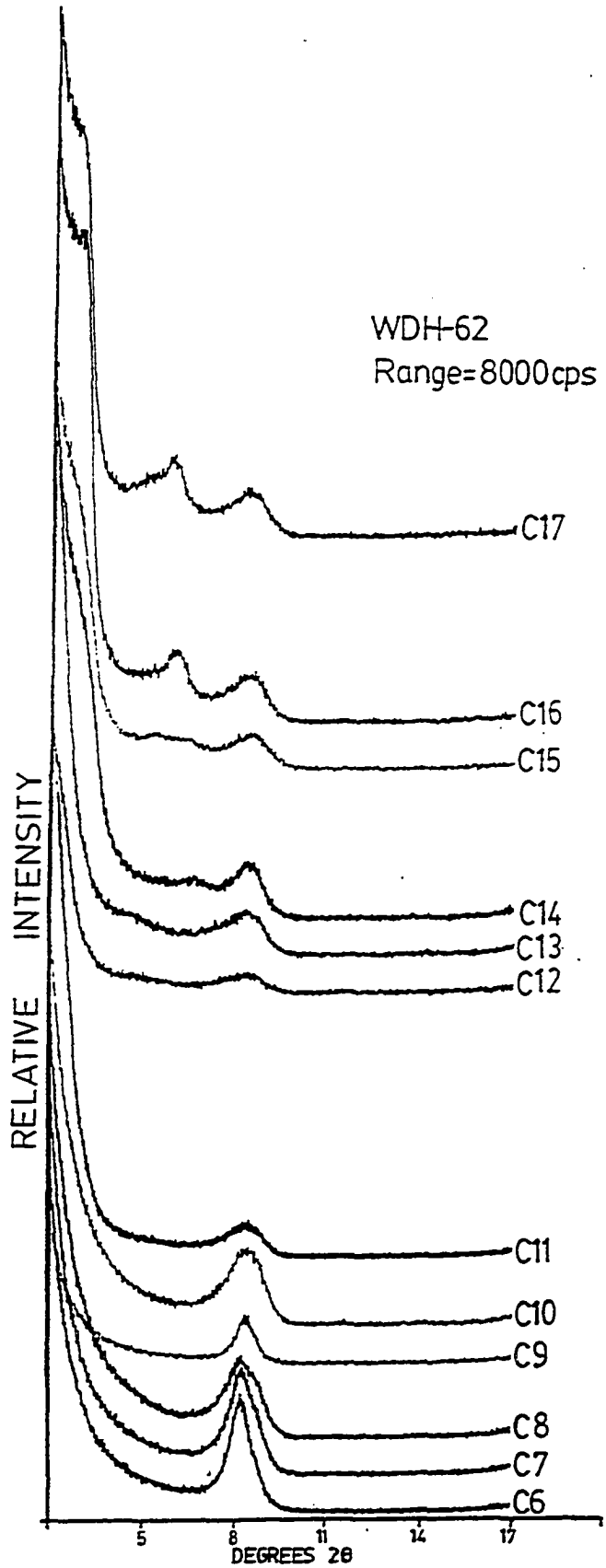

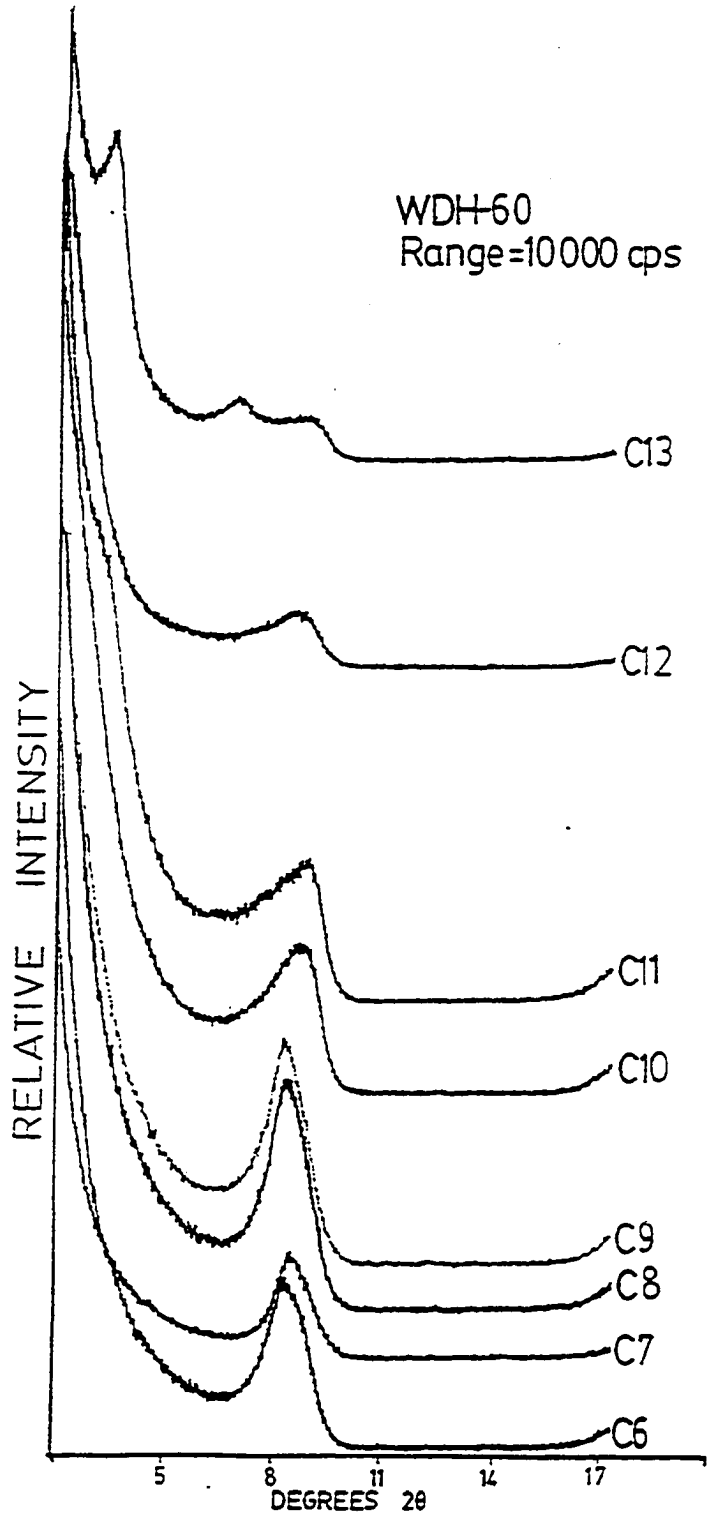

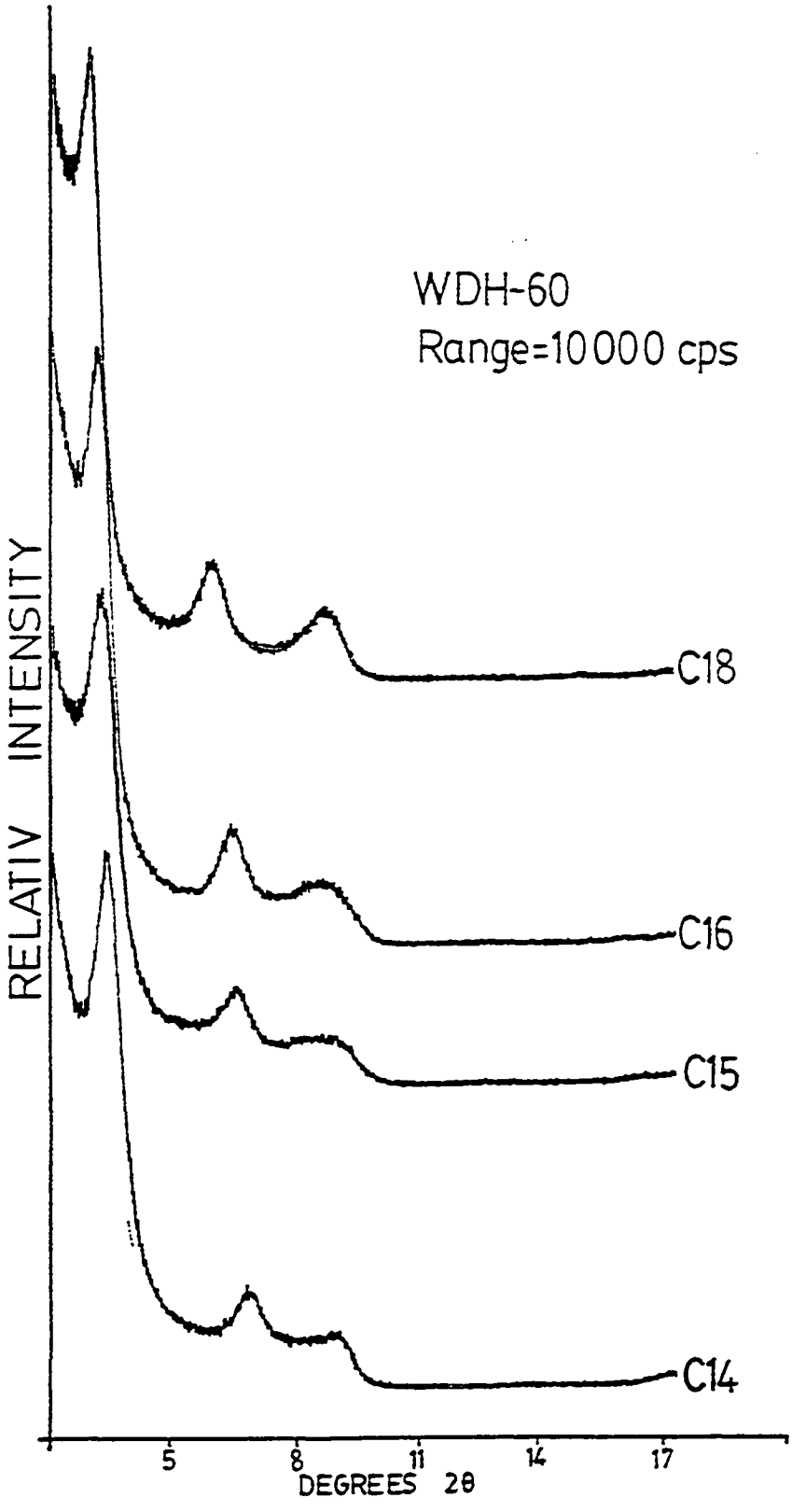

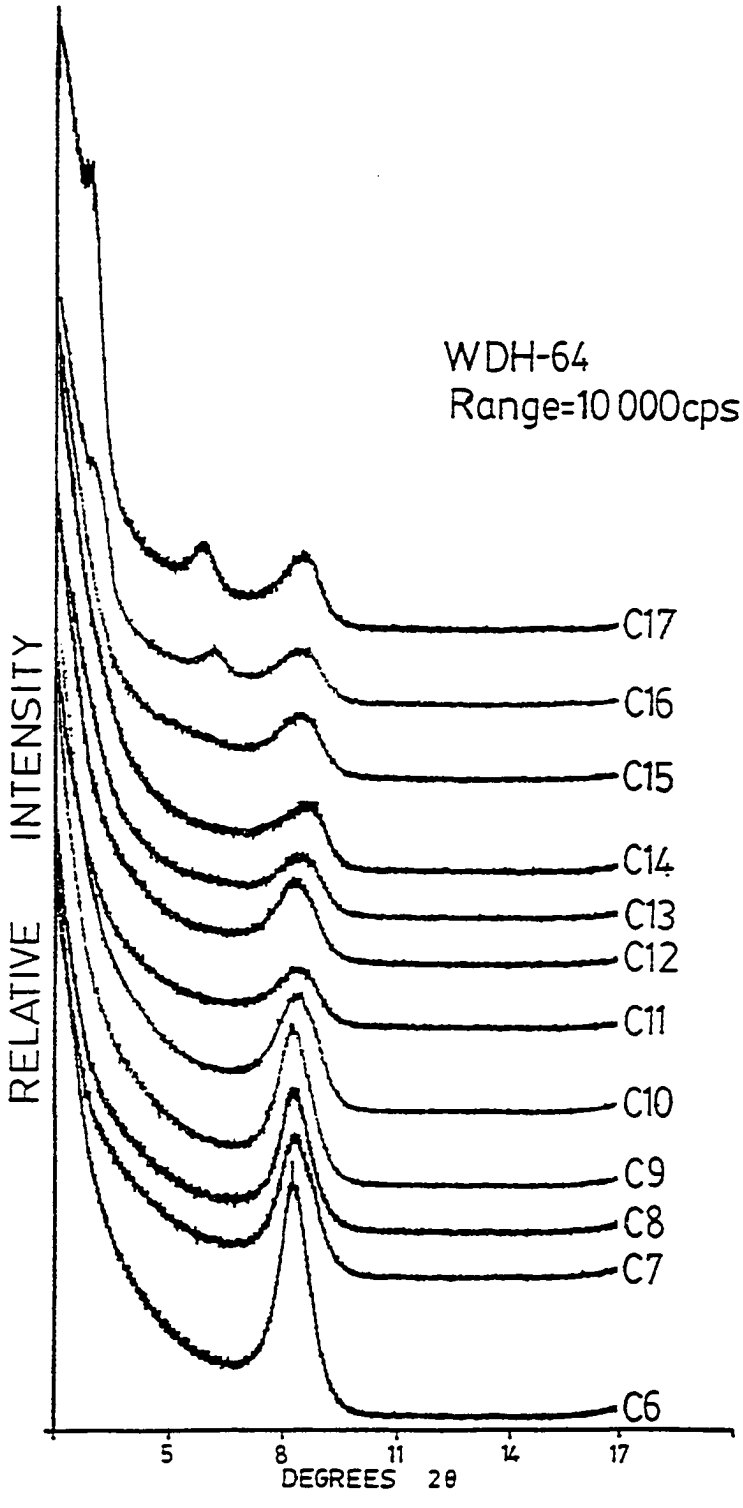

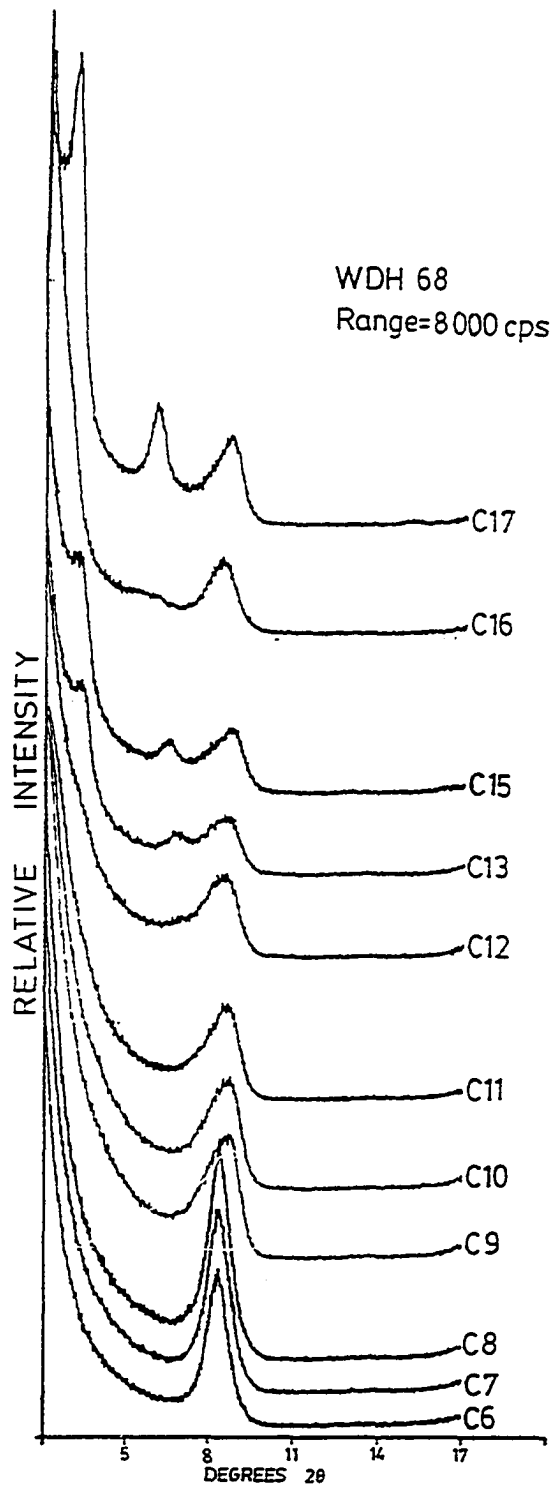

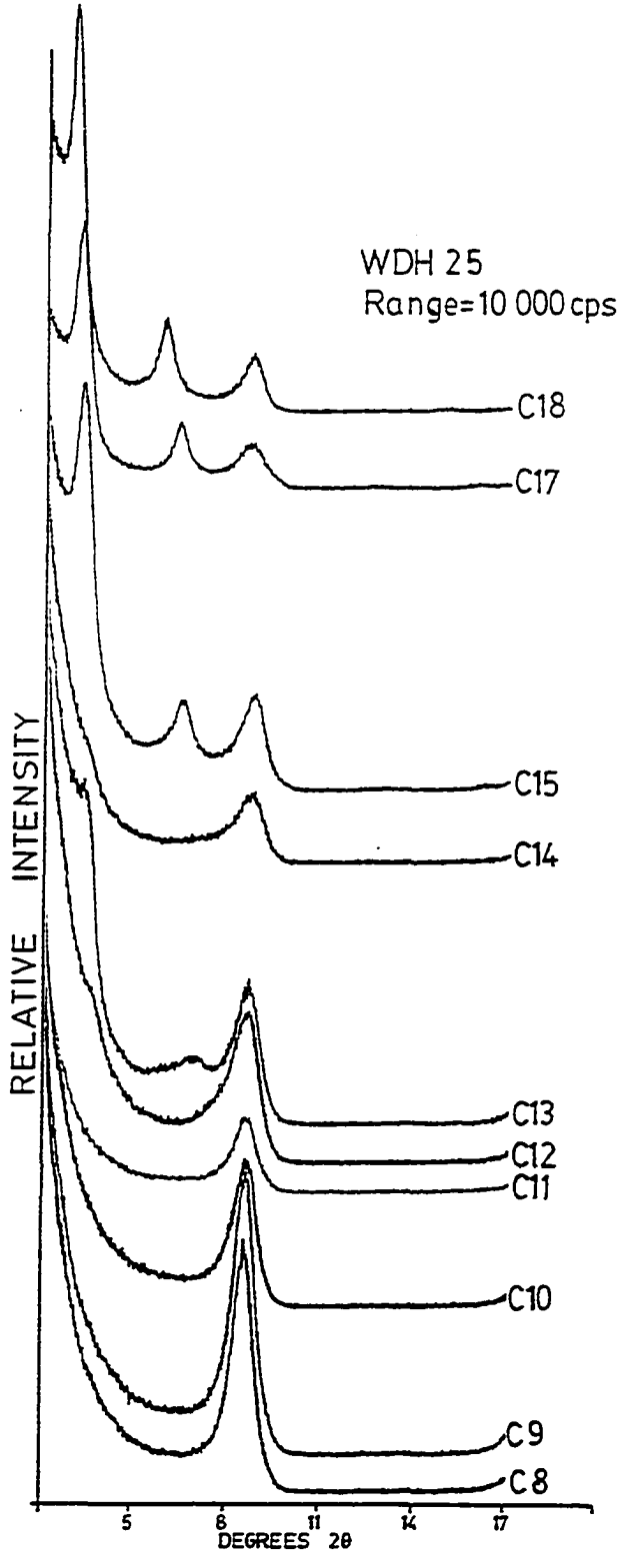

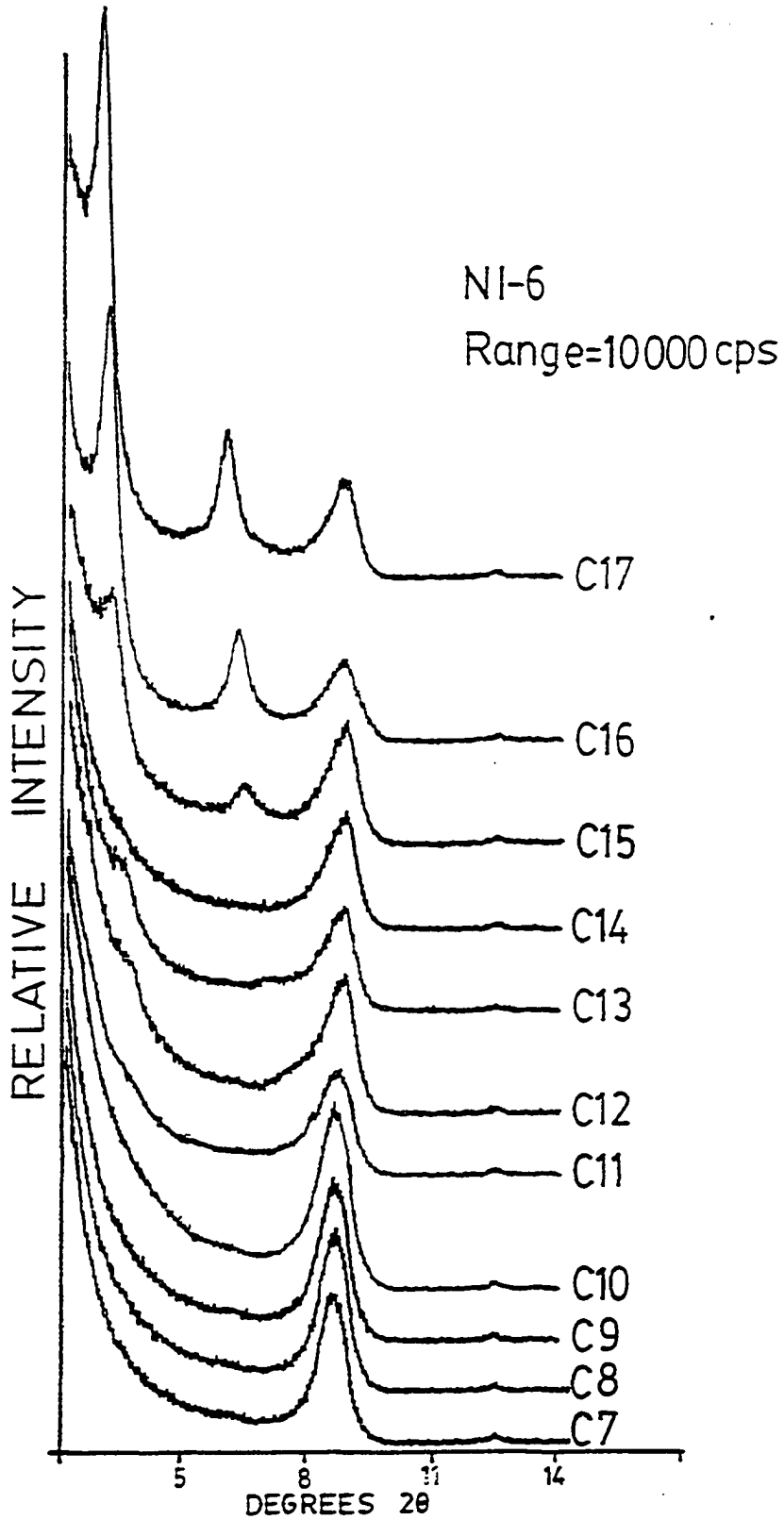

APPENDIX C

Sample localities and bed thicknesses

Sample	Age/Location	Bed Thickness(cm)
SI-9	Ludlow (Silurian). Mortimer Forest near Ludlow, southern England.	5
SI-44	Bringewoodian (Silurian). Perton Quarry, Woolhope Inlier, Shropshire, southern England.	65
SI-47	Upper Wenlock (Silurian). Bagpiper's Trump, Westwood, Woolhope Inlier, southern England.	9
SI-53	Wenlock (Silurian). Haugh Wood section, Woolhope Inlier, Shropshire, southern England.	3
SI-55	Wenlock-?-(Silurian). Woolhope Quarry, Woolhope Inlier, southern England.	18
SI-59	Wenlock-?-(Silurian). Overbury Quarry, Shropshire, southern England.	No data
SI-64	Ludlow (Silurian). Sleaves Oak Quarry, Shropshire, southern England.	11
WDH-25	Upper Ludlow (Silurian). Newtown, Wales.	8
WDH-60	Llandovery (Silurian). Dob's Linn, southern Uplands, Scotland.	9
WDH-62	same as WDH-60	22
WDH-64	same as WDH-60	10
WDH-68	same as WDH-60	17
NI6	Wenlock (Silurian). County Down, Northern Ireland.	No data
MLH	Rocklandian (Middle Ordovician). Hickman Creek at Wesley Chapel, Jessamine County, central Kentucky.	18